



Delft University of Technology

Docking of Surgical Guides

Mattheijer, Joost

DOI

[10.4233/uuid:8264bbbd-376c-4d08-8067-39255ab6fb03](https://doi.org/10.4233/uuid:8264bbbd-376c-4d08-8067-39255ab6fb03)

Publication date

2019

Document Version

Final published version

Citation (APA)

Mattheijer, J. (2019). *Docking of Surgical Guides*. [Dissertation (TU Delft), Delft University of Technology]. <https://doi.org/10.4233/uuid:8264bbbd-376c-4d08-8067-39255ab6fb03>

Important note

To cite this publication, please use the final published version (if applicable).
Please check the document version above.

Copyright

Other than for strictly personal use, it is not permitted to download, forward or distribute the text or part of it, without the consent of the author(s) and/or copyright holder(s), unless the work is under an open content license such as Creative Commons.

Takedown policy

Please contact us and provide details if you believe this document breaches copyrights.
We will remove access to the work immediately and investigate your claim.

Docking of Surgical Guides



Joost Mattheijer

Docking of Surgical Guides

Joost Mattheijer

Docking of Surgical Guides

Proefschrift

ter verkrijging van de graad van doctor

aan de Technische Universiteit Delft,

op gezag van de Rector Magnificus Prof. dr. ir. T.H.J.J. van der Hagen,

voorzitter van het College voor Promoties,

in het openbaar te verdedigen op

woensdag 30 oktober 2019 om 10:00 uur

door

Joost MATTHEIJER

Ingenieur in Biomedical Engineering,

Technische Universiteit Delft, Nederland

geboren te Alkmaar, Nederland

Dit proefschrift is goedgekeurd door de promotoren:

Prof. dr. J. Dankelman

Prof. dr. R.G.H.H. Nelissen

Samenstelling promotiecommissie:

Rector Magnificus

voorzitter

Prof. dr. J. Dankelman

Technische Universiteit Delft, promotor

Prof. dr. R.G.H.H. Nelissen

U Leiden, Technische U Delft, promotor

Prof. dr. E.R. Valstar[†]

U Leiden, Technische U Delft, promotor

Onafhankelijke commissieleden:

Prof. dr. ir. R.H.M. Goossens

Technische Universiteit Delft

Prof. dr. J.A.N. Verhaar

Erasmus Medisch Centrum, Erasmus Universiteit

Prof. dr. ir. J. Harlaar

Technische Universiteit Delft

Dr. P. C. Jutte

UMC Groningen, Rijksuniversiteit Groningen

Prof. dr. ir. P. Breedveld

Technische Universiteit Delft, reservelid

Overige commissieleden:

Dr. ir. B.L. Kaptein

Leids Universitair Medisch Centrum

This research is supported by the NWO Domain Applied and Engineering Sciences (AES) (formerly known as the Technology Foundation STW), which is part of the Netherlands Organization for Scientific Research (NWO), and which is partly funded by the Ministry of Economic Affairs (Project NIG 10812).

Cover design by J. Mattheijer based on illustration by T.O. Herrebrugh.

Printed by Ipskamp Printing

ISBN 978-94-028-1758-4

Copyright © 2019 by J. Mattheijer

All rights reserved. No part of this thesis may be reproduced, stored in a retrieval system, or transmitted in any form or by any means without written permission of the author.



TABLE OF CONTENTS

	Samenvatting	7
	Summary	11
CHAPTER 1	General Introduction	15
CHAPTER 2	Shaping Patient Specific Surgical Guides for Arthroplasty to Obtain High Docking Robustness	29
CHAPTER 3	Docking Robustness of Patient Specific Surgical Guides for Joint Replacement Surgery	57
CHAPTER 4	Docking Accuracy of Patient Specific Surgical Guides for Joint Replacement Surgery	87
CHAPTER 5	A Novel Intraoperatively Adjustable Patient Specific Surgical Guide for Knee Replacement Surgery	109
CHAPTER 6	General Discussion and Conclusion	127
	Dankwoord	137
	Curriculum Vitae	139
	List of Publications	141

SAMENVATTING

Verkeerde uitlijning van implantaatcomponenten is een onderliggende oorzaak voor het falen van knieprotheses. Patiëntspecifieke Chirurgische Mallen – in het engels: Patient Specific Surgical Guides (PSSG's) – worden gebruikt om de postoperatieve positie van het implantaat te verbeteren ten opzichte van een preoperatief geplande positie. De PSSG's worden op maat gemaakt om te passen op de anatomie van de patiënt en om boorgaten en zaagsleuven uit te lijnen ten opzichte van het bot. Dit proefschrift verschaft methodes voor preoperatieve optimalisatie van de contactgeometrie en intraoperatieve aanpassingen voor een verbeterde uitlijning.

The chirurg plaatst de PSSG op het bot door gebruik te maken van de overeenkomende geometrie en behoudt de positie door het uitvoeren van kracht. De toegestane variatie in de werklijn van deze kracht is afhankelijk van de afmetingen van de PSSG en wordt aangeduid als plaatsingsrobustheid – in het engels: docking robustness (Hoofdstuk 2 en 3).

In hoofdstuk 2 worden methodes van robotisch grijpen en werkstukopspanning gebruikt bij het creëren van een nieuwe methode voor de evaluatie van plaatsingsrobustheid van tweedimensionale PSSG's. Ontwerpgereedschappen worden gepresenteerd bestaande uit visualisatiekaarten en maten. Wrench space kaarten worden gebruikt om een contactset te selecteren welke de toegestane variatie in de werklijn van de aandrukkracht maximaliseert. Application angle kaarten maken het mogelijk om een robuuste locatie voor het aandrukvlak te vinden gebaseerd op gradiënt grijsinten. De contactefficiëntie maat η_c wordt gebruikt voor kwantificatie van het geselecteerde bot-mal contact. De malefficiëntie maat η_g wordt gebruikt om de volledige mal te kwantificeren inclusief een aandrukvlak waarop de chirurg kracht kan uitvoeren. Robuustheid R is een intuïtieve maat welke de toegestane variatie in de aandrukkracht op het slechtste punt op het aandrukvlak kwantificeert. De ontwerpgereedschappen worden gebruikt in een stapsgewijze optimalisatie van de afmetingen van een tweedimensionale chirurgische mal. De PSSG's die resulteren in elke optimalisatiestap worden gevalideerd in fysieke experimenten. De fysieke experimenten laten zien dat er maar een kleine afwijking van 0.7 graden is van de berekende waarden, en dus, dat de methodes valide zijn voor dimensionering van PSSG's.

In hoofdstuk 3 wordt het robuustheidsraamwerk uitgebreid met gereedschappen voor driedimensionale PSSG's. De visualisatiekaarten en maten worden diensovereenkomstig aangepast. De robuustheidskaarten worden nu gerepresenteerd door snedes van een gradiëntvolume. Een robuuste locatie voor het aandrukvlak wordt gevonden door gebruik te maken van snedes in meerdere richtingen. Maten η_c , η_g , en R worden op dezelfde manier als bij tweedimensionale PSSG's gebruikt, echter is de berekening aangepast aan

de hogere dimensie van de wrench space. De ontwerpgereedschappen worden gebruikt in de optimalisatie van een PSSG voor de distale femur. De optimalisatie laat zien dat een groter aantal geoptimaliseerde contacten resulteert in een hogere contactefficiëntie. Een aantal van 12 geoptimaliseerde contacten resulteert namelijk in $\eta_c = 0.74$ (uit een maximum van 1.00), waar 6 geoptimaliseerde contacten resulteert in $\eta_c = 0.18$.

Wanneer de PSSG geplaatst wordt op het gewrichtsvlak van de patiënt, beïnvloeden geometrische botverschillen met het virtuele beeld (i.e. het CT of MRI beeld) de positionering. Incorrecte positionering van de PSSG werkt rechtstreeks door in de positionering van implantaatonderdelen. Het effect van de geometrische botverschillen wordt onderzocht in hoofdstuk 4 en 5.

In hoofdstuk 4 worden maten voor plaatsingsnauwkeurigheid gecreëerd om het effect van geometrische botverschillen op de PSSG positie te kwantificeren. De maten worden berekend door Monte Carlo simulaties van de plaatsing. In elke herhaling worden willekeurige geometrische botverschillen en een willekeurige aandrukkracht gegenereerd. Een Iterative Closest Point algoritme wordt gebruikt om een plaatsing op het bot te vinden waarbij ten minste zes contacten in aanraking zijn met het bot (i.e. minimaal contact). Plaatsingsnauwkeurigheid wordt vervolgens berekend uit de spreiding in positieafwijkingen van de gesimuleerde plaatsingen. In een voorbeeld worden rotatie-plaatsingsnauwkeurigheid en contactefficiëntie gecombineerd om optimale locaties voor contact te vinden. De combinatie van deze maten maakt het mogelijk een chirurgische mal te maatvoeren welke zowel stabiel als nauwkeurig geplaatst kan worden.

In hoofdstuk 5 wordt een nieuwe PSSG gepresenteerd welke intraoperatief kan worden aangepast om botverschillen op te vangen. De PSSG bevat veerplunjers voor de geometrische passing en visualisatie van botcontact. Groene pineindes steken uit de veerplunjers wanneer deze in contact zijn met het bot. De visuele terugkoppeling wordt door de chirurg gebruikt om de kwaliteit van de geometrische passing te bepalen. Veerplunjers kunnen worden verwijderd wanneer wordt verwacht dat dit de plaatsing verbetert. De PSSG is getest in een experiment waarbij gebruikers gevraagd wordt om te detecteren of er een verstoorde passing aanwezig is en optioneel een veerplunjer te verwijderen om een goede passing te verkrijgen. Gebruikers met voorgaande ervaring met de PSSG waren beter in staat verstoringen te herkennen en te verwijderen gedurende het plaatsingsproces dan onervaren gebruikers. Uitgebreide training wordt daarom voorgesteld wanneer de PSSG wordt doorontwikkeld voor klinisch gebruik.

Een algemene discussie en conclusie worden gepresenteerd in hoofdstuk 6. Voor verdere ontwikkeling is 3D printen de meest haalbare oplossing om een instrument te maken welke patiëntspecifiek en zowel compact als gemakkelijk in gebruik is. Omdat de anatomie

complexer is dan alleen de (kraakbeen-)botoppervlakten waarop de PSSG uiteindelijk geplaatst wordt, is additionele terugkoppeling naar de chirurg gedurende plaatsing van de PSSG noodzakelijk voor de kwaliteit van de passing. Elektrische contactschakelaars kunnen bijvoorbeeld worden gebruikt om contact met het (kraakbeen-)botoppervlak te detecteren. Deze contactinformatie zou bij voorkeur worden gepresenteerd met een simpel signaal aan de chirurg om te kunnen onderscheiden in de kwaliteit van passing. Nauwkeurigheid en simpliciteit moeten worden gecombineerd om de chirurg niet af te leiden van het operatiegebied van de patiënt en de operatie op een juiste manier te sturen.

SUMMARY

Malalignment of implant components is a root cause for knee prosthesis failure. Patient Specific Surgical Guides (PSSGs) are used to improve the postoperative position of the implant relative to a preoperative planned position. The PSSGs are tailor made to match the patient's bony anatomy and align drill holes and saw slots relative to the bone. However, correct PSSG alignment (and thus prosthesis alignment) is heavily dependent on the geometric fit with the matching anatomy. This thesis provides methods for preoperative optimization of the matched contact and intraoperative adjustments for improved alignment.

The surgeon docks the PSSG onto the bone by making use of the matching geometry and maintains the position by applying force. The variation allowed in the line of action of this force depends on PSSG dimensions and is referred to as docking robustness (Chapter 2 and 3).

In Chapter 2, methods from robotic grasping and workpart fixturing are employed in the creation of a new method for evaluating docking robustness of two-dimensional PSSGs. Design tools are presented comprising visualization maps and measures. Wrench space maps are used to select a contact set that maximizes the allowed variation in the application force. Application angle maps allow to find a robust location for the application surface based on gradient shading. The contact efficiency measure η_c is used to quantify the selected bone-guide contact. The guide efficiency measure η_g is used to quantify the complete guide including an application surface for the surgeon to push on. Robustness R is an intuitive measure that quantifies the angular deviation allowed in the application force at the worst point on the application surface. The design tools are utilized in a step-by-step optimization of the dimensions of a two-dimensional surgical guide. The PSSGs that result in every optimization step are validated with physical experiments. The physical experiments show that there is only a small deviation of 0.7 degrees from calculated values, and thus, that the methods are valid in dimensioning of PSSGs.

In Chapter 3, the docking robustness framework is expanded with tools for three-dimensional PSSGs. The visualization maps and measures are accommodated accordingly. The robustness maps are now represented by slices of a gradient volume. A robust location for the application surface is found by employing slices in multiple directions. Measures η_c , η_g , and R are used in the same manner as for two-dimensional PSSGs, though calculation is adjusted to the higher dimensional wrench space. The design tools are utilized in the optimization of a PSSG for the distal femur. The optimization shows that the number of optimized contacts can considerably increase contact efficiency. That is, 12

optimized contacts result in $\eta_c = 0.74$ (out of a maximum of 1.00), where 6 optimized contacts result in $\eta_c = 0.18$.

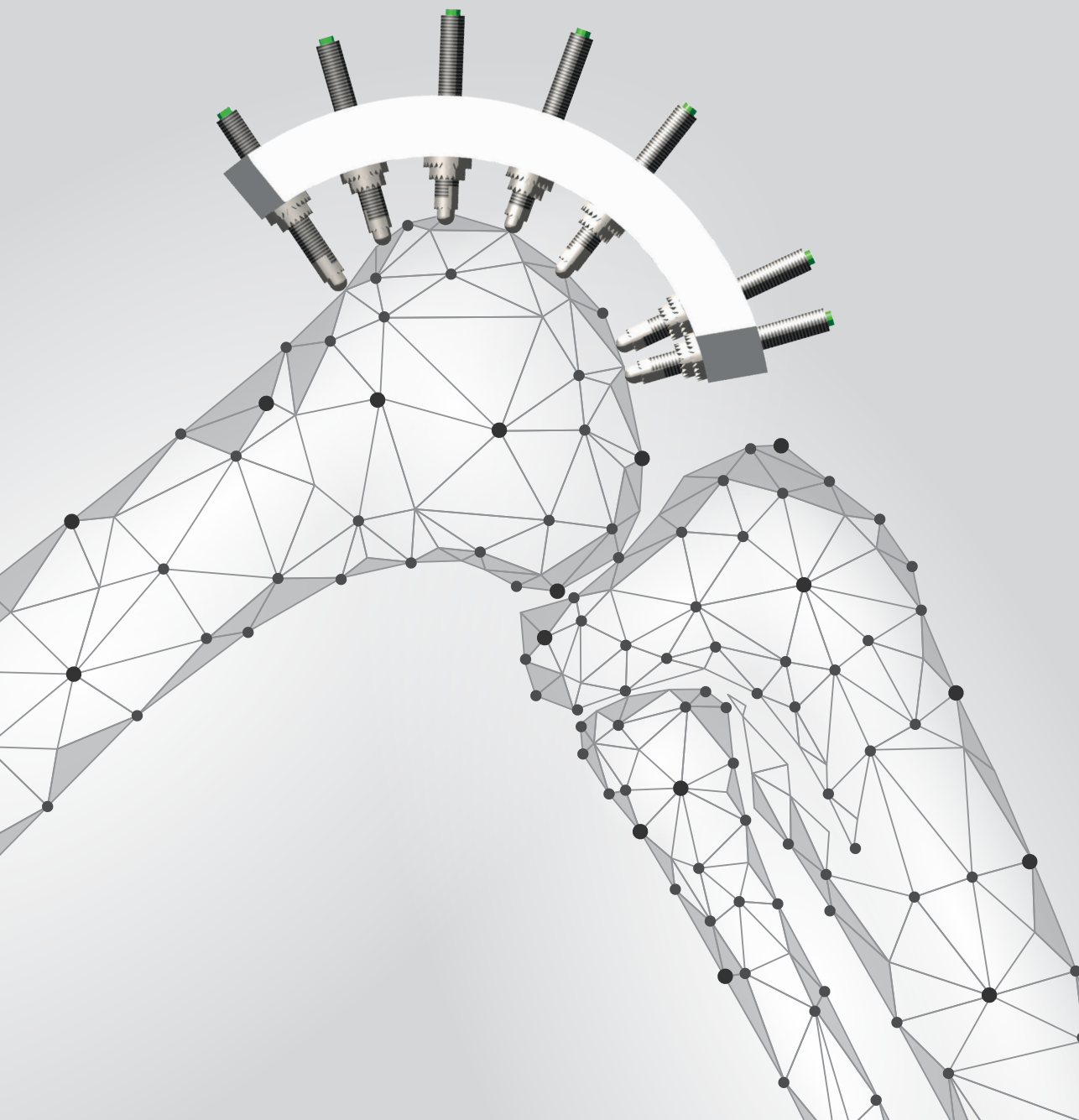
When the PSSG is docked onto the patient's joint surface, geometrical bone deviations from the virtual image (i.e. the CT or MRI image) may influence positioning. Incorrect positioning of the surgical guide directly translates to positioning of the implant components. The effect of the geometrical bone deviations is investigated in Chapter 4 and 5.

In Chapter 4, docking accuracy measures are created for quantifying the effect of geometrical bone deviations on the PSSG's position. The measures are evaluated by Monte Carlo simulations of the docking. In every repetition, random bone deviations and a random application force are generated. An Iterative Closest Point algorithm is used to find a docked position on the bone where at least six contacts touch the bone (i.e. minimal contact). Docking accuracy is subsequently calculated from the dispersion in positional errors of the simulated dockings. In an example, rotational docking accuracy and contact efficiency are combined to find optimal locations for contact. The combination of these measures allows dimensioning a surgical guide that can be docked both stable and accurate.

In Chapter 5, a novel PSSG is presented which allows intraoperative adjustments to accommodate bone deviations. The PSSG contains spring plungers for the geometric fit and visualization of bone contact. Green pin ends protrude from the spring plungers when in contact with the opposing bone. The visual feedback is used by the surgeon to assess the quality of the geometric fit. Spring plungers can be removed when considered to improve the fit. The PSSG is tested in an experiment where users are asked to detect whether disturbance is present and optionally remove a spring plunger in order to obtain a proper geometric fit. Users with former experience with the PSSG were better able to recognize and remove disturbances during the PSSG docking process than unexperienced users. Extensive training is therefore suggested when the PSSG is further developed for clinical practice.

A general discussion and conclusion are presented in Chapter 6. For future development 3D printing is the most viable solution for creating a device that is patient specific and both compact and easy to use. Since the anatomy is more complex than just the (cartilage) bony surfaces where the PSSG is ultimately positioned, additional feedback to the surgeon while placing the PSSG is necessary for the quality of the fit. Electrical contact switches can for instance be used to detect contact with the (cartilage) bony surface. This contact information should be presented in a simple signal to the surgeon to differentiate the

quality of the fit. Accuracy and simplicity should be combined in order to not distract the surgeon from patient's operating field and aim of the surgery as such.



CHAPTER 1

General Introduction

1 BACKGROUND

Osteoarthritis and rheumatoid arthritis are common diseases which affect the joints of the human body. The joint surface degenerates, wears out, and deforms, making smooth motion difficult and painful. Fortunately, in today's surgery it is possible to get an artificial replacement joint which counteracts for some of these problems. The surgery for the replacement of a joint is known as arthroplasty and when the complete joint is replaced with an artificial one this is known as total arthroplasty.

The knee is the joint mechanism that controls the movement of the tibia relative to the femur. The tibiofemoral joint serves for the hinge-like movement of the knee, realized by the sliding motion of the femoral condyles over the tibial plateau. The patellofemoral joint serves for the muscle force transfer from the upper leg's quadriceps to the tibia in order to extend the knee. The patella acts like a leverage in this force transfer. The knee has ligaments to limit movement in certain directions. The medial and lateral ligaments restrict sideways movement of the tibia. The anterior and posterior cruciate ligament prevent forward and backward movement of the tibia. Total Knee Arthroplasty comprises the replacement of the articulating surfaces of the tibiofemoral joint and optionally the patellofemoral joint. Only the tibiofemoral joint will be considered in this introduction.

Orthopaedic surgeons generally make a preoperative surgical planning, to select the most appropriate type and size of prosthetic components and the most optimal position of the components with respect to the patient's anatomy. To reveal the patient's anatomy, an image scan is made of the affected area, in general only standard radiographs in two directions. In few cases a CT or MRI scan is made. Relevant anatomical landmarks are often also located (or measured) at the radiograph as reference measures for the alignment of prosthetic components during surgery. This planning is transferred to actual surgery using guidance instruments.

Malalignment of the prosthetic components is a root cause for failure of knee prostheses [1]. In the Netherlands, the reason for 27.1% of major knee revision surgeries is malalignment [2]. Other reasons for knee revision surgery can be indirectly rooted to malalignment (i.e. instability of the joint 24.1%, loosening of prosthetic components 32.3% and dislocation of prosthetic components 2.6%). Finding appropriate location and orientation of implant components is a complex task in knee surgery and for that matter any arthroplasty surgery due to difficult to assess anatomical references. For instance, in knee replacement surgery, the hip center is an important reference for femoral component alignment, though its exact location is covered by many layers of soft tissue. As for shoulder surgery it is difficult to align the glenoid component perpendicular to the

axis through the middle of the scapular bone. These two examples stress the potential caveats of placing artificial joints in an anatomic optimal way.

This introduction presents an overview of surgical instrumentation used in total knee arthroplasty (TKA). Conventional instrumentation as well as the alternative methods of Computer Assisted Surgery (CAS) and Patient Specific Surgical Guides (PSSGs) are discussed. Information is obtained by reading manufacturers surgical guides, analyzing (online) video, attending surgeries and acquiring the expert opinion of orthopaedic surgeons. Additionally a literature survey is performed to obtain information about current developments. The different types of surgical instrumentation (i.e. conventional, CAS or patient-specific instrumentation) are analyzed on their benefits and shortcomings. Due to the large amount of conventional instrumentation on the market, only the three companies with the largest market share are considered, that is, ZimmerBiomet, DePuy and Stryker [2]. For these three companies, only one prosthesis per company is random selected.

2 CONVENTIONAL INSTRUMENTATION

In the conventional surgical technique, a radiograph is made of the affected area. Sizing templates of the implants are superimposed over radiographs to select the appropriate size for prosthetic components and their optimal position. This procedure is done on 2D images. During surgery, the orthopaedic surgeon uses alignment instruments in order to line up cutting and drilling guides, which position is based on these preoperative two-dimensional measurements. The alignment instruments reference with anatomical landmarks that can be palpated on the skin or bony landmarks like for example the inner axis of a long bone (known as the intramedullary canal). Since the positioning of the implant also depends on ligament balancing to have a stable joint, experience of the surgeon is an important factor to obtain optimal prosthesis alignment. Conventional arthroplasty instrumentation used by orthopaedic surgeons generally comprises many tools. The variety in patient's anatomy and (in)stability of the joint are important factors in sizing of those toolboxes. Toolboxes that comprise dozens of tools are therefore very common.

The manufacturers of knee prosthesis generally use similar procedures for joint replacement [3-6]. The procedure of TKA can roughly be divided into four major steps, namely: preparation of the femur, preparation of the tibia, trial reduction and final component placement.

2.1 Preparation of the femur

For preparation of the femur, the shape of the distal femur is adjusted to fit an artificial component (Figure 1). The adjusted shape is usually created by saw cuts that roughly represent the contour of the articulating surface. The surface cuts that generally make up the contour are the distal, anterior and posterior cut, and two chamfer cuts. The distal cut is often made first. Hereto, a distal cut guide is placed onto the anterior femur. By inserting an intramedullary rod into the intramedullary canal, a hard reference is created to place the distal cut guide into the desired valgus angle. Subsequently a sizer, which measures the anterior-posterior size, is often used to determine the appropriate size of the final femur component. The remaining cuts of the contour are generally made with a 4-in-1 cut guide. The amount of external rotation of the final femur component can be determined by rotational adjustment of the 4-in-1 cut guide to the proximal tibia cut or to the epicondylar axis. For cruciate sacrificing prostheses, a notch cut is generally created. The notch should be placed correctly in the mediolateral direction for a smooth working prosthesis.

2.2 Preparation of the tibia

For preparation of the tibia, the proximal tibia needs to be cut. An alignment tower is used in standard instrumentation. For the initial placement, an ankle clamp at the lower part of the assembly is aligned with the malleoli and the proximal part with the medial one third of the tibial tubercle. The varus/valgus angle of the cut can be adjusted translating the rod mediolaterally at the lower part of the assembly. The slope of the cut can be adjusted by translating the rod in the anterior or posterior direction at the lower part of the assembly. The height of the cut is relative to one of the condyles and is adjusted by vertical translation of the cut plane and assessed with a stylus. Often a keel is created for fixation of the tibial component. The keel is created with a punch.

2.3 Trial reduction

For the trial reduction, the appropriate size trial components are selected, the joint is reduced, and motion is assessed. The thickness of the tibial insert can be adjusted to obtain proper stiffness for the joint.

2.4 Final component placement

After trial reduction, the appropriate size components are selected and placed. Some prosthesis components are press-fit and have a porous coating for bone ingrowth, whereas others are fixed with cement.

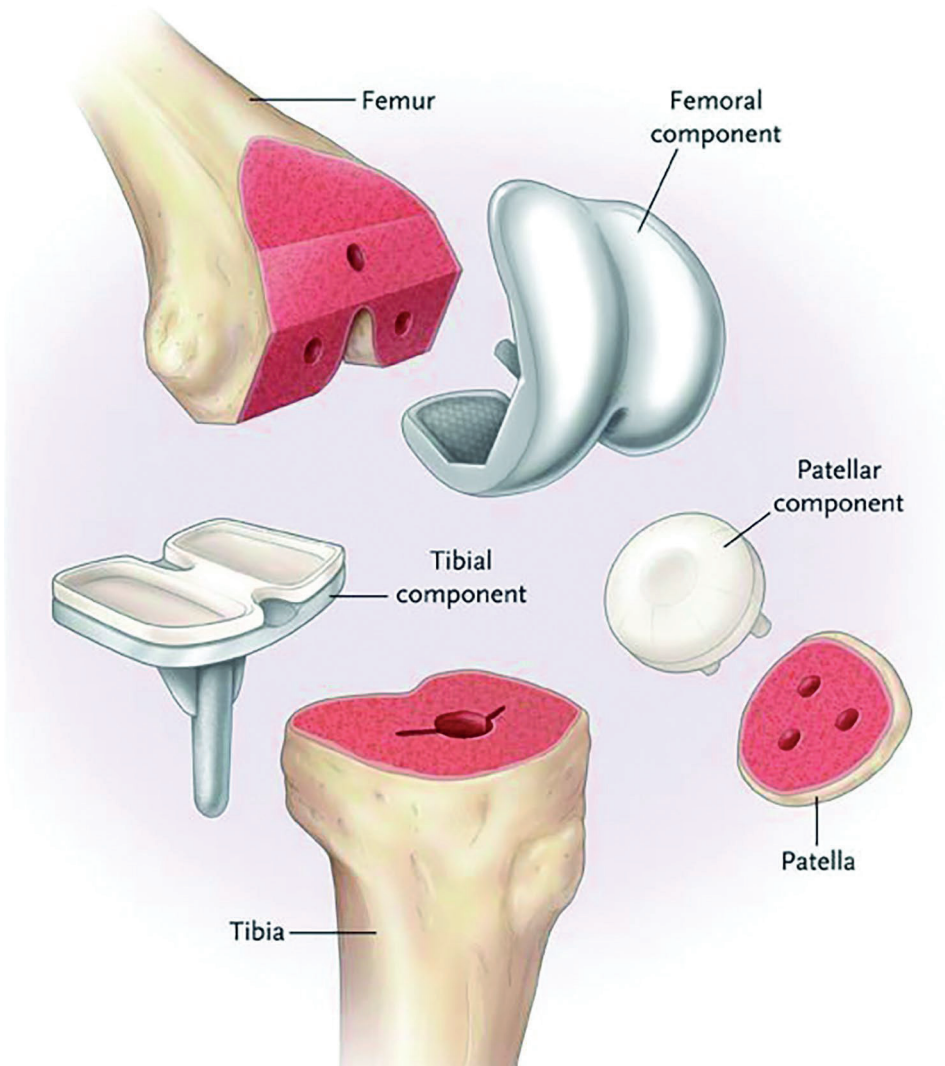


Figure 1. Total Knee Arthroplasty components and the required surgical resections [7].

3 COMPUTER ASSISTED SURGERY

In Computer Assisted Orthopaedic Surgery (CAS), computer technology is applied before, during and possibly after surgery to improve the outcome of the orthopaedic procedure. Preoperatively, the surgery can be planned onto a virtual model of the patient's anatomy. Intra-operatively, the position of instruments can be tracked relative to the patient's anatomy. Post-operatively, the outcome can be validated by making an additional scan. The following paragraphs outline different kinds of CAS techniques.

In one CAS technique, a virtual model of the affected anatomy is obtained by making a preoperative scan, where CT has the preference above MRI because of its superiority in bone segmentation [8, 9]. Intraoperatively, a surgical navigation system continuously tracks the position of trackers which are attached to the relevant bones of the patient and to surgical instrumentation. The movement of the bones and instrumentation can thereby be made visible. The communication between the navigation system and the trackers can be optical, ultrasonic, magnetic or mechanical [8]. Optical communication is mostly used nowadays. The other communication methods appeared to be unsuccessful in the past; ultrasonic communication appeared to be sensitive for temperature changes; magnetic communication has the advantage of communication through objects, though it has the disadvantage that the magnetic field is disturbed by metal objects [10]; mechanical links have also been used but appeared to be clumsy in practice.

The shape of the instruments is generally programmed into the computer of the navigation system, whereby it is always known where for example the axis of a drill is. The location of the relevant bones must be registered for every surgery, i.e. matching the location of the virtual bone model with the real anatomy of the patient. Hereto, a feature-based registration method as paired-point-registration can be used. In this method, pairs of distinct points are identified in the virtual model as well as the real anatomy of the patient. Mistakes can easily be made with this method, because it is difficult to exactly find the same point in the virtual model and the real anatomy. Percutaneous markers have been suggested as an alternative, but never gained clinical acceptance due to the extra operation which is needed before the preoperative scan [8].

In another CAOS technique, no preoperative scans are made of the patient's anatomy. Instead, the patient's anatomy is identified intraoperatively using a tracking instrument; a method known as Surgeon Defined Anatomy (SDA) [8]. The tip of the tracking instrument is used to locate points on the bony anatomy of the patient and the points are subsequently reconstructed into lines and surfaces. In contrary to the aforementioned CT-based technique, cartilage is considered with this method. The reconstruction of bone axes, which is important for the alignment of prosthesis components, can also be performed using this technique. In knee surgery for example, the tibia axis can be reconstructed by tracking points on the ankle and the proximal tibia. The hip center, which is also an important reference in knee surgery, can be reconstructed by passive movement of the hip. An alternative to the standard SDA technique is a method known as bone morphing [11, 12]. Bone morphing uses a database of virtual bone models and a specific point set on the bony anatomy tracked by the surgeon. Computer software selects the virtual bone model that best fits the selected point set and subsequently morphs the virtual bone model to exactly fit the tracked points. The overall advantage of both SDA techniques is that no scan is required before operation.

In yet another CAOS technique, fluoroscopy is used intraoperatively to produce an image for navigation [8]. Hereto, a tracker is firmly attached to the bony anatomy, whereafter a C- or O-arm is positioned (robotically) around the patient and recreates either two-dimensional multiplanar X-ray images or a three-dimensional fluoro-CT [8, 13]. The surgeon then uses tracked instruments to operate the patient, while a video screen visualizes the path of the instruments over the just acquired images. When surgery is finished, new image(s) may be acquired to check the result.

4 PATIENT SPECIFIC SURGICAL GUIDES

Patient Specific Surgical Guides (PSSGs) are instruments for the positioning of drilling and cutting guidance instruments, exclusively designed for a specific (individual) patient. A CT or MRI scan is made preoperatively to determine the geometry of the patient's bony anatomy. During surgery the 3D printed patient specific surgical guides fit to the patient's specific anatomy so that cutting slots and drill holes for the saw and drill guides are correctly aligned.

Many companies are nowadays making patient specific instrumentation for the knee [14-20]. Generally, there are two types of patient specific instrumentation: surgical guides for the positioning of pins (Figure 2A) and surgical guides for the positioning of pins and saw slots (Figure 2B). The process to come to PSSGs is basically as follows. The patient comes to the hospital to make a CT or MRI scan of the affected joint. The scan is sent to the company, who makes the PSSGs. From the scan, the bony anatomy is identified by segmentation software or manual segmentation. A virtual model of the prosthesis is superpositioned over the segmented bony anatomy. This proposition is sent to the orthopaedic surgeon. When desired, the surgeon can adjust alignment of the joint and positioning of the prosthesis. The adjusted proposition is sent back to the company. The virtual models of the surgical guides are fitted onto the virtual bony anatomy, so that drill guides and saw slots are positioned correctly. Finally, physical instrumentation is produced from the surgical guide models by 3D printing.

Usage of PSSGs in other types of joint replacement procedures is being researched as well. Valstar et al. [21, 22] investigated the positioning of the glenoid component with patient specific surgical guides, resulting in two template designs (Figure 3). Initial experiments were performed on cadaver scapulae to test the design and functioning of the drill guides. The results were promising but require improvement. The drill guides were superpositioned onto a virtual bone model derived by CT, and hence, cartilage covering the glenoid was not considered for surgical guide positioning. Knife contacts of the surgical guide had the purpose to cut through the cartilage. However, the cartilage still had a significant impact on the final position of the implant.

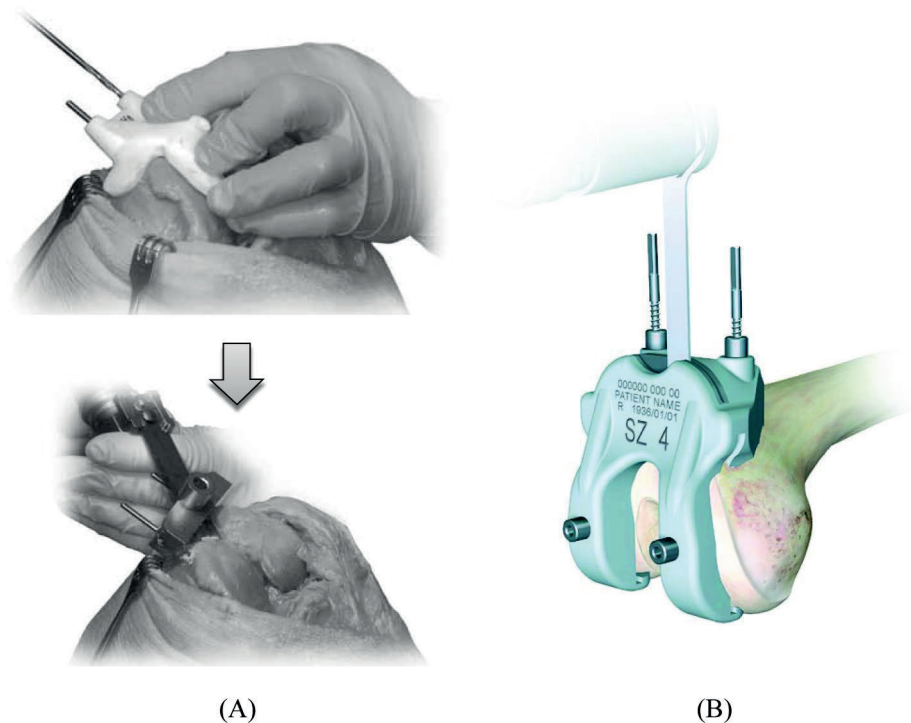


Figure 2. Patient specific templates. (A) Surgical guide for the placement of pins [23]. The pins are subsequently used for the positioning of further instrumentation. (B) Surgical guide for the placement of pins and the creation of a saw cut [24]. The pins are subsequently used for the positioning of further instrumentation.

In general, imaging of the knee is either done by Computed Tomography (CT) or Magnetic Resonance Imaging (MRI). CT is superior in bone identification [8, 9], providing superior bone-soft tissue contrast and a relatively undistorted image. Though development in segmentation techniques can possibly make MRI a good competitor. A disadvantage of CT is that cartilage is poorly visible. Surgical guides designed using CT or MRI can nevertheless both support onto cartilage as well as compact bone. However, surgical guides designed using CT must make an estimation of the amount of cartilage present. For alignment of the prosthesis, often the hip and ankle are included in the imaging process. This is done either by propagation of the CT/MRI or by making an accompanying long leg x-ray.

Most surgical guide manufacturers propose mechanical alignment of the prosthesis, where the tibia component is placed perpendicular to the tibia axis and a straight line can be drawn in the coronal plane through the centers of the hip, knee and ankle. Other manufacturers propose for anatomic or kinematic alignment, i.e. restoration of the original alignment of the knee before affection [25-27]. Eckhoff et al. [28] showed in a study of 180 healthy knees, that the natural angular offset of the tibia relative to mechanical alignment

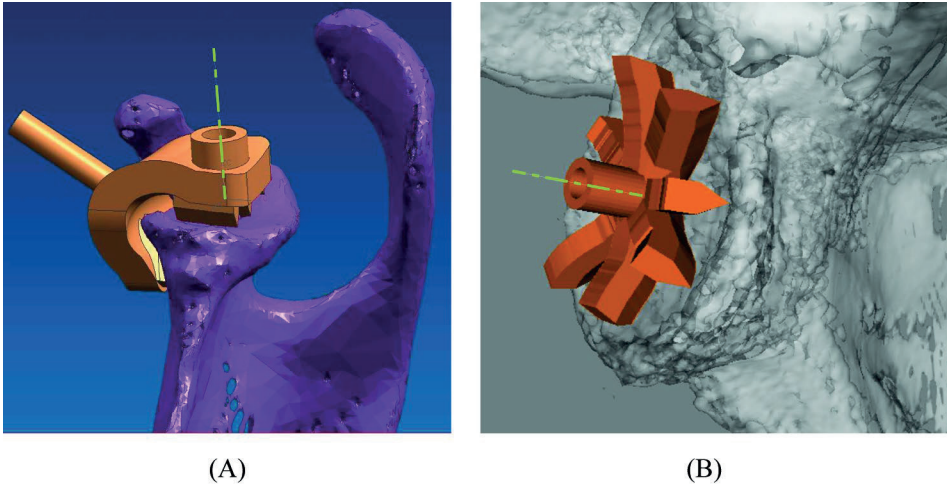


Figure 2. Two shoulder template designs of Valstar et al. [21, 22], which both incorporate knife contacts. (a) The knives contact the glenoid and the anterior surface next to the glenoid. (b) The knives contact the glenoid only. As can be depicted from the picture, positioning of the glenoid with respect to the perpendicular axis of the scapular blade through the glenoid is difficult to achieve during the small surgical exposure area.

is $2.8 \pm 2.2^\circ$ for varus angulation and $2.7 \pm 3.2^\circ$ for valgus angulation. Anatomic alignment is said to be accounting for this natural variability in the human knee by mimicking the unaffected knee in placement of the prosthesis components.

Accuracy of surgical guide alignment has been evaluated by several researchers. Hafez et al. [29] performed a study on 6 plastic bone models. A navigation system was used to track PSSG and bone and allowed to compare the actual position with the planned position. The study showed that the mean error for bone resection alignment is within 1.7° and 0.8 mm. In other studies [25-27, 30] prosthesis alignment was post-operatively compared with neutral mechanical alignment. Spencer et al. [27] showed a post-operative alignment error of $1.2 \pm 2.4^\circ$ varus ($N = 21$), where Howell et al. [25] showed in a similar study $1.4 \pm 2.8^\circ$ valgus ($N = 48$). Post-operative joint alignment however is regarded as an indirect manner for PSSG accuracy evaluation, as exact location of resection cuts is not considered.

The number of instruments required for TKA is greatly reduced by PSSGs. The alignment instruments required in conventional instrumentation are not needed here, as alignment is incorporated in the PSSGs themselves. Operation time is expected to be reduced due to the reduced number of steps. Spencer et al. [27] compared TKA performed with conventional instrumentation ($N = 30$) to TKA performed with PSSGs ($N = 21$). In their study the duration of the tourniquet time (i.e. the time arterial blood flow is restricted) was used as an outcome measure. Tourniquet time was shorter when using PSSGs (80 ± 17 min) compared to the conventional method (93 ± 12 min). Hafez et al. [29] showed in a study with plastic bone models that less time was required for bone resection when using PSSGs

(11-13 min) instead of the conventional instrumentation (15-30 min). Another advantage of PSSGs is that the femur's intramedullary canal (which is a reference for alignment rods in conventional instrumentation), does not have to be opened. The insertion of intramedullary alignment rods can lead to a higher risk of bleeding, infection, fat embolism and fractures [29, 31].

5 AIM OF THIS THESIS

PSSGs incorporate registration in the geometric fit and are therefore designed to decrease operation time compared to the conventional method and CAS. Alignment of the PSSGs however is dependent on the quality of the geometric fit. Moreover, the geometric fit is the primary feedback for the surgeon to judge alignment. In this thesis we aim to develop methods for preoperatively optimizing PSSG settings and intraoperatively allowing adjustments for increased alignment. The preoperative planning tools allow the surgeon to optimize the PSSG for geometric fit and accurate placement. The intraoperative tools allow the surgeon to check alignment and possibly perform adjustments when required.

6 THESIS OUTLINE

6.1 Docking Robustness in 2D

An analytical method is created for the evaluation of the geometrical fit between two-dimensional PSSGs and bone (Chapter 2). Measures and visualization maps are introduced, which allow developers to optimize PSSGs dimensions for robust docking. An example two-dimensional bone model is used to find optimal locations for contact and a PSSG surface whereon the surgeon can push. The methods are validated in a physical experiment.

6.2 Docking Robustness in 3D

The two-dimensional method for docking robustness is generalized to three-dimensional PSSGs (Chapter 3). The measures and visualization maps are made appropriate for evaluation of three-dimensional docking. A virtual model of the distal femur is used in the optimization of contact locations and the location of the PSSG surface. A bone-guide contact set with minimal contact points is compared to a contact set that increases the docking robustness with additional contact points.

6.3 Docking Accuracy in 2D/3D

The positional error of the PSSG due to geometrical deviations between the CT/MRI image and the bone as observed during surgery is investigated (Chapter 4). Translational and

rotational docking accuracy measures are created to find the expected positional error of the PSSG. Repeated simulations of guide placement are used in the calculation of docking accuracy. Linear and non-linear docking accuracy are compared in the dimensional optimization of a PSSG.

6.4 Intraoperatively Adjustable PSSG

A PSSG is designed incorporating a novel mechanism to visualize bone contact (Chapter 5). The surgical guide has a base plate wherein spring plungers are inserted to create a geometrical fit. The spring plungers have protruding green pin ends to show when contact is made. The PSSG is assessed in a user experiment where the geometrical fit was intentionally either disturbed or undisturbed. Users were requested to assess the geometrical fit and remove one spring plunger when they thought this disturbed the positioning.

REFERENCES

- [1] Ritter, M. A., Faris, P. M., Keating, E. M., and Meding, J. B., 1994, Postoperative Alignment of Total Knee Replacement Its Effect on Survival. *Clin Orthop Relat Res*, **299**, pp. 153–156.
- [2] Reus, A., Spekenbrink-Spooren, A., van Steenberghe, L. N., Denissen, G. A. W., Rijnsburger, E., and van der Togt, C. R., 2018, Online LROI annual report 2018, Tech. rep., Dutch Arthroplasty Register (LROI), 's-Hertogenbosch, The Netherlands.
- [3] Biomet Orthopedics Inc., Warsaw, IN, USA, 2011, *Premier, Total Knee Instrumentation, Surgical Technique, Vanguard® Complete Knee System*.
- [4] DePuy Orthopaedics Inc., Warsaw, IN, USA, 2010, *Sigma, High Performance Instruments, Balanced, Surgical Technique*.
- [5] Stryker Orthopaedics Inc., Mahwah, NJ, USA, 2010, *Triathlon Knee System, Surgical Protocol, Posterior Stabilized and Cruciate Retaining*.
- [6] Zimmer Inc., Warsaw, IN, USA, 2010, *Zimmer NexGen Flexion Balancing Instruments, Fixed Bearing Knees, Surgical Technique*.
- [7] Leopold, S. S., 2009, Minimally invasive total knee arthroplasty for osteoarthritis, *N Engl J Med*, **360**(17), pp. 1749–1758.
- [8] Langlotz, F. and Nolte, L. P., 2004, Technical approaches to computer-assisted orthopedic surgery, *European Journal of Trauma*, **30**(1), pp. 1–11.
- [9] White, D., Chelule, K. L., and Seedhom, B. B., 2008, Accuracy of MRI vs CT imaging with particular reference to patient specific templates for total knee replacement surgery, *Int J Med Robotics Comput Assist Surg*, **4**(3), pp. 224–231.

- [10] Meskers, C. G. M., Fraterman, H., Van der Helm, F. C. T., Vermeulen, H. M., and Rozing, P. M., 1999, Calibration of the “Flock of Birds” electromagnetic tracking device and its application in shoulder motion studies, *J Biomech*, **32**(6), pp. 629–633.
- [11] Fleute, M., Lavallée, S., and Julliard, R., 1999, Incorporating a statistically based shape model into a system for computer-assisted anterior cruciate ligament surgery, *Med Image Anal*, **3**(3), pp. 209–222.
- [12] Stindel, E., Briard, J. L., Merloz, P., Plaweski, S., Dubrana, F., Lefevre, C., and Troccaz, J., 2002, Bone morphing: 3D morphological data for total knee arthroplasty, *Comput Aided Surg*, **7**(3), pp. 156–168.
- [13] Patil, S., Lindley, E. M., Burger, E. L., Yoshihara, H., and Patel, V. V., 2012, Pedicle screw placement with O-arm and stealth navigation, *Orthopedics*, **35**(1), pp. e61–e65.
- [14] Biomet UK Ltd, Bridgend, South Wales, UK, 2011, *Signature, Personalized Arthritis Care*.
- [15] DePuy Orthopaedics Inc., Warsaw, IN, USA, 2011, *TruMatch, Personalized Solutions*.
- [16] Stryker Orthopaedics Inc., Mahwah, NJ, USA, 2010, *Customized Patient Instruments*.
- [17] Medacta International, Castel San Pietro, Switzerland, 2011, *MyKnee, Patient Matched Instruments*.
- [18] Smith & Nephew Inc., Andover, MA, USA, 2011, *Visionaire, Patient Matched Technology*.
- [19] Wright Medical Technology Inc., Arlington, TN, USA, 2011, *Prophecy, Pre-Operative Navigation Guides, Surgical Technique*.
- [20] Zimmer Inc., Warsaw, IN, USA, 2011, *Patient Specific Instruments*.
- [21] Valstar, E. R., van Brussel, K., Kaptein, B. L., Stoel, B. C., and Rozing, P. M., 2003, CT-based personalized templates for accurate glenoid prosthesis placement in total shoulder arthroplasty, *Proceedings of The 3rd Annual Meeting of the International Society for Computer Assisted Orthopaedic Surgery*.
- [22] Botha, C. P., 2005, Techniques and software architectures for medical visualisation and image processing, Ph.D. thesis.
- [23] Zimmer Inc., Warsaw, IN, USA, 2011, *Patient Specific Instruments, Surgical Techniques for NexGen Complete Knee Solution*.
- [24] DePuy Orthopaedics Inc., Warsaw, IN, USA, 2010, *Customized Patient Instruments, Primary Cruciate Retaining Surgical Technique*.
- [25] Howell, S. M., Kuznik, K., Hull, M. L., and Siston, R. A., 2008, Results of an initial experience with custom-fit positioning total knee arthroplasty in a series of 48 patients, *Orthopedics*, **31**(9), pp. 857–863.
- [26] Klatt, B. A., Goyal, N., Austin, M. S., and Hozack, W. J., 2008, Custom-fit total knee arthroplasty (OtisKnee) results in malalignment, *J Arthroplasty*, **23**(1), pp. 26–29.

- [27] Spencer, B. A., Mont, M. A., McGrath, M. S., Boyd, B., and Mitrick, M. F., 2009, Initial experience with custom-fit total knee replacement: intra-operative events and long-leg coronal alignment, *Int Orthop*, **33**(6), pp. 1571–1575.
- [28] Eckhoff, D. G., Bach, J. M., Spitzer, V. M., Reinig, K. D., Bagur, M. M., Baldini, T. H., and Flannery, N. M. P., 2005, Three-dimensional mechanics, kinematics, and morphology of the knee viewed in virtual reality, *J Bone Joint Surg Am*, **87-A**(Suppl. 2), pp. 71–80.
- [29] Hafez, M. A., Chelule, K. L., Seedhom, B. B., and Sherman, K. P., 2007, Computer-Assisted Total Knee Arthroplasty Using Patient-Specific Templates: the Custom-made Cutting Guides, *Navigation and MIS in Orthopedic Surgery*, Springer, pp. 182–188.
- [30] Lombardi Jr, A. V., Berend, K. R., and Adams, J. B., 2008, Patient-specific approach in total knee arthroplasty. *Orthopedics*, **31**(9), pp. 927–930.
- [31] Hafez, M. A., Chelule, K. L., Seedhom, B. B., and Sherman, K. P., 2006, Computer-assisted Total Knee Arthroplasty Using Patient-specific Templating, *Clin Orthop Relat Res*, **444**, pp. 184–192.



CHAPTER 2

Shaping Patient Specific Surgical Guides for Arthroplasty to Obtain High Docking Robustness

Joost Mattheijer^{1,2}

Just L. Herder³

Gabriëlle J.M. Tuijthof^{2,4}

Rob G.H.H. Nelissen¹

Jenny Dankelman²

Edward R. Valstar^{1,2,†}

¹Leiden University Medical Center, Dept. of Orthopaedics, Leiden, The Netherlands

²Delft University of Technology, Dept. of BioMechanical Eng., Delft, The Netherlands

³Delft Univ. of Tech., Dept. of Precision and Microsystems Eng., Delft, The Netherlands

⁴Academic Med. Center, Dept. of Orthopaedic Surgery, Amsterdam, The Netherlands

ABSTRACT

Patient Specific Surgical Guides (PSSGs) are used in joint replacement surgery to simplify the surgical process and to increase the accuracy in alignment of implant components with respect to the bone. Each PSSG is fabricated patient specifically and fits only in the planned position on the joint surface by the matching shape. During surgery, the surgeon holds the PSSG in the planned position and the incorporated guidance is used in making the essential cuts to fit the implant components. The shape of the PSSG determines its docking robustness (i.e. the range of forces that the surgeon may apply without losing the planned position). Minimal contact between the PSSG and the joint surface is desired, as this decreases the likelihood of interposition with undetected tissues. No analytical method is known from literature where the PSSG shape can be optimized to have high docking robustness and minimal bone-guide contact. Our objective is to develop and validate such an analytical method. The methods of motion restraint, moment labeling and wrench space – applied in robotic grasping and workpart fixturing – are employed in the creation of this new method. The theoretic approach is utilized in an example by optimizing the PSSG shape for one joint surface step-by-step. The PSSGs that arise from these optimization steps are validated with physical experiments. The following design tools for the analytical method are introduced. The optimal location for bone-guide contact and the application surface where the surgeon may push can be found graphically respectively by the use of the wrench space map and the application angle map. A quantitative analysis can be conducted using the complementary wrench space metrics and the robustness metric R . Utilization of the analytical method with an example joint surface shows that the PSSG's shape can be optimized. Experimental validation shows that the standard deviation of the error between the measured and calculated angular limits in the docking force is only 0.7° . The analytical method provides valid results and thus can be used for the design of PSSGs.

Keywords: Orthopedics, Patient Specific Surgical Guides, Docking, Wrench Space.

1 INTRODUCTION

In joint replacement surgery, worn out and painful joints – such as the hip or knee – are replaced with a prosthesis. The surgical procedure starts with an incision exposing the joint surfaces. Alignment instruments are subsequently used to determine where bone cuts need to be made in order to place the prosthesis with the correct alignment and orientation. This process can be problematic and is prone to errors since only a small part of the involved bones – the joint – is exposed. The main part of the bones adjacent to the joint is still covered by soft tissues such as skin, muscles, ligaments, and fat. Correct alignment is important as it determines the survival of the prosthesis. In knee replacement surgery for example, alignment of the prosthetic components using the hip center of rotation is crucial [1-3], though its exact location is hard to determine because it is situated deep under the skin (i.e. somewhere in the groin area).

Computer Assisted Surgery (CAS) techniques have been used in joint replacement surgery for two decades [4-6] in order to obtain a more accurate alignment of prosthetic components [7-11]. In many of these techniques, a virtual surface model of the involved bones is created based on a three-dimensional scan obtained from Computed Tomography (CT) or Magnetic Resonance Imaging (MRI). This virtual model makes it possible to plan the surgical procedure in advance. In other CAS techniques, a biomechanical model is acquired during surgery [12]. Key is how to transfer the planned surgery to the surgical theatre. Generally, there are two approaches used today: Camera-based CAS and Patient Specific Surgical Guides (PSSG).

Camera-based CAS relies on time consuming registration of the actual bone surfaces as exposed during surgery and the virtual bone models [4-6]. Markers attached to the bones, instruments and prosthesis components are subsequently tracked by a camera.

For the PSSG method [13-15], the virtual bone model is used to design guides, representing the negative imprint of the joint surface (Figure 1). The surgical guide models are fabricated using Computer Numerical Control Machining or Rapid Prototyping techniques. During surgery, the guides are supposed to dock in the planned position only, taking away the need for a time-consuming registration process as needed with camera-based CAS. Guidance holes and slots included in the guides are correctly aligned by the docking. Therefore, they can directly be used to guide surgical instruments like a drill or oscillating saw.

Regarding docking, the bone-guide contact is designed to result in a unique location and orientation of the guide. Irregularities that are not visible on the virtual bone models – like soft tissues – can be present on the real bony anatomy during surgery. These unforeseen deviations might ruin the fit of the guide and bone and can result in incorrect positioning.

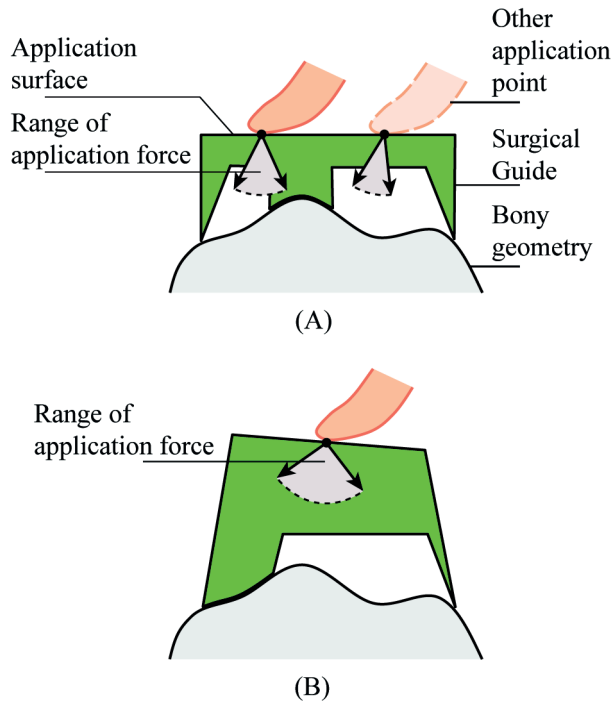


Figure 1. (A) The surgical guide is held into its planned position by an application force of the surgeon. The location of the bone-guide contact and application surface bound what forces may be applied. Pushing at a different location might result in a different range in the application force. (B) A guide with different contact and application surface might result in different range in forces that may be applied.

The chance to come into conflict with the deviations is less likely for guides that require less contact.

The goal of this paper is to propose and validate a method for the design of surgical guides and to analyze the effect of the guide's shape on docking robustness. The bony geometry will be used as an input to find suitable locations for bone-guide contact and the application surface. A guide with a high robustness will remain docked under a wide variation in the location and direction of the application force, and is therefore desired. Besides high robustness, minimal contact is desired as this reduces the likelihood of meeting disturbances that might obstruct the fit.

The structure of the paper is as follows. First assumptions are made and methods are described concerning static equilibrium of the surgical guide docked onto the joint surface (Section 2, "Methods"). These methods are employed in the development of design tools (Section 3, "Design Tools"). The design tools are subsequently utilized in an example by optimizing the shape of a surgical guide step-by-step (Section 4, "Utilization").

The six guides that arise from these optimization steps are validated in an experimental setup (Section 5, "Validation").

2 METHODS

The robustness of the surgical guide will be defined as the range of forces that may be applied onto the application surface – maintaining static equilibrium and thus maintaining the docked position. The range of forces that may be applied onto the guide depends on the bone-guide contact set and the location and shape of the application surface (Figure 1A). The bone-guide contact set defines what external forces on the surgical guide are allowed for static equilibrium. The application surface further limits what forces can actually be applied by the surgeon. Another contact set and another location, shape or size of the application surface will result in other limits (Figure 1B). This way surgical guide designs can be compared on their capability to fulfill the robustness requirement.

For a docked condition of the surgical guide, the contact set between bone and guide needs to attain a unique location and orientation, known as deterministic positioning [16]. The contact set between bone and guide can be in the form of points, lines, surfaces or a combination of those. A minimum number of six point contacts is required to attain deterministic positioning in three dimensional space, whereas three contacts are sufficient in a two dimensional environment [16-19].

The shape of the surgical guide as a whole – the bone-guide contact and the application surface – determines the robustness of the guide. To our best knowledge, no method is described in literature concerning the robustness of surgical guides. Research areas that concern the positioning of irregular shaped components are: grasp analysis of robotic hands [20-24] and fixture analysis of workpart fixtures in production lines [16, 25, 26]. In grasping, the fingers of a robotic hand are able to grasp an object and possibly move it to another location. Workpart fixtures are used to hold a workpart in a certain position, so that, for example, a machining operation can be executed. Workpart fixtures can also be configurable, whereby they are able to deal with a variety of workpart shapes.

In both robotic grasping and workpart fixtures, the shape of the object of concern is usually used as an input to find suitable contact points. The location of all contact points of either the robotic hand or fixture can be controlled. A different approach is needed for surgical guides, where the shape of the object – the guide – is not the input but the outcome of the analysis. The bone-guide contact is dictated by the bony geometry and can be controlled by changing the guide's shape. The location of the closing contact – the

surgeon's thumb or finger – can be controlled partially by shaping the application surface. Yet, the surgeon is free in choosing where to push on the application surface.

The methods of motion restraint, moment labeling and wrench space, applied in grasping/fixturing, seem suitable in the creation of an analytical method to determine the surgical guide's shape. All these methods concern the immobilization of objects. Motion restraint concerns the kinematic restraint of objects in contact with each other and was first described in 1876 by Reuleaux [27]. Moment labeling [28] and the wrench space method [17, 18, 28] can be used to determine if objects are in static equilibrium and moreover if objects are completely immobilized by a certain force, a condition known as force closure [17].

2.1 Assumptions

The effect of the guide's shape onto the robustness will be isolated in the analysis by making the following assumptions.

- 1) *The guide is in its planned position.*
- 2) *The shape of the actual bony geometry and the reconstructed bony geometry is identical.*

In actual clinical situations, a virtual reconstruction of the bone is created by CT or MRI for designing the surgical guides. Deviations in geometry may be present between the actual bone shape and the reconstructed bone shape (e.g. by undetected soft or hard tissues). Developing guides with a small contact area is one of the targets of this study because this decreases the likelihood of interposition with these undetected deviations. Though we are aware that interposition is still possible, the deviations are not considered in this article.

- 3) *Both the surgical guide and the bony geometry are assumed rigid.*

The planned position can be best replicated, when both the surgical guide and the bony geometry are rigid. Therefore it is preferable to use hard material for the surgical guide. The bony geometry however consists of the relatively hard cortical bone or the relatively soft cartilage. When the surgical guide is designed to dock onto cartilage, the surgeon's docking force will cause the cartilage to deform. The contact is sagging into the cartilage creating extra sliding resistance [29, 30] which aids in the guide's robustness. Thus, assuming both the guide and the bony geometry as rigid can be considered as a worst case scenario.

- 4) *Friction between the bone-guide interface is neglected.*

When friction is taken into account, all the contact reaction forces are bound by a friction cone. This aids in the guide's robustness as there is more freedom for the reaction forces and thus this can be considered as a worst case scenario as well.

- 5) *The weight of the surgical guide is negligible compared to the surgeon's application force.*

Surgical guides are usually made of plastic and as a result are relatively light compared to the force that the surgeon is able to apply.

2.2 Motion Restraint

In the planned position, the bone-guide contact is supposed to keep the guide docked in place. The location of the bone-guide contact determines to what degree motion is restrained and consequently to what application forces the guide may be subjected.

When considering two objects in contact, one object may move freely to some degree and at the same time is restrained to move by the other object [27]. The motion restraint can be described by defining in which direction an object that is making contact with another object is able to rotate (Figure 2). An arbitrary object making contact with another object can make positive rotations (counterclockwise) about every point to the left side of the contact normal \mathbf{n}_c , and can make negative rotations (clockwise) about every point to the right side of the contact normal \mathbf{n}_c . On the normal line itself points can be chosen for both positive and negative rotation. Note that curvature is not taken into account here. When curvature is taken into account objects can be immobilized with fewer than four contacts [31]. For surgical guides this would imply fewer than three bone-guide contacts as the closing contact is of the surgeon's thumb or finger. To the best of our knowledge it is not known if deterministic positioning (i.e. acquiring a unique position of the surgical guide) is possible with fewer than three bone-guide contacts. For more information about the effect of curvature on restraint, see the work by Rimon and Burdick [24].

For an object having multiple contact points, the restraint of the individual contact points can be combined to find the restraint for the object as a whole - see Figure 3A for two contact points and Figure 3B for three contact points. Positive rotation is only possible in areas where for all contact points positive rotation is possible. Likewise, negative rotation is only possible in areas where for all contact points only negative rotation is possible. No rotation is possible in areas where positive and negative rotation interfere. In these areas no point can be chosen to rotate the guide. At the border of the positive and negative rotation field, respectively positive and negative rotation is still possible.

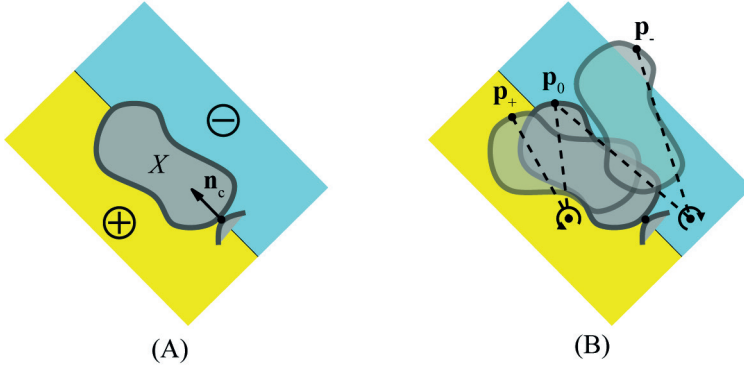


Figure 2. (A) The surgical guide is held into its planned position by an application force of the surgeon. The location of the bone-guide contact and application surface bound what forces may be applied. Pushing at a different location might result in a different range in the application force. (B) A guide with different contact and application surface might result in different range in forces that may be applied.

2.3 Moment Labelling

The allowed variation in the application force can be assessed by a technique called moment labelling [28]. This technique is applied analogous to the motion restraint method and can be described as follows. The line of action and direction of a normal force can be represented by the set of points formed by two half spaces (Figure 2): points left and right to the normal around which the normal force produces respectively a positive and a negative moment. When multiple normal forces act on an object, as indicated in Figure 3, the half spaces of the individual contact normals can be combined. The area where all the positive half spaces intersect contains points around which all normal forces produce a positive moment and similarly the area where all the negative half spaces intersect contains points around which all normal forces produce a negative moment. For static equilibrium the application force (e.g. \mathbf{f}_{a1} or \mathbf{f}_{a2}) has to satisfy the following conditions: (1) the line of action does not intersect the positive and negative area; (2) the direction is such that it causes an opposing moment to all points in the positive and negative area.

For a guide having two contact points the conditions for the application force imply that the line of action must be in one line with the intersection point of the two contact normals (Figure 3A). So, when an application force acts on a certain point on the guide, there is only one possibility for the line of action (e.g. \mathbf{f}_{a1} or \mathbf{f}_{a2}), making docking of the guide impossible. Choosing the application point elsewhere on the application surface will require a different direction of the application force. Any deviation in this direction will result in movement of the guide. For a guide having three or more contact points, docking is possible (Figure 3B). The line of action may vary for a said application point, as long as above-mentioned conditions are met (i.e. the application force is within the gray bounds shown in Figure 3B).

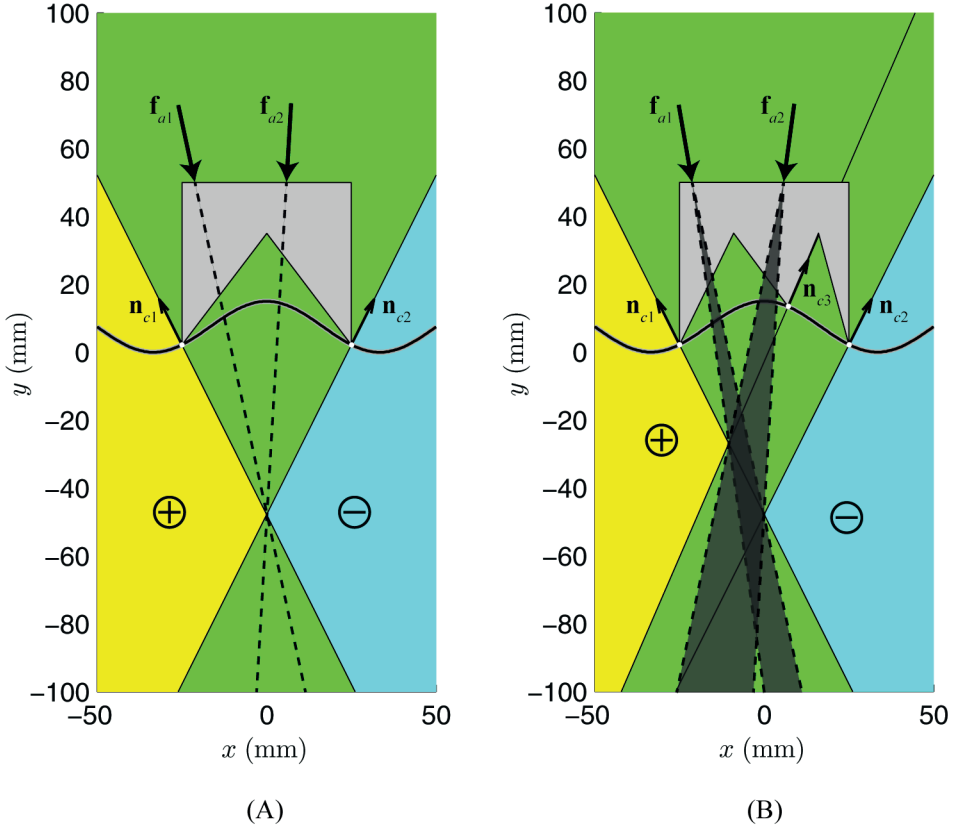


Figure 3. Surgical guide having respectively (A) two and (B) three bone-guide contact points. Guide (A) remains its position when the contact normals and the line of action of the application force, all intersect in one point. For every other application point, the angle of application must be different to maintain static equilibrium, e.g. f_{a1} or f_{a2} . Every deviation in the line of action will cause motion and thus this guide cannot be docked. Guide (B) can be docked onto the bony geometry. For each application point, there is a range in which the angle of application may be varied (gray areas), e.g. f_{a1} or f_{a2} . This range may vary for every other application point. Force f_{a2} has a broader range than f_{a1} .

2.4 Wrench Space Method

The domain of the application force can be further investigated by the use of the wrench space method [28]. Each force \mathbf{f} acting on the guide can be represented by a corresponding wrench \mathbf{w} , a generalized vector consisting of the force itself and the torque τ_0 it produces around the origin of a chosen coordinate system $\mathbf{w} = [f_x, f_y, \tau_0]^T$. All the components of the wrench together locate the line of action and the direction of the force in physical space. When the force \mathbf{f} is considered to act on the guide at point \mathbf{p} , its torque equals $\tau_0 = |\mathbf{p}, \mathbf{f}|$ for two dimensional guides and $\tau_0 = \mathbf{p} \times \mathbf{f}$ for three dimensional guides.

For static equilibrium of the guide, the sum of external forces and torques (induced by the external forces) must both equal zero. Consequently, also the sum of external wrenches must equal zero.

$$\sum \mathbf{w}_{ext} = \mathbf{0} \quad (1)$$

The guide is subjected to an application wrench \mathbf{w}_a and i bone-guide contact wrenches \mathbf{w}_{ci} . The force magnitude of each contact wrench may vary, but the direction is always normal to the bony geometry. Note that the force magnitudes can only be non-negative, as a contact can be pushed into the bony geometry, but there is no restriction for the contact being pulled away. For convenience, the force magnitude λ_{ci} for the normalized contact force $\hat{\mathbf{f}}_{ci}$ can be taken out of the wrench equation resulting in a modified contact wrench $\mathbf{w}'_{ci} = [\hat{\mathbf{f}}_{ci}, [\mathbf{p}_{ci}, \hat{\mathbf{f}}_{ci}]]^T$ for two dimensional guides and $\mathbf{w}'_{ci} = [\hat{\mathbf{f}}_{ci}, \mathbf{p}_{ci} \times \hat{\mathbf{f}}_{ci}]^T$ for three dimensional guides.

The application wrench \mathbf{w}_a is needed to completely immobilize the surgical guide, a condition known as force closure [17]. Force closure is attained when all wrenches taken together positively span the entire wrench space [17, 18]. This is equivalent to the condition that the origin lies in the interior of the convex hull constructed of all the wrenches [32, 21]. Therefore, a certain variation is allowed in the application wrench \mathbf{w}_a , dependent on where the guide makes contact with the bony geometry. The surgical guide is in force closure, when the application wrench meets the following equation.

$$\mathbf{w}_a = -\sum_{i=1}^n \lambda_{ci} \mathbf{w}'_{ci}, \quad \lambda_{ci} \geq 0 \quad (2)$$

Or in other words, force closure is attained when the application wrench \mathbf{w}_a is in the negative span of the contact wrenches [25].

$$\mathbf{w}_a \in \text{neg}([\mathbf{w}'_{c1} \dots \mathbf{w}'_{cn}]) \quad (3)$$

Figure 4A shows three different force closure situations for three different application points onto the same guide. When force is applied at \mathbf{p}_{a1} or \mathbf{p}_{a2} , force closure may be attained. When force is applied at \mathbf{p}_{a3} , force closure is impossible; every force will result in motion of the guide.

In the wrench space representation of Figure 4B, the force closure situation for the guide and the three different application points can be verified. All wrenches in this representation are modified wrenches \mathbf{w}' , corresponding to normalized forces; and instead of f_x - and f_y -components, the direction of force is indicated with an angle relative to the

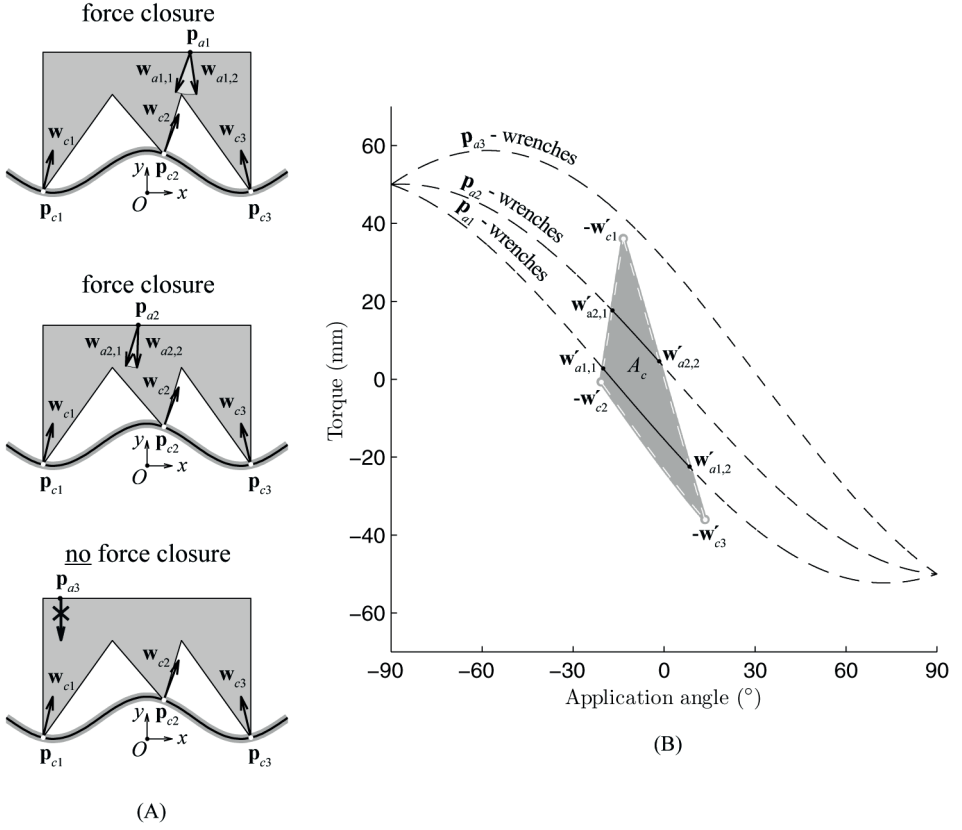


Figure 4. Range of wrenches that is allowed for three example application points. The wrench limits shown in physical space (A) correspond to the wrench limits shown in wrench space (B). (A) Force closure may be attained when pushing at point p_{a1} and p_{a2} . Force closure may not be attained when pushing at p_{a3} , as all forces will result in movement of the guide. (B) The negated contact wrenches span subspace A_c . All the wrenches going through one point in physical space are located on a curve in the wrench space. The intersection of the curve with subspace A_c determines the wrench limits where between an application wrench will result in force closure.

negative y -axis of physical space. Note that, because force is normalized the wrenches lie on a cylinder with radius one, which is rolled out for this representation. The negated contact wrenches $-w'_{ci}$ span the subspace A_c wherein the application wrench w'_a must fall for force closure. All possible wrenches going through one point in physical space, like an application point p_a , are located in wrench space on the same plane going through the origin. The intersection of this plane with the wrench space cylinder gives a curve when the cylinder is rolled out. This curve shows the application wrenches that are possible for said application point in the wrench space representation. The equation for the application wrench curve is defined as follows.

$$\mathbf{w}'_a(\vartheta_a) = \begin{bmatrix} \vartheta_a \\ -p_{a,x} \cos(\vartheta_a) - p_{a,y} \sin(\vartheta_a) \end{bmatrix} \quad (4)$$

Where ϑ_a denotes the application angle. So, the location of an application point in physical space determines its corresponding curve in wrench space. The intersection of the curve with the subspace \mathcal{A}_c determines what set of wrenches for that specific point will result in force closure. For point \mathbf{p}_{a1} , the set of force closure wrenches is bounded by $\mathbf{w}'_{a1,1}$ and $\mathbf{w}'_{a1,2}$. The set shows a wider range in the application angle than point \mathbf{p}_{a2} and so more variation is allowed in the angle of the application force (Figure 4A). Because no intersection is present between the wrench curve corresponding to point \mathbf{p}_{a3} , no wrench through this point will result in force closure.

3 DESIGN TOOLS

By making use of the wrench space method, an optimal shape for surgical guides can be found. Graphical techniques are introduced which aid in this design process and metrics are created to quantify the quality of the surgical guide's shape.

3.1 Wrench Space Map

Figure 5B shows the wrench space when contact occurs at the indicated points (i.e. the contact wrench space \mathcal{A}_c indicated light gray) and when contact occurs along the whole length of the bony geometry (i.e. the potential contact wrench space \mathcal{A}_0 indicated dark gray). The allowed space for the application wrench is maximal when the surgical guide has full contact. Contact wrenches along the bony geometry lie in wrench space on a curve (indicated black). All the contact wrenches of this curve together span subspace \mathcal{A}_0 . The contact wrenches on the border of \mathcal{A}_0 form a so-called positive basis and are indicated with thick black line segments and thick black dots (the corresponding contact is indicated alike). A wrench that is a positive linear combination of other wrenches along the curve, lies within \mathcal{A}_0 , and meets following equation.

$$\mathbf{w}_{ci} - [\mathbf{w}_{c1}, \mathbf{w}_{c2} \dots \mathbf{w}_{c(i-1)}, \mathbf{w}_{c(i+1)}, \mathbf{w}_{c(i+2)} \dots \mathbf{w}_{cn}] \cdot \begin{bmatrix} \lambda_{c1}, \lambda_{c2} \dots \lambda_{c(i-1)}, \lambda_{c(i+1)}, \lambda_{c(i+2)} \dots \lambda_{cn} \end{bmatrix}^T = \mathbf{0}, \forall \lambda \geq 0 \quad (5)$$

The contact corresponding to these wrenches (the thin black line segments) can be excluded from the contact set, while remaining a maximal size of \mathcal{A}_0 .

To see what wrenches are allowed onto the application surface it is discretized to a number of points (indicated green in Figure 5A). The wrenches going through these points are located on the green curves in wrench space. The intersection of the green

curves (including the space in between) with the contact wrench space A_c gives the application wrench space A_a . The application wrench space A_a contains all the wrenches that are allowed onto the application surface (in this case A_a equals A_c).

3.2 Application Angle Map

When contact occurs at the indicated white contact, the set of force closure wrenches (spanned by A_c) can be determined for every possible application point in physical space (like the example points of Figure 4). Resulting is the application angle map of Figure 5A. For a certain application point in the map, the arrow field indicates the mean direction to push; and the grayscale color indicates the variation that is allowed in the angle of the application force. The three application points considered in Figure 4 are shown here for reference. Point p_{a1} has a lighter underlying grayscale color than point p_{a2} , indicating that more variation is allowed in the application angle. Point p_{a3} falls out of the map, indicating that no application force is allowed here. The map can be used to adapt the shape of the surgical guide to gain an application surface whereon high variation is allowed in the application angle.

3.3 Wrench Space Efficiency Metrics

The area of the application wrench space A_a (unit: "millimeter \times degree") is a measure for the amount of wrenches that may be subjected to the application surface. Area A_a is a sub-area of the contact wrench space area A_c , containing all the wrenches that may be applied freely when the surgical guide has the indicated contact. Likewise, area A_c is a sub-area of the positive basis wrench space area A_0 , containing all the wrenches that may be applied freely when the surgical guide has full contact. Efficiency metrics η_c , $\eta_{a,c}$ and η_g are created to determine how well the wrench space is covered for a certain design of the surgical guide.

$$\eta_c = A_c / A_0 \quad (6)$$

$$\eta_{a,c} = A_a / A_c \quad (7)$$

$$\eta_g = A_a / A_0 \quad (8)$$

The contact efficiency η_c is helpful in finding a suitable contact set. It is a measure that indicates how well the contact set is chosen relative to full contact. When a contact set is chosen, it is useful to know if all the wrenches that can be subjected to the actual guide, can be subjected onto the application surface. The application surface efficiency $\eta_{a,c}$ is a metric that describes this, showing how well the application surface is chosen for the selected contact set. The overall guide efficiency η_g shows the overall wrench space coverage, defined as the ratio between the application surface wrench area A_a and the

maximum wrench area that can be attained A_0 . The overall guide efficiency η_g can also be seen as the multiplication of the contact efficiency η_c and the application surface efficiency $\eta_{a,c}$.

$$\eta_c \cdot \eta_{a,c} = \eta_g \quad (9)$$

The overall guide efficiency is optimized by successively changing the contact set to obtain high contact efficiency η_c and changing the application surface to obtain high application surface efficiency $\eta_{a,c}$.

3.4 Robustness Metric

In general, the allowed range in the application force's angle differs along the application surface. The robustness metric R is introduced to give an indication of the distribution of this range and hence it is defined as the minimum, median and maximum value of the application force's angle occurring along the application surface. The point discretization shown in Figure 5A (which we arbitrarily have set to twenty-five points) is used to determine the minimum median and maximum value. The robustness metric is an outcome metric which shows what we might expect when choosing a random point on the application surface to hold the guide in place. For the guide of Figure 5A the minimum range of the application angle is zero and thus there is a portion of the application surface where it is not allowed to push. Nevertheless, for fifty percent of the guide the range of the application angle is between the seven and thirty-one degrees.

4 UTILIZATION

An optimal shape for two dimensional surgical guides can be found by applying the design tools described in this paper. The robustness of guide 1 (Figure 5) will be improved by changing its shape in a step-by-step approach. In the first steps (guide 1-4) the contact set will be optimized; in the final steps (guide 5-6) the application surface will be optimized.

4.1 Guide 1

The location of the three contact points of guide 1 (Figure 5) has been randomly selected. The application surface is also set at a random height. The contact efficiency η_c shows that only sixteen percent of the contact potential has been used. On the other hand, the application surface efficiency $\eta_{a,c}$ is maximum and consequently all wrenches that may be subjected to the guide can also be subjected to the application surface. Note that $\eta_{a,c}$ is always maximum when the application surface fully intersects the cone of the application angle map. The application surface is actually too wide, because no force can be subjected

to the parts of the application surface which fall out of the application angle map. The robustness R shows this as the minimum range of the application angle is zero.

4.2 Guide 2

The contact set has been changed to create guide 2 (Figure 6). With only four contacts a large amount of wrench space is covered resulting in high contact efficiency η_c (ninety percent). Note that hereto the contact points have been selected from the four subsections of the positive basis. The application surface efficiency $\eta_{a,c}$ and the overall guide efficiency η_g are also affected by the changing the contact set, though we address these metrics in subsequent steps (guide 5-6) when the application surface is optimized. The robustness R of the surgical guide is improved significantly. For half of the length of the application surface the range in the application angle is seventy-one degrees. The minimum range is now not zero anymore and so it is allowed to push on every location of the application surface. We can also see this because the application surface falls now completely within the cone of the application angle map.

4.3 Guide 3

By adding two more contacts (Figure 7) the contact efficiency η_c increases to almost maximal (ninety-nine percent). The minimum of the robustness metric R also increases a bit which can also be seen in the robustness map as for the outer points of the application surface the gray value becomes lighter.

4.4 Guide 4

The contact efficiency η_c is maximal when all the positive basis contact is selected (Figure 8). If we do not want the application surface to change, the robustness R is also maximal.

4.5 Guide 5

By making the application surface narrower it falls within the whitest part of the grayscale map (Figure 9). Consequently, the range of the application angle is high at every point which we can see back in the values of the robustness metric R . On the other hand we see that the design of the surgical guide is not efficient as the application surface efficiency $\eta_{a,c}$ is quite low (fifty-four percent).

4.6 Guide 6

For guide 6, the application surface is made as wide as possible while remaining within the white portion of the grayscale map (Figure 10). The result is a surgical guide with high robustness R (the minimum value is sixty-seven), maximal contact efficiency η_c and close to maximal application surface efficiency $\eta_{a,c}$ (ninety-eight percent). Note that maximal application surface efficiency $\eta_{a,c}$ is not desired as this would imply that the cone of the

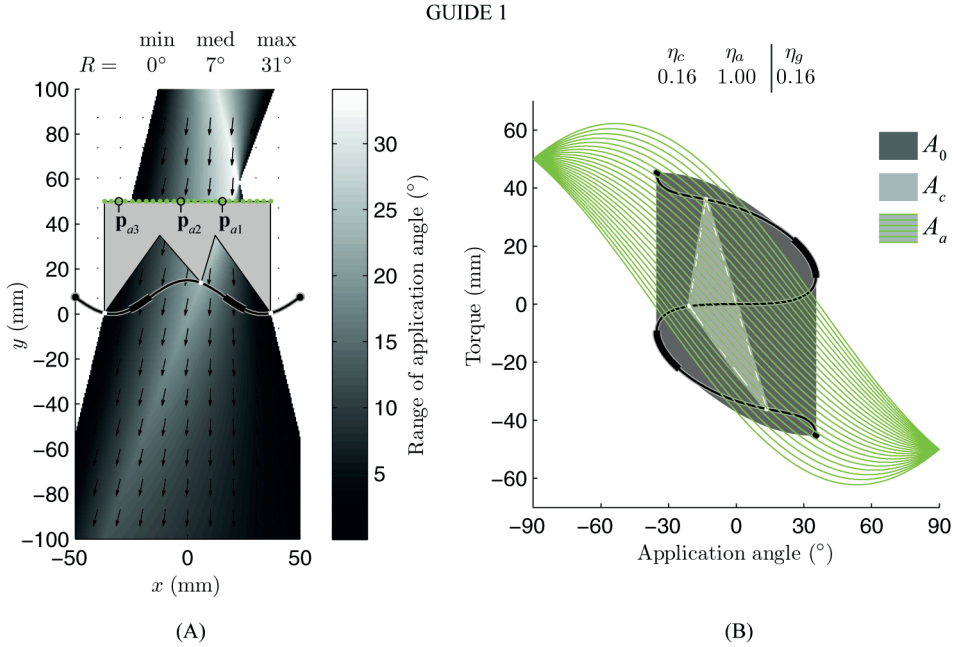


Figure 5. Guide 1: three random contact points with the application surface at a random height. (A) The guide in position on the bony geometry. Contact is indicated white on the bone line. In the background is the application angle map which shows for a certain application point: the mean direction to push (arrow field); and the range in which the application angle may be varied (grayscale color). The robustness metric R is given to show the docking quality of the actual guide. (B) The wrench space for the guide. Each green wrench space curve corresponds to a green point on the application surface and shows the wrenches that are possible through these points. Area A_0 shows the wrench space covered when the guide has full contact or positive basis contact (without consideration of the application surface); area A_c shows the wrench space covered when the guide has the indicated white contact (also without consideration of the application surface); and area A_a shows the wrench space of wrenches that can actually be subjected onto the application surface. The wrench space metrics η_c , $\eta_{a,c}$ and η_g show how well wrench space is covered.

application angle map is completely intersected. Consequently, a slightly too wide application surface (e.g. due to manufacturing errors) would cause the minimum value of the robustness metric to be zero degrees. The contact efficiency η_c together with the application surface efficiency $\eta_{a,c}$ results in a surgical guide efficiency η_g that is close to maximal (ninety-eight percent). The wide application surface combined with the high robustness ensures that the surgical guide will remain docked under a large variation in the location and direction of the application force.

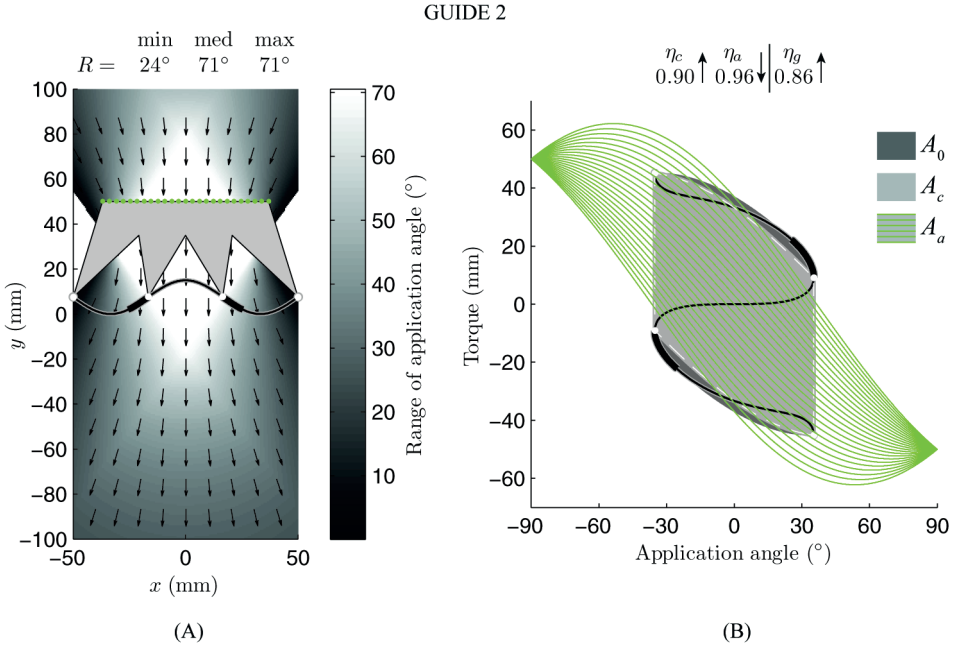


Figure 6. Guide 2: the contact is changed to four logical contact points which are selected from the positive basis contact. (A) The guide in position on the bony geometry. Contact is indicated white on the bone line. In the background is the application angle map which shows for a certain application point: the mean direction to push (arrow field); and the range in which the application angle may be varied (grayscale color). The robustness metric R is given to show the docking quality of the actual guide. (B) The wrench space for the guide. Each green wrench space curve corresponds to a green point on the application surface and shows the wrenches that are possible through these points. Area A_0 shows the wrench space covered when the guide has full contact or positive basis contact (without consideration of the application surface); area A_c shows the wrench space covered when the guide has the indicated white contact (also without consideration of the application surface); and area A_a shows the wrench space of wrenches that can actually be subjected onto the application surface. The wrench space metrics η_c , $\eta_{a,c}$ and η_g show how well wrench space is covered.

5 VALIDATION

The six surgical guides that result from the design process in the section utilization (Figure 5-10) were validated in an experimental setup (Figure 11). In the experiment we have tried to mimic the assumptions made in this article as good as possible.

5.1 Materials

Friction is assumed to be negligible and thus materials were selected where between the coefficient of friction was low. The materials used for the bony geometry and surgical guides were respectively Stainless Steel (SS 316) and Ultra High Molecular Weight Polyethylene (UHMW-PE). This material combination is also used in endo-prosthesis because of the very low friction component. The shape of the bony geometry and the

GUIDE 3

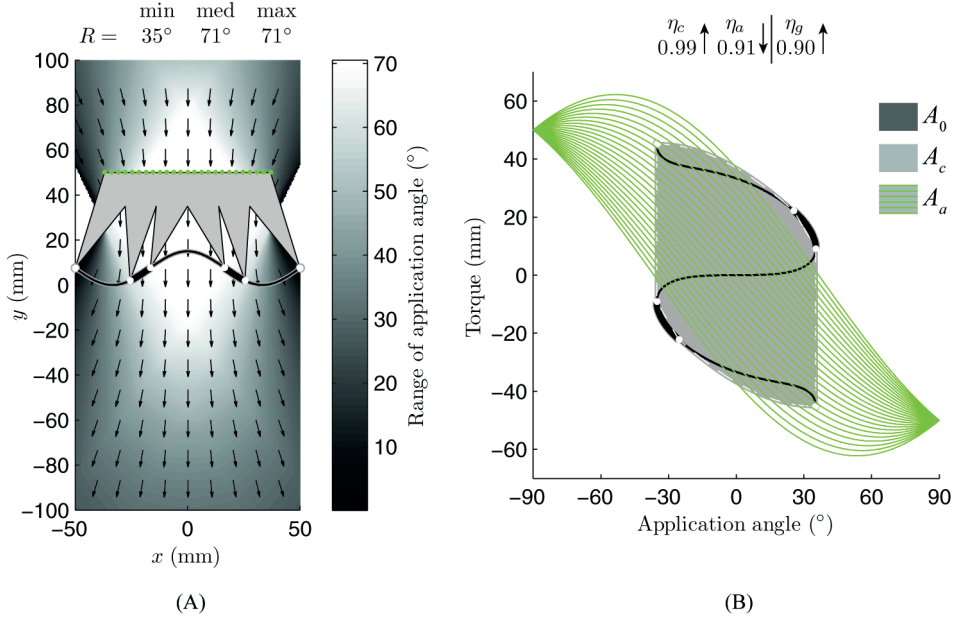


Figure 7. Guide 3: the contact is changed to six logical contact points which are selected from the positive basis contact. (A) The guide in position on the bony geometry. Contact is indicated white on the bone line. In the background is the application angle map which shows for a certain application point: the mean direction to push (arrow field); and the range in which the application angle may be varied (grayscale color). The robustness metric R is given to show the docking quality of the actual guide. (B) The wrench space for the guide. Each green wrench space curve corresponds to a green point on the application surface and shows the wrenches that are possible through these points. Area A_0 shows the wrench space covered when the guide has full contact or positive basis contact (without consideration of the application surface); area A_c shows the wrench space covered when the guide has the indicated white contact (also without consideration of the application surface); and area A_a shows the wrench space of wrenches that can actually be subjected onto the application surface. The wrench space metrics η_c , $\eta_{a,c}$ and η_g show how well wrench space is covered.

surgical guides is purely two dimensional. Computer Numerical Control vertical milling was used to create the shapes. Three grooves were included in the application surface of each guide representing points of application; one at twenty-five, fifty and seventy-five percent of the application surface's length.

5.2 Experimental Setup

An inclination table was created by the use of a digital angle measuring device (Bosch DWM 40 L). One leg of the measuring device was clamped to a vertical panel, while the other leg was still able to incline freely (Figure 11). The clamped leg includes a spirit level by which it was vertically leveled (a plastic plate was used as filling material). The angle between the clamped leg and the free leg (the inclination table) could be read from the

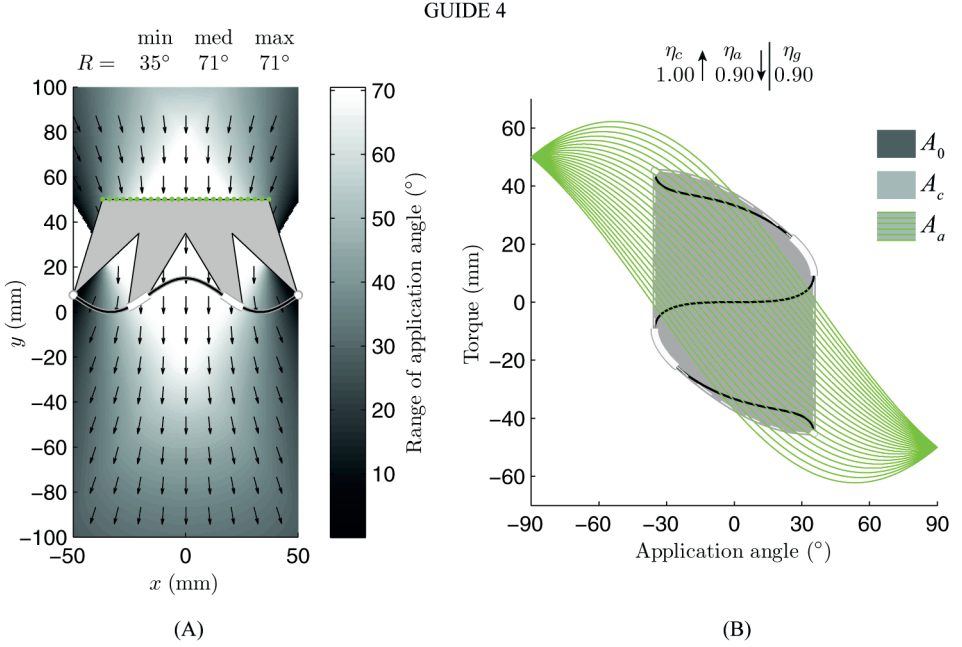


Figure 8. Guide 4: the contact is changed to the positive basis contact. (A) The guide in position on the bony geometry. Contact is indicated white on the bone line. In the background is the application angle map which shows for a certain application point: the mean direction to push (arrow field); and the range in which the application angle may be varied (grayscale color). The robustness metric R is given to show the docking quality of the actual guide. (B) The wrench space for the guide. Each green wrench space curve corresponds to a green point on the application surface and shows the wrenches that are possible through these points. Area A_0 shows the wrench space covered when the guide has full contact or positive basis contact (without consideration of the application surface); area A_c shows the wrench space covered when the guide has the indicated white contact (also without consideration of the application surface); and area A_a shows the wrench space of wrenches that can actually be subjected onto the application surface. The wrench space metrics η_c , η_a , and η_g show how well wrench space is covered.

digital display on the measuring device. The bony geometry was fixed to the inclination table. When the surgical guide was on the bony geometry, the application force was represented by a weight: a bar was laid into a groove of the application surface and at both ends of this bar a weight hanger was hung. The total weight of the bar and the two weight hangers (including the slotted weight) was 1058 grams. As in the assumptions of the analytical method, the weight of the surgical guide (between 26-59 grams) was negligible compared to the applied load.

One measurement was executed as follows. The surgical guide was placed onto the bony geometry in the planned position. The weight for the application force was hung in one of the grooves of the application surface. The angle of the application force was changed by slowly increasing or decreasing the angle of the inclination table by hand. When the

GUIDE 5

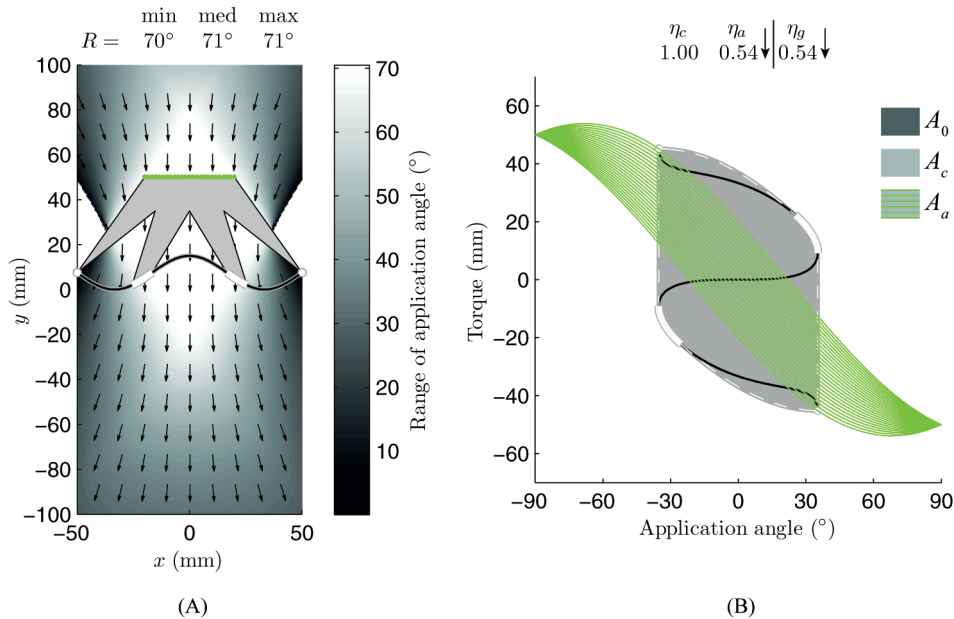


Figure 9. Guide 5: the application surface is made narrower so that it falls within the white part of the grayscale map. (A) The guide in position on the bony geometry. Contact is indicated white on the bone line. In the background is the application angle map which shows for a certain application point: the mean direction to push (arrow field); and the range in which the application angle may be varied (grayscale color). The robustness metric R is given to show the docking quality of the actual guide. (B) The wrench space for the guide. Each green wrench space curve corresponds to a green point on the application surface and shows the wrenches that are possible through these points. Area A_0 shows the wrench space covered when the guide has full contact or positive basis contact (without consideration of the application surface); area A_c shows the wrench space covered when the guide has the indicated white contact (also without consideration of the application surface); and area A_a shows the wrench space of wrenches that can actually be subjected onto the application surface. The wrench space metrics η_c , η_a , and η_g show how well wrench space is covered.

guide started to move (e.g. fell or slid) the angle on the digital display of the measuring device was noted. For each application point five repetitions were performed for both upwards and downwards inclination. Guides 2-6 are symmetrical and thus point 3 of those guides (at seventy-five percent of the application surface's length) was omitted from the experiment. This resulted in a total of one-hundred-and-thirty measurements for the six surgical guides.

An identical inclination test was done to measure the friction between flat surfaces of the materials. The friction test included five repetitions for both upwards and downwards inclination.

Two corrections have been applied to the measured values. The first was done to correct the horizontality of the inclination table as this depended on the spirit level of the clamped

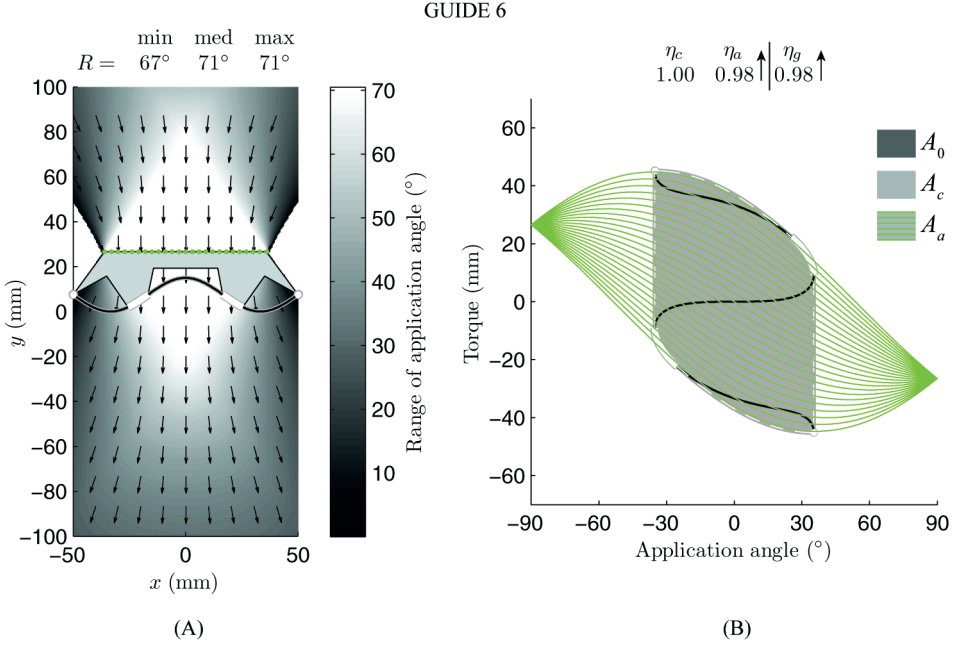


Figure 10. Guide 6: the application surface is made as wide as possible within the white part of the grayscale map. (A) The guide in position on the bony geometry. Contact is indicated white on the bone line. In the background is the application angle map which shows for a certain application point: the mean direction to push (arrow field); and the range in which the application angle may be varied (grayscale color). The robustness metric R is given to show the docking quality of the actual guide. (B) The wrench space for the guide. Each green wrench space curve corresponds to a green point on the application surface and shows the wrenches that are possible through these points. Area A_0 shows the wrench space covered when the guide has full contact or positive basis contact (without consideration of the application surface); area A_c shows the wrench space covered when the guide has the indicated white contact (also without consideration of the application surface); and area A_a shows the wrench space of wrenches that can actually be subjected onto the application surface. The wrench space metrics η_c , $\eta_{a,c}$ and η_g show how well wrench space is covered.

leg (which is not very accurate). The symmetry of guides 2-6 was used to calculate the correction value for horizontality. In the middle point of guides 2-6 the application range should be symmetrical as the guides are symmetrical. Therefore, the correction value for horizontality was calculated as the mean of all measurements for the middle point of guides 2-6. The second correction was for friction as this was neglected in the analytical method. The mean angle of friction was calculated from the friction test and was 5.2° . This value was subtracted from or added to the measured limits (dependent on whether it was a minimum or maximum application angle).



Figure 11. Experimental setup for testing the limits of the range of the application angle. A digital angle measuring device is used to create an inclination table. One leg of the measuring device is clamped to a vertical panel while the other leg can move freely. The bony geometry is fixed onto the inclination table (the free leg). For an experiment the guide is placed onto the bony geometry in the planned position. Weight is hung in one of the grooves of the application surface, representing an application force.

5.3 Results

The measured values from the experiment are very close to the calculated values from the analytical method (Figure 12). The standard deviation of the error between all calculated and measured values is only 0.7° . As expected from the analytical method, Guide 1 (Figure 5) performs far worse than all the other guides. Guides 2-6 actually all show very similar results for the measured limits of the application angle. Reason for this is that the chosen application points all fall within the white area of the grayscale map of those guides (Figure 6-10). Guides 5 and 6 are expected to perform better than guides 2-4 on the outer ends of the application surface (where no measurement was done). The range of the application angle for Guides 5 and 6 is high and rather constant over the length of the application

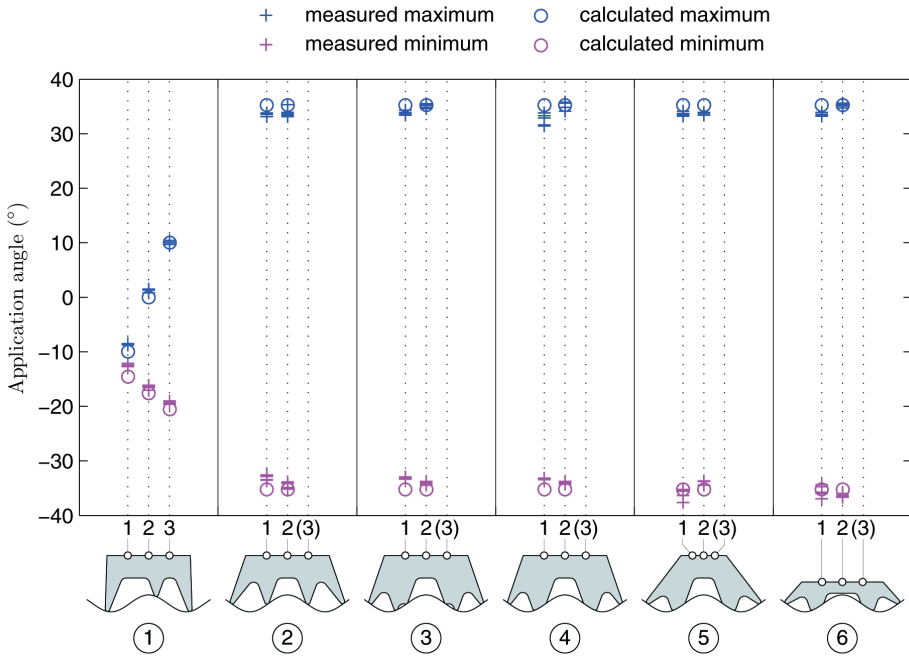


Figure 12. Comparison between the measured limits of the application angle (indicated with +) and the calculated limits of the application angle (indicated with o) for guides 1-6. Every individual measurement is displayed in the graph. Upper limits are indicated blue; lower limits are indicated magenta. Application points are at twenty-five, fifty and seventy-five percent of the length of the application surface. Application point 3 is excluded from the experiment for the symmetrical guides (i.e. guides 2-6) because the limits of the application angle are expected to be identical to those of point 1.

surface, which can be seen from the robustness metric R in Figure 9 and 10. Of Guides 5 and 6, Guide 6 is preferred because of its wider application surface.

6 DISCUSSION

The analytical method outlined in this paper gives developers and designers the opportunity to find an optimal shape for robust patient specific surgical guides. Design tools are presented which aid in the development of the guide. By only selecting positive basis contact, a guide is created that attains maximal contact efficiency η_c (Figure 8). More contact is not needed as it does not contribute to the robustness of the guide. A suitable location and shape for the application surface, where the surgeon may push, can be found by use of the application angle map (Figure 9-10). When the application surface is chosen as wide as possible within the whitest part of the map, the application surface efficiency $\eta_{a,c}$ is close to maximal and the values of the robustness metric are high (Figure 10). When one gets more experienced with the design tools and desires even less contact, a subset of the positive basis contact can be chosen (as with the guides of Figure 6 and 7)

combined with a logical location for the application surface (as with the guide of Figure 10). The resulting guide will only slightly compromise the robustness.

In the design process of surgical guides for clinical usage, virtual models of the patient's bony anatomy are used to find suitable contact. It should be clearly noted that such a virtual model will never represent the real bony geometry exactly. Soft as well as hard tissues might be present which were not segmented in the virtual bone models. When using the described method to design surgical guides, one might want to select a region wherefore segmentation is likely to be accurate – for instance, regions on the cortical bone when CT is used as an imaging modality.

The shape of the bone-guide contact is not only of importance in finding a stable position for the surgical guide, but also determines the validity with respect to the preoperatively plan for the guide position. In the design process of a guide, considerations have to be addressed to obtain a stable position that is at the same time identical to the planned position. When a guide is designed to have full contact, the likelihood of meeting irregularities on the bone or soft tissue interposition is high. As a result, the guide might not be docked stable and consequently rocking can occur when the surgeon is trying to hold it in position. Therefore, one might consider using the minimum amount of contact in designing the guide. The minimum amount of contact for deterministic positioning is three and six, respectively for two- and three-dimensional guides [16-19]. When a surgical guide is designed to have minimal contact, a stable position is likely to be found and rocking will not occur. Although, one cannot be sure if the final position is identical to the planned position – interposition of tissue under one contact point might result in a stable but wrong position. By adding extra contact to the minimal contact set, a self-checking mechanism is incorporated within the guide. If the guide with the additional contact has a good fit, one can be reasonably sure that tissue interposition has not occurred.

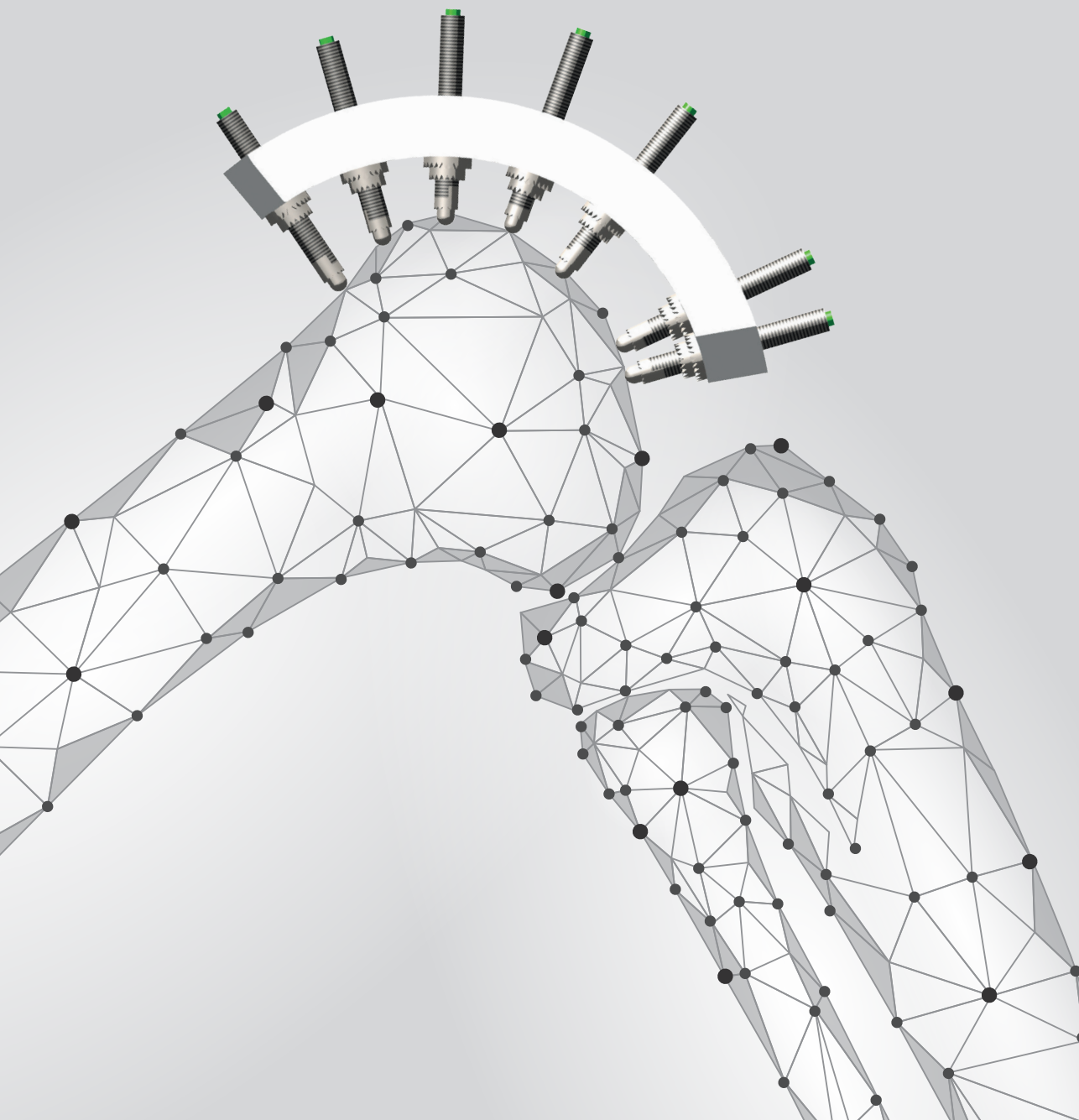
Experimental validation shows that the analytical method is able to predict the outcome of two-dimensional surgical guides (Figure 12). The standard deviation between the measured and calculated values is only 0.7°. The guides can be fully shaped with the described method and the minimal contact set that is obtained reduces the likelihood of tissue interposition. More research is required to investigate the errors that could arise when tissue interposition occurs or when the virtual model deviates from the real anatomy. Moreover, extrapolation to three dimensions is necessary to enable the development of guides that can be used in the surgical environment. The positive basis method to remove redundant contact is also applicable for three-dimensional guides. The reduction to a point contact set and shaping of the application surface remains a challenge.

REFERENCES

- [1] Lotke, P. A. and Ecker, M. L., 1977, Influence of positioning of prosthesis in total knee replacement. *J Bone Joint Surg Am*, **59-A**(1), pp. 77–79.
- [2] Jeffery, R. S., Morris, R. W., and Denham, R. A., 1991, Coronal alignment after total knee replacement, *J Bone Joint Surg Br*, **73-B**(5), pp. 709–714.
- [3] Eckhoff, D. G., Bach, J. M., Spitzer, V. M., Reinig, K. D., Bagur, M. M., Baldini, T. H., and Flannery, N. M. P., 2005, Three-dimensional mechanics, kinematics, and morphology of the knee viewed in virtual reality, *J Bone Joint Surg Am*, **87-A**(Suppl. 2), pp. 71–80.
- [4] Jaramaz, B., Hafez, M. A., and DiGioia, A. M., 2006, Computer-assisted orthopaedic surgery, *Proceedings of the IEEE*, **94**(9), pp. 1689–1695.
- [5] Kowal, J., Langlotz, F., and Nolte, L. P., 2007, Basics of computer-assisted orthopaedic surgery, *Navigation and MIS in Orthopedic Surgery*, Springer, ed., Springer, pp. 2–8.
- [6] Sugano, N., 2003, Computer-assisted orthopedic surgery, *J Orthop Sci*, **8**(3), pp. 442–448.
- [7] Balthis, H., Perlick, L., Tingart, M., Lüring, C., Zurakowski, D., and Grifka, J., 2004, Alignment in total knee arthroplasty, *J Bone Joint Surg Br*, **86-B**(5), pp. 682–687.
- [8] Sparmann, M., Wolke, B., Czupalla, H., Banzer, D., and Zink, A., 2003, Positioning of total knee arthroplasty with and without navigation support: a prospective, randomised study, *J Bone Joint Surg Br*, **85-B**(6), pp. 830–835.
- [9] Stöckl, B., Nogler, M., Rosiek, R., Fischer, M., Krismer, M., and Kessler, O., 2004, Navigation improves accuracy of rotational alignment in total knee arthroplasty, *Clin Orthop Relat Res*, **426**, pp. 180–186.
- [10] Chauhan, S. K., Scott, R. G., Breidahl, W., and Beaver, R. J., 2004, Computer-assisted knee arthroplasty versus a conventional jig-based technique: a randomised, prospective trial, *J Bone Joint Surg Br*, **86-B**(3), p. 372.
- [11] Matziolis, G., Krockner, D., Weiss, U., Tohtz, S., and Perka, C., 2007, A Prospective, Randomized Study of Computer-Assisted and Conventional Total Knee Arthroplasty, Three-Dimensional Evaluation of Implant Alignment and Rotation, *J Bone Joint Surg Am*, **89-A**(2), pp. 236–243.
- [12] van der Linden-van der Zwaag, H. M. J., Valstar, E. R., van der Molen, A. J., and Nelissen, R. G. H. H., 2008, Transepicondylar axis accuracy in computer assisted knee surgery: a comparison of the CT-based measured axis versus the CAS-determined axis, *Comput Aided Surg*, **13**(4), pp. 200–206.
- [13] Hafez, M. A., Chelule, K. L., Seedhom, B. B., and Sherman, K. P., 2007, Computer-Assisted Total Knee Arthroplasty Using Patient-Specific Templates: the Custom-made Cutting Guides, *Navigation and MIS in Orthopedic Surgery*, Springer, pp. 182–188.

- [14] Klatt, B. A., Goyal, N., Austin, M. S., and Hozack, W. J., 2008, Custom-fit total knee arthroplasty (OtisKnee) results in malalignment, *J Arthroplasty*, **23**(1), pp. 26–29.
- [15] Spencer, B. A., Mont, M. A., McGrath, M. S., Boyd, B., and Mitrick, M. F., 2009, Initial experience with custom-fit total knee replacement: intra-operative events and long-leg coronal alignment, *Int Orthop*, **33**(6), pp. 1571–1575.
- [16] Asada, H. and By, A. B., 1985, Kinematic analysis of workpart fixturing for flexible assembly with automatically reconfigurable fixtures, *IEEE J Robot Autom*, **RA-1**(2), pp. 86–94.
- [17] Dizioglu, B. and Lakshminarayana, K., 1984, Mechanics of form closure, *Acta Mech*, **52**(1), pp. 107–118.
- [18] Salisbury, J. K. and Roth, B., 1983, Kinematic and Force Analysis of Articulated Mechanical Hands, *J Mech Transm-T ASME*, **105**(1), pp. 35–41.
- [19] Mishra, B., Schwartz, J. T., and Sharir, M., 1987, On the existence and synthesis of multifinger positive grips, *Algorithmica*, **2**(1), pp. 541–558.
- [20] Ohwovoriole, E. N., 1987, Kinematics and friction in grasping by robotic hands. *J Mech Transm-T ASME*, **109**(3), pp. 398–404.
- [21] Nguyen, V. D., 1988, Constructing force-closure grasps, *Int J Robotics Res*, **7**(3), pp. 3–16.
- [22] Markenscoff, X., Ni, L., and Papadimitriou, C. H., 1990, The geometry of grasping, *Int J Robot Research*, **9**(1), pp. 61–74.
- [23] Trinkle, J., 1992, On the stability and instantaneous velocity of grasped frictionless objects, *IEEE T Robot Autom*, **8**(5), pp. 560–572.
- [24] Rimon, E. and Burdick, J. W., 1998, Mobility of bodies in contact - Part I: A 2nd-order mobility index for multiple-finger grasps, *IEEE T Robot Autom*, **14**(5), pp. 696–708.
- [25] Brost, R. C. and Goldberg, K. Y., 1996, A complete algorithm for designing planar fixtures using modular components, *IEEE T Robot Autom*, **12**(1), pp. 31–46.
- [26] Chou, Y. C., Chandru, V., and Barash, M. M., 1989, A mathematical approach to automatic configuration of machining fixtures: analysis and synthesis, *J Eng Ind*, **111**(4), pp. 299–306.
- [27] Reuleaux, F., 1876, *The kinematics of machinery: outlines of a theory of machines*, Macmillan, pp. 103–112.
- [28] Mason, M. T., 2001, *Mechanics of Robotic Manipulation*, The MIT Press.
- [29] Dodou, D., Breedveld, P., and Wieringa, P. A., 2006, The role of geometry in the friction generated on the colonic surface by mucoadhesive films, *J Appl Phys*, **100**(1), p. 014904.
- [30] Bowden, F. P., Moore, A. J. W., and Tabor, D., 1943, The ploughing and adhesion of sliding metals, *J Appl Phys*, **14**(2), pp. 80–91.
- [31] Bicchi, A. and Kumar, V., 2000, Robotic grasping and contact: a review, *IEEE International Conference on Robotics and Automation* (Vol. 1), pp. 348–353.

- [32] Goldman, A. J. and Tucker, A. W., 1956, Polyhedral convex cones, *Linear inequalities and related systems*, Princeton University Press, pp. 19–39.



CHAPTER 3

Docking Robustness of Patient Specific Surgical Guides for Joint Replacement Surgery

Joost Mattheijer^{1,2}

Just L. Herder³

Gabriëlle J.M. Tuijthof^{2,4}

Edward R. Valstar^{1,2,†}

¹Leiden University Medical Center, Dept. of Orthopaedics, Leiden, The Netherlands

²Delft University of Technology, Dept. of BioMechanical Eng., Delft, The Netherlands

³Delft Univ. of Tech., Dept. of Precision and Microsystems Eng., Delft, The Netherlands

⁴Academic Med. Center, Dept. of Orthopaedic Surgery, Amsterdam, The Netherlands

ABSTRACT

In joint replacement surgery, Patient Specific Surgical Guides (PSSGs) are used for accurate alignment of implant components. PSSGs are designed preoperatively to have a geometric fit with the patient's bone such that the incorporated guidance for drilling and cutting is instantly aligned. The surgeon keeps the PSSG in position with a pushing force and it is essential that this position is maintained while drilling or cutting. Hence, the influence of the location and direction of the pushing force should be minimal. The extent that the pushing force may vary is what we refer to as docking robustness. In this article, we present a docking robustness framework comprising the following quantitative measures and graphical tool. Contact efficiency η_c is used for the quantification of the selected bone-guide contact. Guide efficiency η_g is used for the quantification of the whole guide including an application surface whereon the surgeon can push. Robustness maps are used to find a robust location for the application surface based on gradient colors. Robustness R is a measure indicating what angular deviation is minimally allowed at the worst point on the application surface. The robustness framework is utilized in an optimization of PSSG dimensions for the distal femur. This optimization shows that twelve contacts already result in a relatively high contact efficiency of 0.74 ± 0.02 (where the maximum of 1.00 is obtained when the guide is designed for full bone-guide contact). Six contacts seem to be insufficient as the obtained contact efficiency is only 0.18 ± 0.02 .

Keywords: Robustness, Form Closure, Surgical Guides, Joint Replacement, Grasping, Fixtures.

1 INTRODUCTION

When a hip or knee joint is painful and has severe damage due to arthritis, the cartilage and some of the underlying bone can be removed and replaced with a joint replacement prosthesis. Replacement is done by making the appropriate saw cuts and drill holes such that the artificial components fit in the intended position. The use of Patient Specific Surgical Guides (PSSGs) is a fairly new method used to guide these saw cuts and drill holes accurately and time efficiently [1-4]. The PSSGs are dimensioned to dock in a unique position onto the patient's bone so that incorporated saw and drill guidance is correctly aligned (Figure 1). In the docked position, the PSSG is immobilized by a geometric fit with the bone and a pushing force of the surgeon. In clinical practice, the line of action of this pushing force should be allowed to vary to some extent while the PSSG remains docked stably. The allowed variation in the line of action depends on the PSSG's dimensions and is topic of this article.

The geometric fit of PSSGs is different for each patient (i.e. patient specific) and achieved either by three-dimensional printing [5, 6] or by setting a configurable PSSG. Printed PSSGs are already used in clinical practice today [1-4] whereas configurable PSSGs are still in a more conceptual phase [7]. The downside of printed PSSGs is that they can only be used one time for one patient due to the varying bone geometry. In contrast, configurable PSSGs can be used for multiple patients by changing settings. Haselbacher [7] shows an example of a configurable PSSG consisting of a plate with a grid of threaded holes and threaded pins which can be set to a desired depth. The grid of pins can be set to match the bone of a specific patient. Either printed or configurable, patient-specific dimensioning of the PSSGs is done pre-operatively such that it matches the patient's virtual bone model as obtained by MRI (Magnetic Resonance Imaging) or CT (Computed Tomography).

The contact geometry plays an important role in the design of the surgical guide. In case of a configurable surgical guide, the number of contacts determines the complexity of the instrument. Minimally six contacts are required for a fully determined position [8]. More contacts leads to an over-determined equilibrium, and as a result, bony deviations, deviations from the bone model not predicted by preoperative MRI or CT, may cause rocking of the surgical guide. The likelihood of encountering these bony deviations is maximal for a surgical guide that is designed for full contact. For a surgical guide with the minimum number of contacts, the likelihood of encountering bony deviations at the contact points is minimal. On the other hand, the surgical guide with full contact will most likely remain docked under larger variation in the surgeon's pushing force.

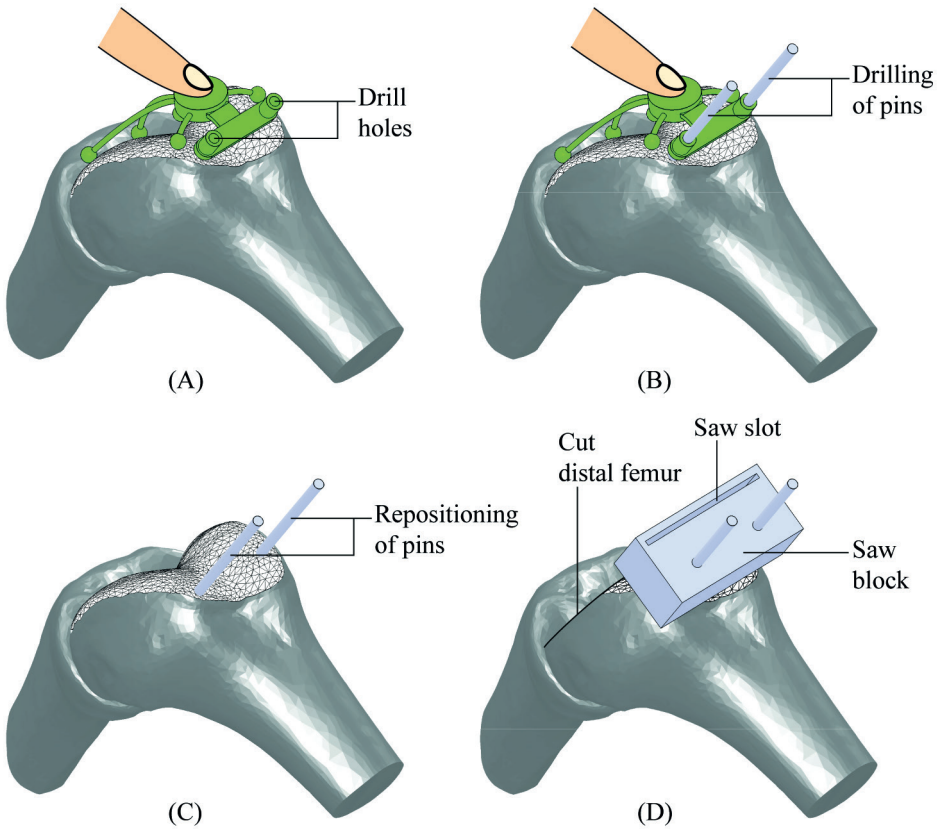


Figure 1. An artist impression of a surgical guide and its usage in knee replacement is shown. (a) The surgical guide is docked onto the distal femur by a geometric fit and a pushing force of the surgeon. (b) The drill holes are used to drill pins into the bone. (c) The pins and surgical guide are removed, whereupon the pins are repositioned. (d) The pins are used to guide a saw block in place and the saw slot is used to cut the distal femur.

When the surgeon uses the guidance of the PSSG for the creation of saw cuts and drill holes, it is crucial that the docked position onto the bone is maintained. Hence, the influence of the location and direction of the surgeon's pushing force onto the guide should be minimal. To what extent the line of action of the pushing force may be varied depends on the guide dimensions and will be referred to as *docking robustness*. In previous work [9], we focused on two-dimensional guides and created measures for the quantification of docking robustness and accompanying graphical tools for the optimization of guide dimensions.

The goal of this article is to develop measures for the quantification of docking robustness of three-dimensional PSSGs. With these new measures, existing printed guides can be assessed, and moreover optimal settings for the geometric fit of configurable guides can be found. The higher dimensional problem, compared to two-dimensional guides [9],

requires considerable adjustment of measures and graphical tools. Although our work is primarily focused on PSSGs, it is closely related and applicable to the fields of workpart fixturing and robotic grasping. In workpart fixturing, objects are fixed in a desired position to enable machine processing [8, 10, 11]. In robotic grasping, the fingers of robotic hands are configured to hold and manipulate objects [12-14].

The remainder of this article is structured as follows. First the assumptions, constraints and static condition for the surgical guide docked onto the bone are considered (Section 2). Next, the framework for the quantification of docking robustness is presented (Section 3). Using the measures and graphical tool from the robustness framework, optimal PSSG dimensions are sought for docking with the distal femur (Section 4).

2 DOCKING OF SURGICAL GUIDES

The design of a femoral PSSG for knee replacement surgery is taken as example in this article. Figure 2 shows the knee with the femur and tibia in typical angles for knee replacement surgery. These angles and the geometry of the tibia and femur remain constant throughout the article. Nevertheless, the methods applied to quantify docking robustness and optimize PSSG dimensions are generic.

When the PSSG is held in the intended position by an application force \mathbf{f}_a of the surgeon, both the bones and PSSG hardly move, hence we consider this a static condition (Figure 2). The line of action \mathbf{l}_a of the application force \mathbf{f}_a is allowed to vary to some extent, however, it should not cause dislocation of the surgical guide. Taking one specific point \mathbf{p}_a on the application surface \mathcal{S} , the direction \mathbf{d}_a of the application line \mathbf{l}_a is allowed to vary within the limits of a convex cone \mathcal{D}_a . These limits differ for every point on \mathcal{S} . Before examining the static condition and the limits to \mathbf{l}_a in more detail, assumptions are made and constraints are set.

2.1 Assumptions

- 1) *The PSSG is located at the intended position.*
- 2) *The shapes of the actual bony geometry and the virtual bony geometry are identical.*

The exact bony geometry is assumed to be known for the design of the surgical guide and is represented by a triangular mesh. Consequently, the surgical guide can make contact at all contacts when docked. In actual clinical practice, bony deviations (due to data segmentation inaccuracies not predicted by MRI or CT) may influence the geometric match between the surgical guide and bone. When the surgical guide has only six contacts, i.e. minimal contact, bony deviations will

only cause a slight error in the guide's position, and consequently, also only a small effect on robustness is to be expected. When the surgical guide has more contacts, the guide will either adapt to the bone due to the softness of the cartilage or rock on the bone near the planned position. In case the guide adapts, its position is slightly affected, but contact is granted at every contact point. Consequently, only a small effect on robustness is expected here as well. In case the surgical guide rocks on the bone, there are multiple fully determined positions possible. In each of these positions, there are minimally six contacts contacting the bone. The joined robustness of these individual positions is expected to be almost the same as the unaffected robustness. In the remainder of this article, bony deviations are not considered. Instead, this work can be used to find multiple optimal guides with different contact sets, which in a later stage can be assessed for sensitivity concerning bony deviations.

3) *The PSSG and bony geometry are considered rigid.*

When both the PSSG and bone are completely rigid, the position of the PSSG can be replicated at best. However, the cartilage layer covering the bone is relatively soft. Thus when the surgeon applies a force to a sufficiently stiff PSSG, the contacts will subside into the cartilage. This subsidence creates extra sliding resistance [15, 16] and therefore aids in the docking robustness. Hence, a worst case scenario is considered by assuming both the PSSG and bone to be rigid.

4) *The region on the femur that is suitable for contact is the cartilage portion which is not blocked by the tibia (Figure 2).*

During surgery the femur is not exposed entirely and some of the exposed bony surface is difficult to reach or cannot be reached at all via regular surgical access. This poses a natural limitation to the region of the bony surface that can be used for docking.

5) *The bone-guide interface is considered frictionless.*

Friction at the bone-guide interface creates extra sliding resistance and thus neglecting friction for this interface can be considered as a worst-case scenario.

6) *The guide-finger interface is considered not to cause slip.*

The friction coefficient of the guide-finger interface depends on the contacting materials. In this article, it is considered maximal; thus, the pushing force of the surgeon can be in any direction as long as it is directed below \bar{S} .

2.2 Constraints

- 1) *The allowed contact region is restricted to \mathbf{B} (Figure 2) so that docking and undocking of the PSSG can be performed by a linear motion in line with the gravitational direction \mathbf{g} .*

The purpose of this constraint is two-fold. First, the linear motion facilitates the ease of docking by the surgeon and second, it is a precondition to set up the framework for docking robustness. No contact set can be chosen within region \mathbf{B} which completely immobilizes the PSSG. A pushing force of the surgeon is always needed for complete immobilization. Region \mathbf{B} only contains triangles that have an outward normal which makes an angle less than seventy-five degrees with $-\mathbf{g}$. This angle is set at an arbitrary value below maximum (i.e. ninety degrees) to prevent jamming of the PSSG.

- 2) *Only the triangles' centroids \mathbf{P}_b of the allowed contact region \mathbf{B} can be selected for contact.*

We justify the restriction by the notion that contact with a complete triangle instead of its centroid can only lead to higher docking robustness. A chosen contact set \mathbf{P}_c is selected from \mathbf{P}_b and contains the contact points $\mathbf{p}_{c,i}$ ordered in columns.

- 3) *The dimensions and planned location of the application surface \mathbf{S} are set.*

The application surface \mathbf{S} is defined to be a thirty millimeter diameter disc which is expected to be suitably large for applying pressure with one finger. The planned location for \mathbf{S} is set initially close to the bone in horizontal direction, as depicted in Figure 2. In Section 4, the contact locations for the PSSG will be optimized and therewith an alternative (optimal) location for \mathbf{S} is assessed for robustness.

2.3 Static Condition

The static condition of the surgical guide is investigated with respect to an arbitrary global frame. The stated assumptions and constraints allow us to assume that the surgical guide is subjected to forces only, i.e. an application force \mathbf{f}_a of the surgeon and contact reaction forces $\mathbf{f}_{c,i}$ normal to the joint surface (Figure 2). The line of action \mathbf{l} of each of these forces can be expressed in Plücker coordinates [17] by

$$\mathbf{q} = \begin{bmatrix} \mathbf{d} \\ \mathbf{m} \end{bmatrix} = \begin{bmatrix} \mathbf{d} \\ \mathbf{p} \times \mathbf{d} \end{bmatrix}. \quad (1)$$

Here, \mathbf{d} is the normalized direction vector of the line and \mathbf{m} the line's moment vector about the origin. The moment vector \mathbf{m} can be determined by taking any point \mathbf{p} on the line (which in our case are the contact points $\mathbf{p}_{c,i}$ and the application point \mathbf{p}_a) and the moment equation $\mathbf{p} \times \mathbf{d}$. The force acting along a line l can be expressed by a wrench [18]. The general form of a wrench is

$$\mathbf{w} = \lambda \begin{bmatrix} \mathbf{d} \\ \mathbf{m} \end{bmatrix} + \xi \begin{bmatrix} \mathbf{0} \\ \mathbf{d} \end{bmatrix}. \quad (2)$$

Thus, a wrench can be constructed by a force with magnitude λ acting along a line plus a moment with magnitude ξ about that same line. The contact geometry of the surgical guide is able to resist a general wrench \mathbf{w}_a of the form of Eq. (2). The contact wrenches $\mathbf{w}_{c,i}$ only act along the contact lines $l_{c,i}$ (i.e. normal to the bony geometry), hence, ξ equals zero for those wrenches. Regarding a general wrench \mathbf{w}_a and contact wrenches $\mathbf{w}_{c,i}$ static equilibrium is obtained when the sum of wrenches equals zero.

$$\sum \lambda_{c,i} \mathbf{q}_{c,i} + \mathbf{w}_a = \mathbf{0}, \quad \forall \lambda_{c,i} \geq 0. \quad (3)$$

This is identical to the more familiar conditions for static equilibrium where the sum of forces and sum of moments equal zero. The force magnitudes $\lambda_{c,i}$ can only be nonnegative as all forces on the surgical guide are unidirectional, i.e. all forces on the surgical guide are compressive. Eq. (3) can be rewritten to find the limits for the application wrench

$$\mathbf{w}_a \in K_a = \{ \mathbf{Q}_{nc} \boldsymbol{\lambda}_c \mid \boldsymbol{\lambda}_c \geq \mathbf{0} \}. \quad (4)$$

Here, \mathbf{Q}_{nc} is a matrix containing the negated contact line coordinates $-\mathbf{q}_{c,i}$ as columns, and $\boldsymbol{\lambda}_c$ is a vector containing the corresponding force magnitudes $\lambda_{c,i}$. Wrench space K_a is the description of a polyhedral convex cone in \mathbb{R}^6 [18]. The coordinates of \mathbf{w}_a represent a point in \mathbb{R}^6 which may or may not be contained in K_a . The wrench cone K_a contains all the application wrenches \mathbf{w}_a allowed for the selected contact. Eq. (4) generally states that every allowed application wrench (i.e. $\mathbf{w}_a \in K_a$) can be expressed as a positive linear combination of the negated contact lines \mathbf{Q}_{nc} .

As wrench coordinates are not always line coordinates, additional constraints apply for the application line coordinates \mathbf{q}_a , namely:

$$(\mathbf{w}_a)_1^2 + (\mathbf{w}_a)_2^2 + (\mathbf{w}_a)_3^2 = 1, \quad (5)$$

$$(\mathbf{w}_a)_1 (\mathbf{w}_a)_4 + (\mathbf{w}_a)_2 (\mathbf{w}_a)_5 + (\mathbf{w}_a)_3 (\mathbf{w}_a)_6 = 0. \quad (6)$$

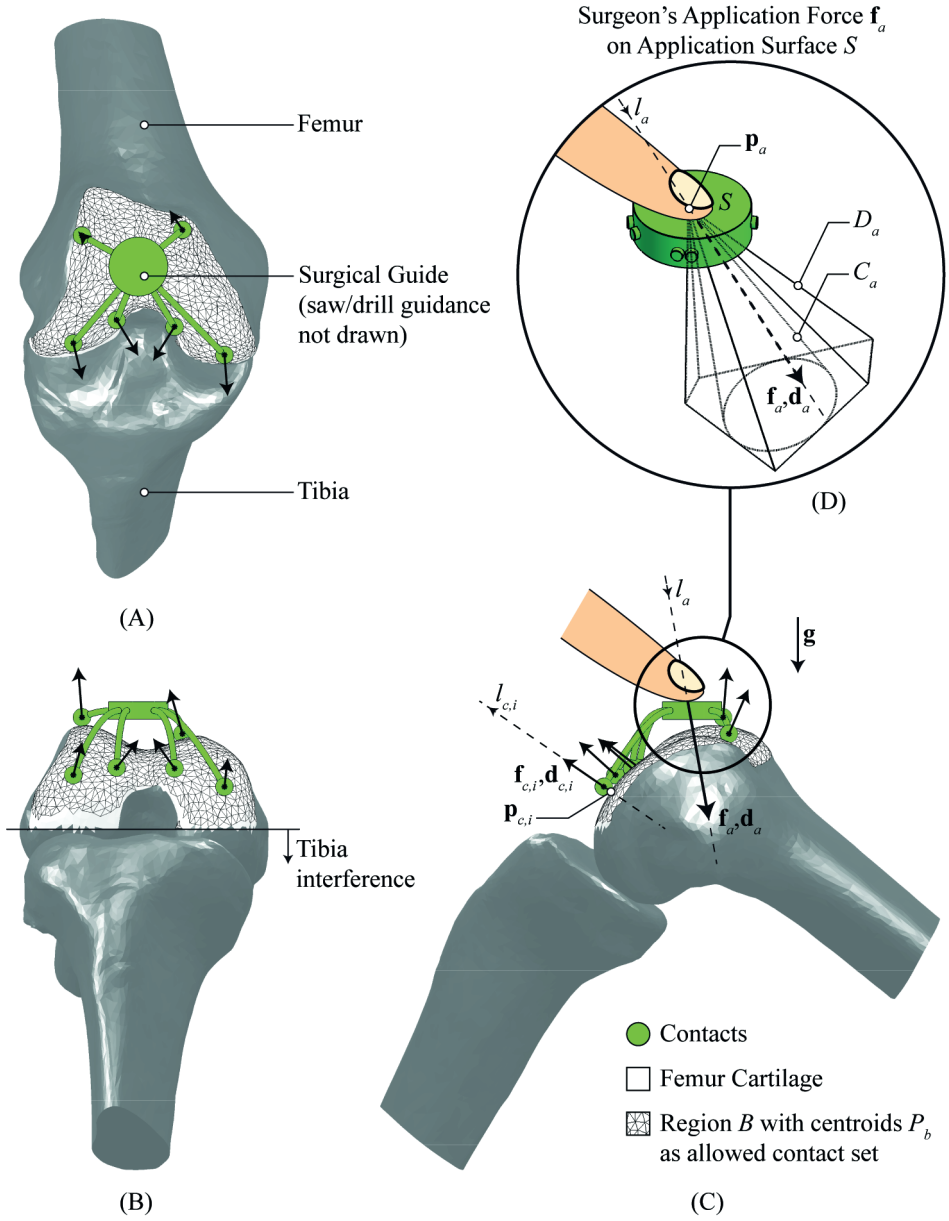


Figure 2. The surgical guide is docked onto the opposing distal femur by a geometric fit and a pushing force of the surgeon. A top view, front view and right view are respectively shown on the knee joint in (A), (B) and (C). The femur and tibia are shown in typical angles for joint replacement surgery. (B) The region of the cartilage which is suitable for contact is the portion that is not interfered by the tibia. (C-D) The surgeon applies force \mathbf{f}_a at an arbitrary point \mathbf{p}_a on the circular application surface S . The resulting contact reaction forces $\mathbf{f}_{c,i}$ act normal to the bony surface. The allowed variation in the application line l_a depends on the contact locations $\mathbf{p}_{c,i}$ and the location of application surface S . (D) For a specified point \mathbf{p}_a , the direction \mathbf{d}_a of application line l_a may vary within a convex cone D_a . Cone C_a is the largest circular cone inscribed in D_a , giving stricter but simpler bounds to the allowed variation of \mathbf{d}_a .

The former constraint is necessary to consider only application lines with unit direction \mathbf{d} . The latter constraint is the Plücker relation [17] and is necessary to consider only line coordinates; in which case the direction components \mathbf{d} are always orthogonal to the moment components \mathbf{m} .

Let the application line space L_a be the set of all application lines allowed for the selected contact, i.e. the lines satisfying Eqs. (4)-(6). Some of the lines within L_a may not be able to be applied onto the application surface S . This depends on the location and dimensions of S and friction with the surgeon's finger. That is, if a certain line l_a intersects the application surface, the surgeon is able to apply force along that line. If in conjunction to that, this line lies within the local friction cone, the surgeon's finger will not slip away. These two conditions can be formulated for the circular disc S (Figure 2). The intersection point of an application line with the plane of S can be found using line geometry [17] by

$$\mathbf{p}_a = \frac{\mathbf{n}_S \times \mathbf{m}_a + (\mathbf{n}_S \cdot \mathbf{p}_{s0}) \mathbf{d}_a}{\mathbf{n}_S \cdot \mathbf{d}_a}. \quad (7)$$

Where, \mathbf{n}_S and \mathbf{p}_{s0} are respectively the outward normal and center of S . This intersection point \mathbf{p}_a is on the circular disc with radius r_S when

$$\|\mathbf{p}_a - \mathbf{p}_{s0}\| \leq r_S. \quad (8)$$

The application line is also within the friction cone (with the maximal friction angle of ninety degrees) when

$$\mathbf{n}_S \cdot \mathbf{d}_a \leq \cos 90^\circ = 0. \quad (9)$$

Let L_{as} be the bounded application line space for the selected contact, i.e. the lines satisfying not only Eqs. (4)-(6) but also Eqs. (7)-(9). Thus, the term bounded implies that these application lines not only satisfy equilibrium, but also satisfy the added condition that forces along these lines can be applied on S . The larger L_{as} , the more variation is allowed in the direction and location of the application line, or in other words, the higher the docking robustness. In the following section, the line space contents L_a and L_{as} will be used in the creation of measures and a graphical tool for robustness assessment.

3 ROBUSTNESS FRAMEWORK

The main goal of this article is the creation of measures for robustness assessment of PSSGs. In this section, these measures are developed and later on they are used to find optimal PSSG dimensions for the distal femur (Section 4). The robustness framework presented here is organized as follows. Contact which does not contribute to the

robustness can be removed by only using *basis contact* (Section 3.1). The robustness of the PSSG can be assessed by *efficiency ratios* for the contact η_c and the guide as a whole η_g (Section 3.2). The allowed variation for an application line is graphically presented by *robustness maps* convenient for locating and dimensioning the application surface (Section 3.3). An insightful *robustness measure* R is created that quantifies the allowed angular variation in the application line at the worst point on the application surface (Section 3.4).

3.1 Basis contact

When a surgical guide with more than the minimum number of contacts is considered, some of the contact may be redundant as it does not contribute to the robustness. In Figure 3 the redundant contact from an initial full contact set $\mathbf{P}_{c,full}$ is removed. Redundant contact for any chosen contact set \mathbf{P}_c is determined as follows.

The columns of \mathbf{Q}_{nc} represent points in \mathbb{R}^6 and some of these points direct the bounding rays of K_a – known as the extreme rays – whereas other points are contained within cone K_a . The points that direct the extreme rays form a positive basis for K_a – i.e. a minimal set to span K_a – and consequently Eq. (4) can be substituted by

$$\mathbf{w}_a \in K_a = \left\{ \mathbf{Q}'_{nc} \boldsymbol{\lambda}'_c \mid \boldsymbol{\lambda}'_c \geq \mathbf{0} \right\}. \quad (10)$$

Here, the apostrophe in \mathbf{Q}'_{nc} and $\boldsymbol{\lambda}'_c$ indicates positive basis. Thus only the negated contact line coordinates that direct the bounding rays of K_a are included in Eq. (10). In Figure 3 the original full contact set $\mathbf{P}_{c,full}$ is replaced by the positive basis contact set $\mathbf{P}'_{c,full}$ containing only the contact points that correspond to the negated contact line coordinates \mathbf{Q}'_{nc} . All removed contact from the original $\mathbf{P}_{c,full}$ can be considered redundant, as it does not affect the robustness of the PSSG. The redundant contact does not enlarge the application line spaces L_a and L_{as} . Any subset from $\mathbf{P}'_{c,full}$ forms a positive basis as well and thus does not contain any redundant contact. Hence, only subsets of $\mathbf{P}'_{c,full}$ will be considered in the remainder of this article.

3.2 Efficiency Ratios

Efficiency ratios for the line spaces L_a and L_{as} are created to assess the robustness of the PSSG design. The larger L_a and L_{as} are, the more variation is allowed in respectively the unbounded and bounded application line – where bounded refers to application lines that can be applied on the application surface S . Line space L_a is dependent on the contact only and is largest when the guide has full or basis contact (with $L_{a,full}$ as the associated line space). In other words, L_a is always a subset of $L_{a,full}$. Line space L_{as} is dependent on all the guide's dimensions (i.e. the contact and the application surface) and

is a subset of L_a . This makes L_{as} a subset of both L_a and $L_{a,full}$. Hence, the relationship of said line spaces is

$$L_{as} \subseteq L_a \subseteq L_{a,full}. \quad (11)$$

Bearing this in mind, the following efficiency ratios are created:

$$\eta_c = \frac{\mu(L_a)}{\mu(L_{a,full})}, \quad (12)$$

$$\eta_g = \frac{\mu(L_{as})}{\mu(L_{a,full})}. \quad (13)$$

Here, μ is a content measure for line spaces which will be defined in the next paragraph. The contact efficiency η_c quantifies the chosen contact set \mathbf{P}_c relative to full or basis contact $\mathbf{P}_{c,full}$ and is therefore helpful in finding a good contact set. The maximum for η_c is one, which is obtained when $\mathbf{P}_c = \mathbf{P}_{c,full}$. When an appropriate contact set is chosen and η_c is acceptable, the guide efficiency η_g can be used to find a suitable application surface. The guide efficiency η_g can be regarded as an overall measure for the surgical guide. For a chosen contact set the maximum for η_g is η_c .

The content measure of a line space $\mu(L)$ quantifies how much variation is allowed in the application line L_a . It is a higher dimensional integral which to our best knowledge cannot be solved analytically. A common technique to approximate higher dimensional integrals is Monte Carlo integration [19]. This numerical integration technique will be used for approximation of $\mu(L)$. For the Monte Carlo integration, a uniform distribution of random lines is generated. The coordinates of these random lines are subsequently tested for containment within the respective line space (e.g. by testing containment within cone K_a for line space L_a). The more random lines are generated, the more accurate the approximation of $\mu(L)$.

The coordinates of the random lines have to satisfy Eqs. (5) and (6), and are generated by

$$\mathbf{q} = \left\{ \left[\mathbf{d}, m \frac{\mathbf{v} \times \mathbf{d}}{\|\mathbf{v} \times \mathbf{d}\|} \right]^T \mid \mathbf{d} \in \mathbb{S}^2, \mathbf{v} \in \mathbb{S}^2, m \in [0, m_{ub}] \right\}. \quad (14)$$

Here, \mathbf{d} is a random direction vector generated by randomly picking a point on the surface of the unit sphere \mathbb{S}^2 (e.g. by Marsaglia's method [20]). Because the radius of the unit sphere equals one, the length of \mathbf{d} equals one as well, and hence, Eq. (5) is satisfied. Vector \mathbf{v} is an intermediate vector also generated by randomly picking a point on the surface of

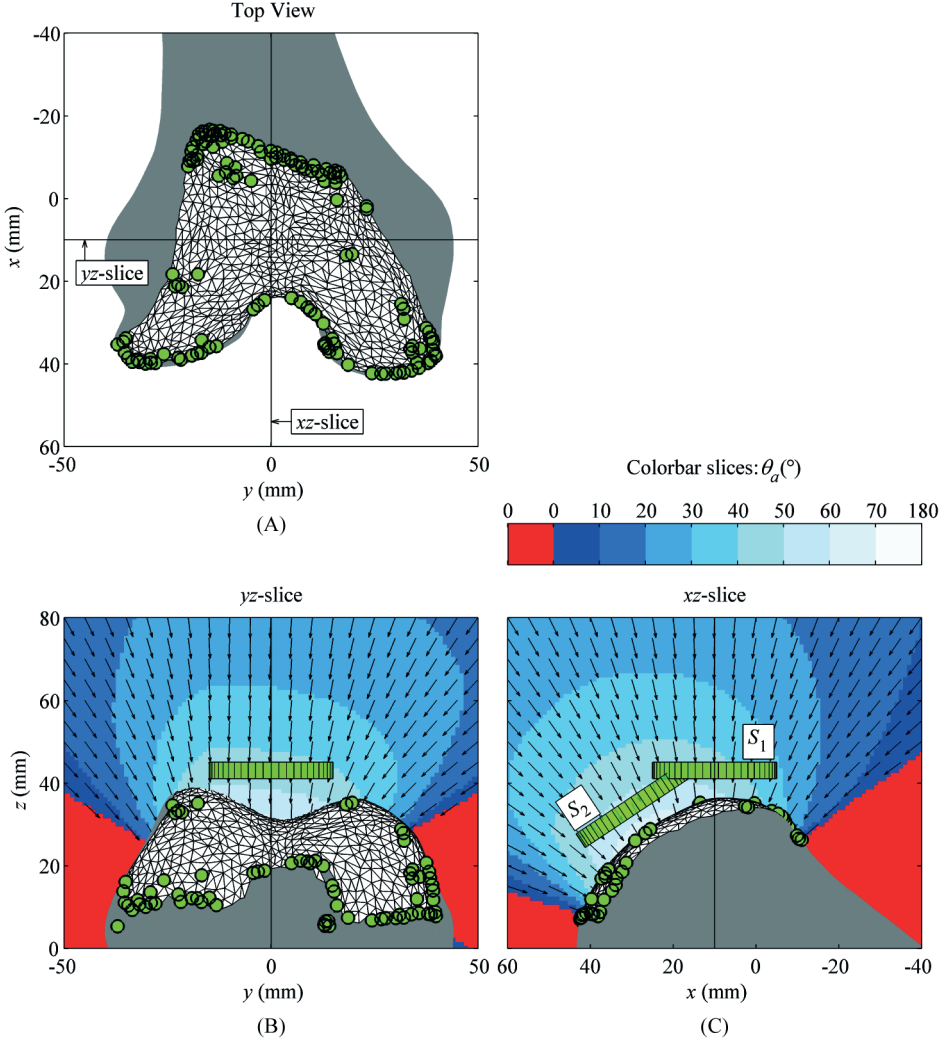


Figure 3. Robustness maps for a guide with basis contact $\mathbf{P}_{c,full}$. The contacts are indicated by the small circles. (A) The top view onto the bony geometry shows all the selected contacts. View (B) and (C) show the robustness maps which are respectively an yz -slice and an xz -slice of the robustness volume. For a certain application point within the robustness maps, the direction of the application line is bounded by a circular cone C_a (as depicted in Figure 2D). The mean direction \mathbf{v}_a and aperture θ_a of C_a is indicated respectively by vector fields and gradient colors. Two locations for the application surface are shown, namely S_1 and S_2 , whereof S_2 is a translation and rotation of S_1 in the xz -plane to a better location and orientation.

the unit sphere \mathbb{S}^2 . The cross product $\mathbf{v} \times \mathbf{d}$ creates a random direction for the moment vector orthogonal to \mathbf{d} ; thereby satisfying Eq. (6). The intensity m of the moment vector is a random value between zero and an upper bound m_{ub} . Without loss of generality, a valid upper bound m_{ub} can be found by only considering convex combinations of the negated contact lines in Eq. (4). Thus, the magnitudes $\lambda_{c,i}$ not only satisfy $\lambda_{c,i} \geq 0$ but also $\sum \lambda_{c,i} = 1$. The length of the moment part in Eq. (4) is the moment intensity equation

$$m = \frac{\left\| \sum \lambda_{c,i} \mathbf{m}_{c,i} \right\|}{\left\| \sum \lambda_{c,i} \mathbf{d}_{c,i} \right\|}. \quad (15)$$

Note that due to constraint 1 of Section 2.2, the direction vectors $\mathbf{d}_{c,i}$ are all directed upward, i.e. they have a positive z -value $(\mathbf{d}_{c,i})_z$. Considering the upward directed $\mathbf{d}_{c,i}$ and convex combinations, the following applies for Eq. (15). The maximum for the numerator is the length of the longest of all $\|\mathbf{m}_{c,i}\|$ and the minimum for the denominator is the smallest of all z -values $(\mathbf{d}_{c,i})_z$. Thus, a valid upper bound is

$$m_{ub} = \frac{\max \left\{ \|\mathbf{m}_{c,i}\| \right\}}{\min \left\{ (\mathbf{d}_{c,i})_z \right\}} \quad (16)$$

Now that random lines can be created by Eqs. (14) and (16), we can return to our objective: measuring the contents of different line spaces in order to determine the contact efficiency η_c and the guide efficiency η_g . The random lines generated by Eq. (14) are checked for containment within the polyhedral convex cones $K_{a,full}$ and K_a . There are several methods to check containment of the random line coordinates within a cone. Fukuda [21] describes a few whereof we use the computationally fastest method which uses a linear program. The number of random lines $h_{a,full}$ and h_a contained within the respective cones gives the line space contents

$$\mu(L_{a,full}) = h_{a,full}, \quad (17)$$

$$\mu(L_a) = h_a. \quad (18)$$

For the random lines contained within K_a it is verified if they can be applied onto S with Eqs. (7)-(9). The number of random lines h_{as} that satisfy these conditions gives the line space content of L_{as}

$$\mu(L_{as}) = h_{as}. \quad (19)$$

The accuracy of the efficiencies η_c and η_g increases with the number of random lines generated. The denominator in both efficiencies (i.e. $\mu(L_{a,full})$) is regarded as a reference set; that is, both efficiencies are maximum when the numerator in Eqs. (12) and (13) equals $\mu(L_{a,full})$. This reference set is used in the determination of the relative error of the Monte Carlo integration [19]

$$\delta\eta_c, \delta\eta_g \approx \frac{1}{\sqrt{\mu(L_{a,full})}}. \quad (20)$$

In Section 4, example PSSGs are optimized on their contact efficiency η_c and assessed on their guide efficiency η_g . The relative errors $\delta\eta_c$ and $\delta\eta_g$ in these calculations are both 0.02.

3.3 Robustness Maps

In this section a graphical tool is presented referred to as *robustness maps* (Figure 3). These maps graphically depict the allowed variation in the application line l_a for a selected contact point set \mathbf{P}_c (e.g. the contact set $\mathbf{P}_{c,full}$ in Figure 3). Hence, the robustness maps are useful in finding a robust location for the application surface \mathcal{S} . For a specific point \mathbf{p}_a in three-dimensional space, the allowed variation in the application line is generally a polyhedral convex cone D_a (Figure 2). For the robustness maps, cones D_a are simplified to circular cones C_a (Figure 2). The next two paragraphs describe how cones D_a and C_a are derived.

3.3.1 Convex Direction Cones

The direction cone for a specific application point \mathbf{p}_a is a polyhedral convex cone D_a (Figure 2) which can be found in the following manner. Considering application point \mathbf{p}_a , the coordinates for every line l_a through that point suffice

$$\mathbf{q}_a(\mathbf{p}_a) = \left\{ \begin{bmatrix} \mathbf{d}_a \\ \mathbf{p}_a \times \mathbf{d}_a \end{bmatrix} \middle| \mathbf{d}_a \in \mathbb{S}^2 \right\}. \quad (21)$$

Here, \mathbf{d}_a can be any point on the surface of the unit sphere \mathbb{S}^2 . The six-dimensional coordinates of $\mathbf{q}_a(\mathbf{p}_a)$ must be within the polyhedral convex cone K_a to keep the surgical guide docked on the bone. Eq. (10) is the extreme ray representation of K_a . A face representation of K_a is used for determination of the directional limits to \mathbf{d}_a and is given by

$$K_a = \{ \mathbf{w}_a \mid \mathbf{N}_a \mathbf{w}_a \geq \mathbf{0} \}. \quad (22)$$

Here, \mathbf{N}_a is a matrix containing the inward normals to the faces of \mathbf{K}_a organized in rows. The conversion of \mathbf{K}_a from ray representation to face representation is nontrivial [22]. Fukuda [23] gives an algorithm for the conversion from one representation to another in both directions. Substitution of Eq. (21) in Eq. (22) gives for specified point \mathbf{p}_a the limits in the six-dimensional line coordinates

$$L_a(\mathbf{p}_a) = \left\{ \mathbf{q}_a \mid \begin{bmatrix} N_{a,11} & N_{a,12} & N_{a,13} \\ N_{a,21} & N_{a,22} & N_{a,23} \\ \vdots & \vdots & \vdots \\ N_{a,m1} & N_{a,m2} & N_{a,m3} \end{bmatrix}, \begin{bmatrix} N_{a,14} & N_{a,15} & N_{a,16} \\ N_{a,24} & N_{a,25} & N_{a,26} \\ \vdots & \vdots & \vdots \\ N_{a,m4} & N_{a,m5} & N_{a,m6} \end{bmatrix} \cdot \begin{bmatrix} \mathbf{d}_a \\ \mathbf{p}_a \times \mathbf{d}_a \end{bmatrix} \geq 0 \right\}. \quad (23)$$

This can be rewritten to obtain the three-dimensional limits that define the direction cone

$$D_a(\mathbf{p}_a) = \{ \mathbf{d}_a \mid \mathbf{G}_a \mathbf{d}_a \geq 0 \} \quad (24)$$

Where, \mathbf{G}_a is a matrix that contains the inward normals to the faces of D_a as rows defined by

$$\mathbf{G}_a = \begin{bmatrix} N_{a,11} & N_{a,12} & N_{a,13} \\ N_{a,21} & N_{a,22} & N_{a,23} \\ \vdots & \vdots & \vdots \\ N_{a,m1} & N_{a,m2} & N_{a,m3} \end{bmatrix} + \begin{bmatrix} N_{a,14} & N_{a,15} & N_{a,16} \\ N_{a,24} & N_{a,25} & N_{a,26} \\ \vdots & \vdots & \vdots \\ N_{a,m4} & N_{a,m5} & N_{a,m6} \end{bmatrix} [\mathbf{p}_a]_{\times}. \quad (25)$$

Here, the cross product $\mathbf{p}_a \times \mathbf{d}_a$ is converted to the matrix multiplication form $[\mathbf{p}_a]_{\times} \mathbf{d}_a$. Eq. (24) gives the direction cone in face representation. This can be transferred backward for visualization purposes to ray representation, as depicted in Figure 2. The ray representation of D_a is given by

$$D_a = \{ \mathbf{D}_a \boldsymbol{\lambda}_a \mid \boldsymbol{\lambda}_a \geq 0 \} \quad (26)$$

Here, \mathbf{D}_a is a matrix containing the extreme rays of D_a as columns.

3.3.2 Circular Direction Cones

The polyhedral convex cone D_a specifies for a single application point \mathbf{p}_a the limits in \mathbf{d}_a (Figure 2). This is rather complex to visualize for a whole volume of application points in \mathbb{R}^3 . Simplification of D_a can be achieved by determining the largest inscribed circular cone C_a contained in D_a , as depicted in Figure 2. Gomez et al. [24] describe a method to determine the directly related largest inscribed spherical circle contained in a convex spherical polygon. This method requires the calculation of the smallest enclosing ball

around the endpoints of the unit normal vectors \mathbf{G}_a . For this purpose we use the ‘minball’ algorithm which is part of an external Matlab toolbox called the Statistical Pattern Recognition Toolbox [25]. For a single point \mathbf{p}_a , cone \mathbf{C}_a is defined by an aperture θ_a (or opening angle) with a maximum of hundred-and-eighty degrees, and a mean direction \mathbf{v}_a . Thereupon, the data can be visualized by gradient maps and vector fields – i.e. robustness maps – as depicted for two slices of the data in Figure 3. Besides simplification, \mathbf{C}_a also further restricts the limits in \mathbf{d}_a . This restriction can be regarded as a safety margin as \mathbf{C}_a is a subset of \mathbf{D}_a .

In Section 4, the robustness maps will be used to optimize the location of the application surface. The optimal application surface \mathbf{S}_2 is located in brighter colors of the robustness maps than the initial application surface \mathbf{S}_1 . Consequently, a surgical guide with \mathbf{S}_2 is more robust and remains docked under larger variation in the line of action of the surgeon’s docking force.

3.4 Robustness Measure

Robustness measure R quantifies the allowed angular variation in the application line at the worst point on the application surface and is created as follows. For a specific point \mathbf{p}_a on the application surface \mathbf{S} , the direction \mathbf{d}_a of the application line has to be within the convex cone

$$\mathbf{D}_{as} = \mathbf{D}_a \cap \mathbf{C}_f. \quad (27)$$

That is, the intersection of the convex cone \mathbf{D}_a defined by Eq. (24) and the local friction cone \mathbf{C}_f . As the friction angle is assumed maximal – i.e. ninety degrees – the local friction cone \mathbf{C}_f is a half space. Cone \mathbf{D}_{as} is simplified to the largest inscribed circular cone \mathbf{C}_{as} in the same manner as described in 3.3.2. The resulting \mathbf{C}_{as} is likewise defined by an aperture θ_{as} and mean direction \mathbf{v}_{as} .

For the robustness measure R , a sufficient number of random points is generated on \mathbf{S} and for each of these points the largest inscribed circular cone \mathbf{C}_{as} is determined. Hence, the robustness measure R is defined as the aperture θ_{as} of the smallest \mathbf{C}_{as} for all the random points. Thereby you always know what angular variation of the application force is minimally allowed on \mathbf{S} . In Section 4, the robustness measure is used to assess example surgical guides.

4 DIMENSIONAL OPTIMIZATION

The measures and graphical tool created in the *robustness framework* (Section 3) are utilized in the following example, where optimal PSSG dimensions are sought for the distal

femur. For the femur shape, we use the mean model from a statistical shape model from a study of Baka et al. [26]. The optimization comprises two steps. In the first step, an optimal contact set \mathbf{P}_c^* with fixed number of contacts k is sought. In the second step, the robustness maps are used to find an optimal location for the application surface \mathcal{S} .

4.1 Contact Set

The contact efficiency η_c is used as function value in the search for an optimal contact set \mathbf{P}_c^* with k contacts. The basis contact set $\mathbf{P}_{c,full}$ is herein used as a superset because every subset of $\mathbf{P}_{c,full}$ is a minimal set. That is, removing any of the contacts of such minimal set would decrease η_c and thus none of the contacts of such minimal set is redundant.

4.1.1 Optimization Method

Optimization of η_c for two-dimensional guides [9] showed that altering the location of one contact can result in local maxima η_c^* . It would therefore be ideal to calculate η_c for all k -numbered contact sets \mathbf{P}_c of $\mathbf{P}_{c,full}$ as it would always result in the global maximum η_c^* . This method is known as brute-force search. For our application, this method is considered too exhaustive to apply though. As an alternative, the contact set \mathbf{P}_c is optimized per contact by brute-force search in the following manner. The optimization initializes with a random k -numbered contact set $\mathbf{P}_c \subseteq \mathbf{P}_{c,full}$. Subsequently, the location of one individual contact is optimized by brute-force search. That is, the function value η_c is calculated for every possible contact location within $\mathbf{P}_{c,full}$ and the location which results in the best η_c is selected. The brute-force search is repeated for every other contact until all are optimized. Subsequently, the resulting contact set \mathbf{P}_c is used as initial set in a following optimization cycle. A number of three cycles is executed to confirm convergence of the optimization.

4.1.2 Results

Figure 7 shows the results of the optimization for even-numbered contact sets ranging from six to eighteen contacts. For each contact set, one hundred thousand random application lines are created to calculate the contact efficiency η_c (the relative error $\delta\eta_c$ equals 0.02). The optimization is converging to an optimum η_c^* for all contact sets, though this optimum is not always reached within one cycle. After about fifteen to twenty iterations, the increase in η_c stays within the error margins for every number of contacts. Furthermore, the optimum η_c^* shows to be increasing with the number of contacts k . This increase shows to be more prominent for low contact numbers, which can be seen in Table 1 by examining η_c^* for six, twelve and eighteen contacts. From six to twelve contacts η_c^* increases with 0.56, whereas from twelve to eighteen contacts η_c^* increases with only 0.14.

4.2 Application Surface

The robustness maps for a guide with basis contact are used to identify an optimal application surface S_2 as alternative for the initial application surface S_1 (Figure 3). The location of S_2 has been obtained by a translation and rotation of S_1 in the xz -plane. Application surface S_2 is located in brighter gradient colors of the robustness maps and consequently more variation is allowed in the application line. Figure 4-6 show the robustness maps for guides with optimum contact P_c^* using respectively six, twelve and eighteen contacts. The robustness maps show that the location of S_2 is also suitable for these contact sets. Table 1 shows the guide efficiency η_g and robustness R corresponding to the contact sets of the figures. As with the contact efficiency η_c , one hundred thousand random application lines are created to calculate the guide efficiency η_g (the relative error $\delta\eta_g$ equals 0.02). Moreover, one thousand random application points are created on the application surface to calculate the robustness R . The increase in η_g and R reflects that the location of S_2 is indeed a more robust location.

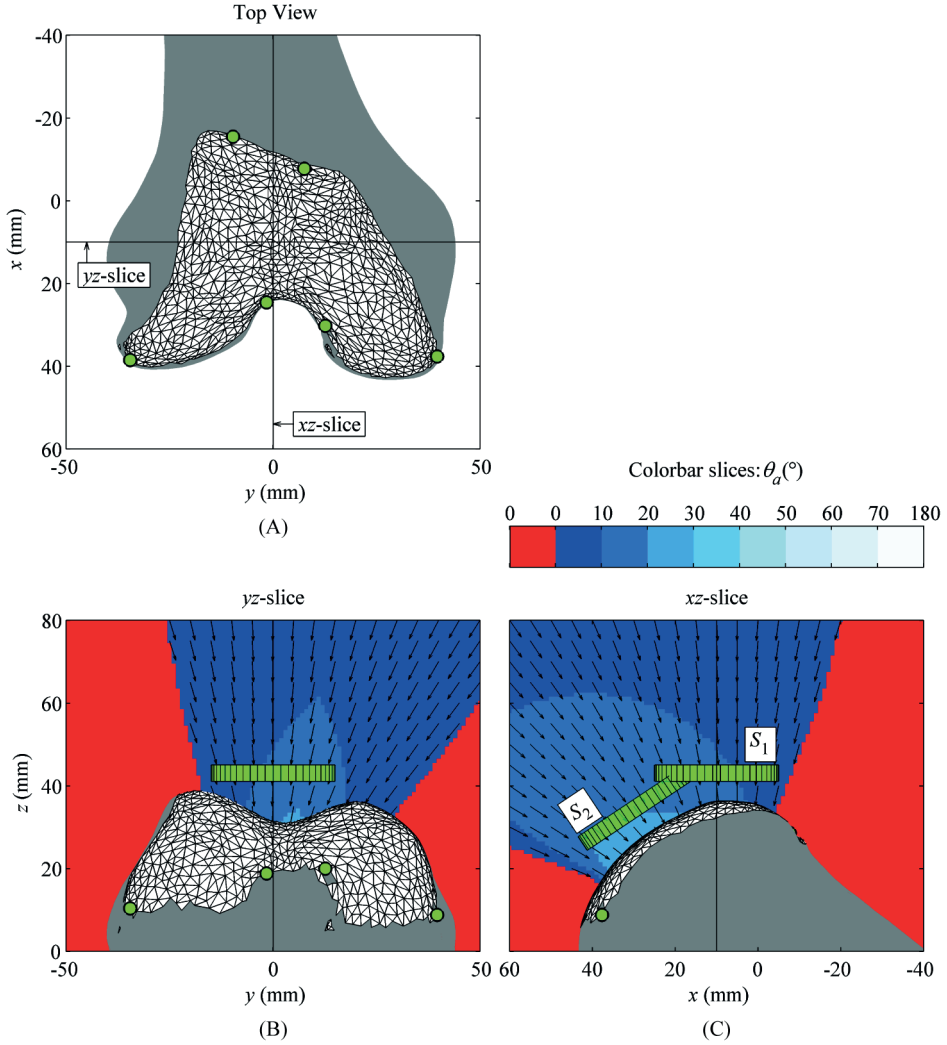


Figure 4. Robustness maps for a guide with six optimized contacts. The contacts are indicated by the small circles. (A) The top view onto the bony geometry shows all the selected contacts. View (B) and (C) show the robustness maps which are respectively an yz -slice and an xz -slice of the robustness volume. For a certain application point within the robustness maps, the direction of the application line is bounded by a circular cone C_a (as depicted in Figure 2D). The mean direction \mathbf{v}_a and aperture θ_a of C_a is indicated respectively by vector fields and gradient colors. Two locations for the application surface are shown, namely S_1 and S_2 , whereof S_2 is a translation and rotation of S_1 in the xz -plane to a better location and orientation.

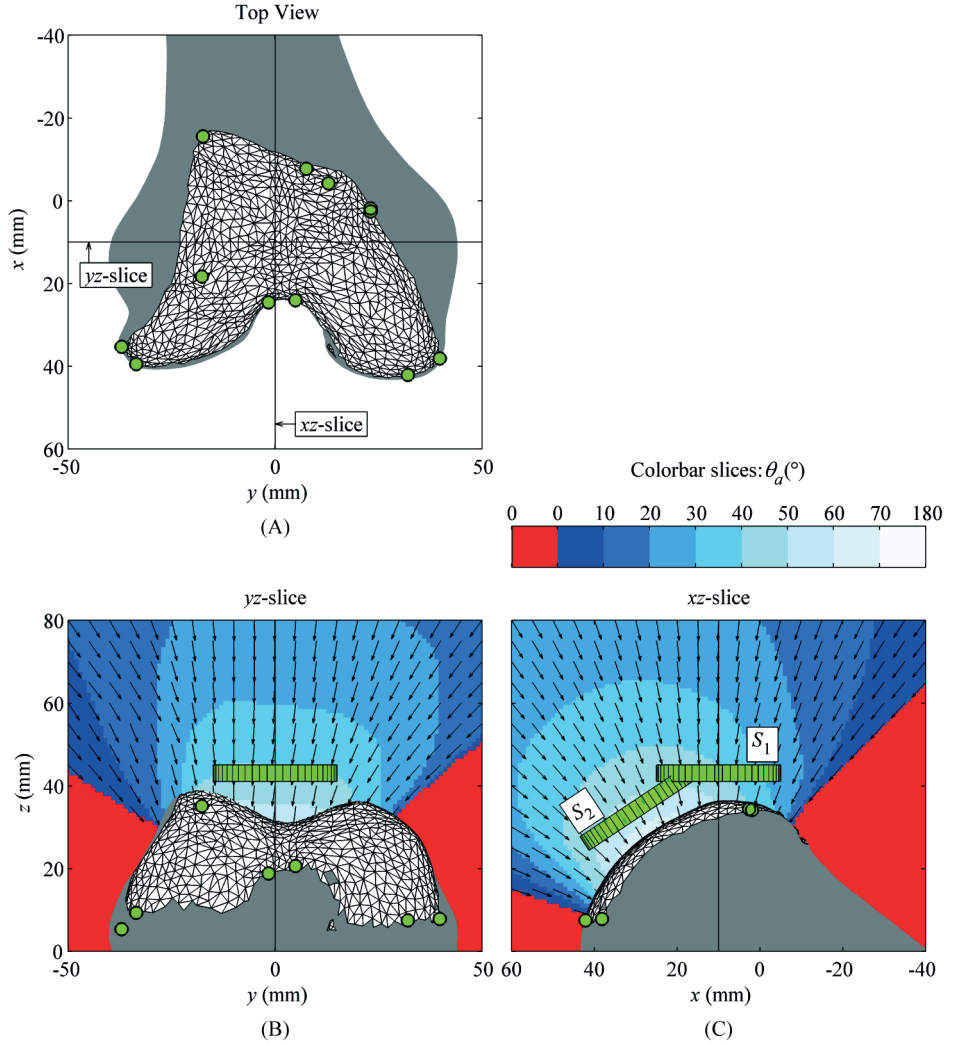


Figure 5. Robustness maps for a guide with twelve optimized contacts. The contacts are indicated by the small circles. (A) The top view onto the bony geometry shows all the selected contacts. View (B) and (C) show the robustness maps which are respectively an yz -slice and an xz -slice of the robustness volume. For a certain application point within the robustness maps, the direction of the application line is bounded by a circular cone C_a (as depicted in Figure 2D). The mean direction \mathbf{v}_a and aperture θ_a of C_a is indicated respectively by vector fields and gradient colors. Two locations for the application surface are shown, namely S_1 and S_2 , whereof S_2 is a translation and rotation of S_1 in the xz -plane to a better location and orientation.

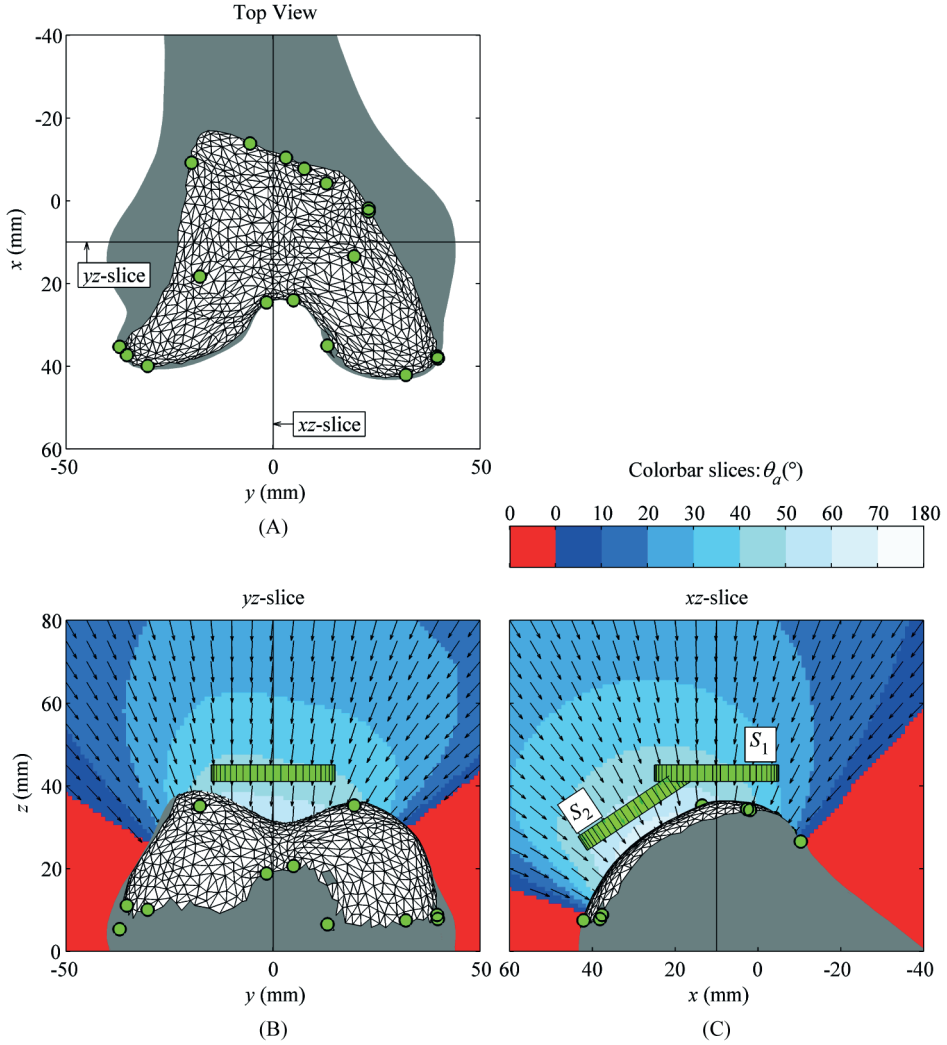


Figure 6. Robustness maps for a guide with eighteen optimized contacts. The contacts are indicated by the small circles. (A) The top view onto the bony geometry shows all the selected contacts. View (B) and (C) show the robustness maps which are respectively an yz -slice and an xz -slice of the robustness volume. For a certain application point within the robustness maps, the direction of the application line is bounded by a circular cone C_a (as depicted in Figure 2D). The mean direction \mathbf{v}_a and aperture θ_a of C_a is indicated respectively by vector fields and gradient colors. Two locations for the application surface are shown, namely S_1 and S_2 , whereof S_2 is a translation and rotation of S_1 in the xz -plane to a better location and orientation.

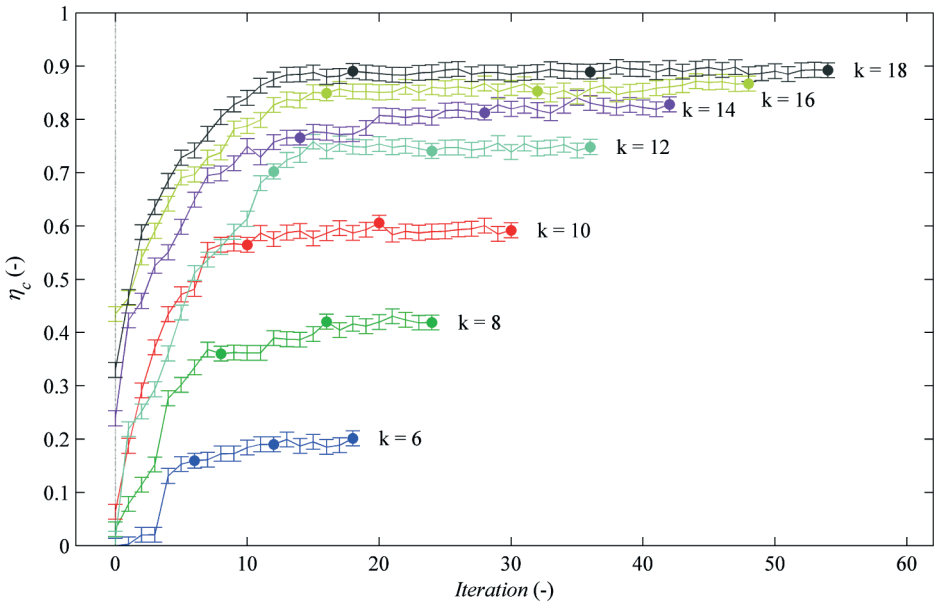


Figure 7. Results of the optimization of η_c for even-numbered contact sets ranging from six to eighteen contacts. The number of contacts is denoted by k . The contacts are optimized one at the time and in three cycles to confirm convergence. The iteration that ends each optimization cycle is denoted by a dot.

Table 2. Measures for a guide with basis contact, and guides with optimized contact with respectively six, twelve and eighteen contacts. Two locations for the application surface, i.e. S_1 and S_2 , are assessed.

Contact set	k	η_c^*	S_1		S_2	
			η_g	R ($^\circ$)	η_g	R ($^\circ$)
Basis	138	1	0.16±0.02	30	0.19±0.02	44
Optimized-6	6	0.18±0.02	0.03±0.02	1	0.07±0.02	10
Optimized-12	12	0.74±0.02	0.14±0.02	24	0.17±0.02	43
Optimized-18	18	0.88±0.02	0.15±0.02	28	0.18±0.02	43

5 DISCUSSION

The robustness framework for surgical guide design created in this article can be used to quantify and graphically present the freedom in the application line of the surgeon's docking force. Though robustness is an important parameter for surgical guide design, research on this topic is scarce. Recently, van den Broeck et al. [27] adopted measures originally created for fixturing and grasping (by Lin et al. [28]) and assessed these for several printed surgical guides. Their measures comprise a translational and rotational stability parameter, which are both dependent on the contact geometry. In the analysis presented in our article, contact is considered redundant when it does not enlarge the allowed variation in the application line. Accordingly, our measures are not affected by redundant contact – in contrast to the measures of van den Broeck et al. Moreover, we chose to take all the dimensions of the surgical guide into consideration, that is the contact geometry \mathbf{P}_c and an application surface \mathcal{S} where the surgeon can push.

In the example of this article, depicted in Figure 2, the surgeon applies a single force onto the application surface. In actual clinical practice, the surgeon may use more than one finger to keep the guide in place. Multiple application forces are indeed allowed onto the surgical guide. When the application lines of these forces are all contained in \mathbf{K}_a , they are accounted for in the efficiency measures η_c and η_g . In fact, some of the application lines may even not satisfy containment in \mathbf{K}_a . As long as the net wrench is contained in \mathbf{K}_a the docking is maintained.

The number of contacts may be an important parameter in the design of configurable PSSGs. Figure 7 shows that the gain in the optimal contact efficiency η_c^* decreases with the number of contacts. With a number of twelve contacts the optimum η_c^* is 0.74 ± 0.02 . Thus, with only a limited number of contacts, the obtained contact efficiency is comparable to full contact. Increasing the number of contacts further somewhat improves η_c^* though at the same time increases the complexity of the PSSG as more contacts need to be configured. Six contacts are minimally needed to fully determine the position of the surgical guide [8]. More contacts results in an over-determined equilibrium and, consequently, deviations (not predicted by the MRI/CT image) may cause problems. When the bone and surgical guide are both rigid, as assumed in this article, rocking may occur. However, the cartilage layer on the bone is relatively soft and thereby may prevent rocking. Though, by the softness of the cartilage the surgical guide might end up in a slightly different position than planned. In the design of surgical guides one can keep this in mind and play with the stiffness of the contacts.

The geometry of the application surface is kept constant throughout this paper. The robustness maps can be used to find a more appropriate geometry for the application

surface. For example, Figure 3-6 show that it would be beneficial to have a curved shape for the application surface in the xz -plane, i.e. an arc which follows the geometry of the bone and the direction vectors of the robustness map. In the yz -plane, a suitable application surface may follow the direction vectors and therewith overlap the concave valley between the condyles. When the application surface would follow the shape of the bone in the yz -plane, the application force may have to be applied at a skew angle at the concave valley.

6 CONCLUSION

Surgical guides for joint replacement surgery are dimensioned to dock in a unique position onto the opposing bone. The docked position is maintained by a geometric fit with the bone and an application force of the surgeon. The allowed variation in the line of action of this application force is referred to as docking robustness. The robustness framework presented in this article can be employed to fully dimension robust surgical guides and to validate existing surgical guides on their robustness. This framework comprises the following quantitative measures and graphical tool. Two efficiency ratios are created to quantify the allowed variation in the application line. Contact efficiency η_c is used when only the contact between guide and bone is considered. Guide efficiency η_g is used when the whole guide is considered including an application surface whereon the surgeon can push. Robustness maps are created to help with finding a robust location for the application surface. The robustness measure R is an intuitive measure defined as the minimally allowed angular deviation at the worst point on the application surface. Optimization of an example surgical guide showed that twelve contacts already results in relatively high contact efficiency, namely 0.74 ± 0.02 (where the maximum of 1.00 is obtained when the guide is designed for full bone-guide contact). Six optimized contacts, on the other hand, seems to be insufficient as the obtained contact efficiency is only 0.18 ± 0.02 . Hence, in designing configurable surgical guides, there is a tradeoff between the complexity of the instrument and its robustness. The robustness maps were used in finding an optimal location for the application surface. These maps can also be used to find a more appropriate shape for the application surface.

7 ACKNOWLEDGMENTS

The authors would like to thank Johannes Maks from the Delft Institute of Applied Mathematics at the Delft University of Technology for his help in finding an upper bound for the moment intensity equation. This research is supported by the Dutch Technology Foundation STW, which is part of the Netherlands Organisation for Scientific Research

(NWO), and which is partly funded by the Ministry of Economic Affairs (project number NIG 10812).

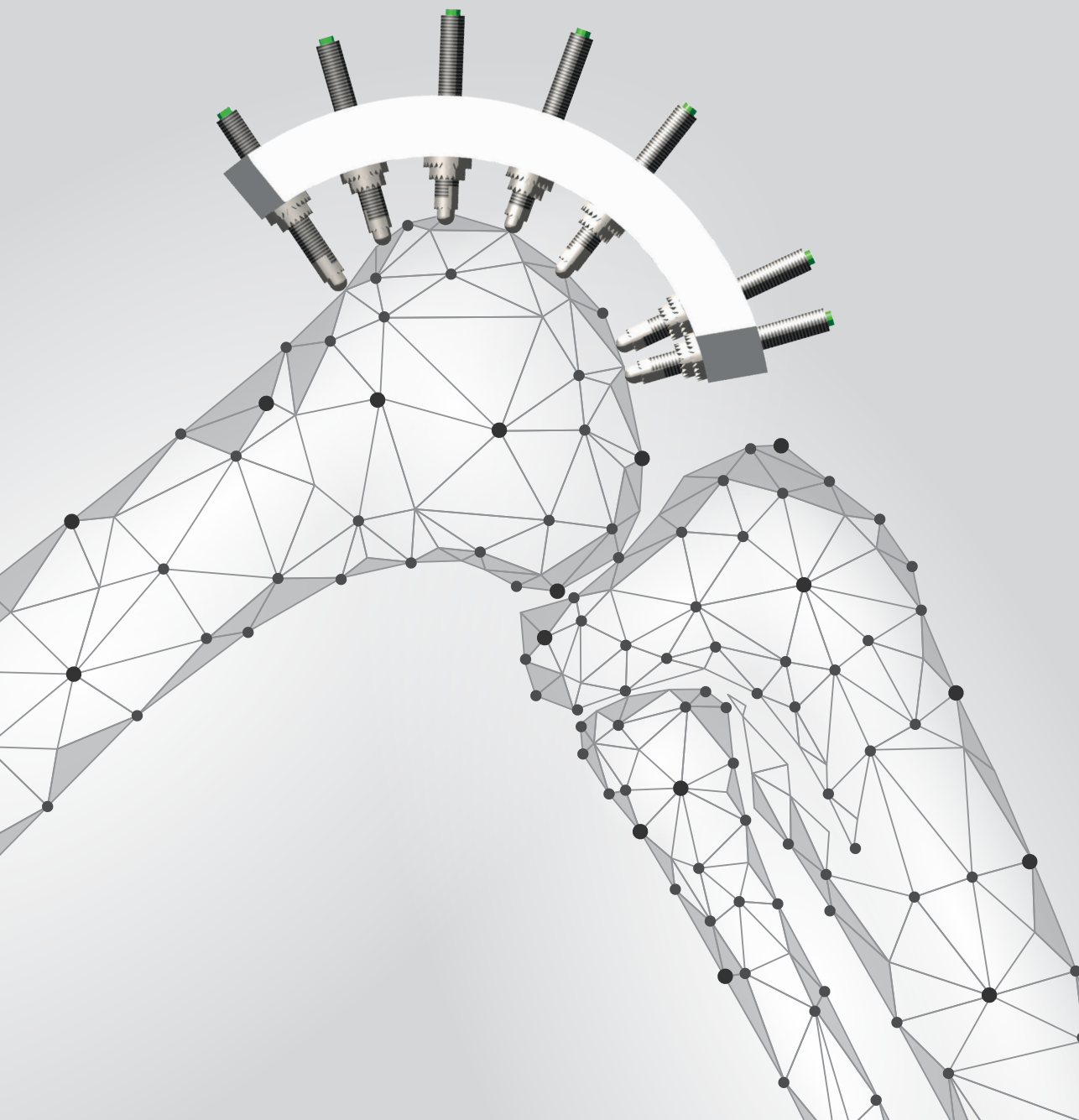
NOMENCLATURE

\mathbf{g}	Gravitational force
\mathcal{S}	Application surface whereon the surgeon applies force
$\mathbf{n}_S, \mathbf{p}_{S0}, r_S$	Outward normal, center and radius of the application surface \mathcal{S}
$\mathbf{p}_a, \mathbf{p}_{c,i}$	Point on \mathcal{S} where the surgeon applies force and the i -th contact point with the bone
B	Region on the bone where contact is allowed
\mathbf{P}_b	Matrix containing the centroids of the triangles of B as columns
\mathbf{P}_c	Matrix containing the contact points $\mathbf{p}_{c,i}$ as columns
$\mathbf{f}_a, \mathbf{f}_{c,i}$	Application force of the surgeon and the i -th contact reaction force
$l_a, l_{c,i}$	Line of action of \mathbf{f}_a and $\mathbf{f}_{c,i}$
$\mathbf{q}_a, \mathbf{q}_{c,i}$	Six-dimensional vector defining the coordinates of the line of action of \mathbf{f}_a and $\mathbf{f}_{c,i}$
$\mathbf{d}_a, \mathbf{d}_{c,i}$	The first three coordinates of \mathbf{q}_a and $\mathbf{q}_{c,i}$ defining the line's direction
$\mathbf{m}_a, \mathbf{m}_{c,i}$	The last three coordinates of \mathbf{q}_a and $\mathbf{q}_{c,i}$ defining the line's moment about the origin (in units of length)
\mathbf{w}_a	Application wrench, i.e. a six-dimensional vector whereof the first three components define the applied force and the last three components define the applied moment (in units of newton \times length)
$\lambda_{c,i}$	Magnitude of the i -th contact force
$\boldsymbol{\lambda}_c$	Vector containing the magnitudes of the contact forces
\mathbf{Q}_{nc}	Matrix containing the negated lines of action $-\mathbf{q}_{c,i}$ as columns
K_a	Application wrench cone
L_a, L_{as}	Application line space without and with consideration of the application surface \mathcal{S}
η_c, η_g	Contact and guide efficiency
D_a, D_{as}	Direction cone for application point \mathbf{p}_a without and with consideration of the application surface \mathcal{S}
\mathbf{N}_a	Inward normals to the faces of cone K_a
\mathbf{G}_a	Inward normals to the faces of cone D_a
C_a, C_{as}	Largest inscribed circular cone in D_a and D_{as}
θ_a, \mathbf{v}_a	Aperture and mean direction of C_a
$\theta_{as}, \mathbf{v}_{as}$	Aperture and mean direction of C_{as}
R	Robustness of the surgical guide

REFERENCES

- [1] Krishnan, S. P., Dawood, A., Richards, R., Henckel, J., and Hart, A. J., 2012, A review of rapid prototyped surgical guides for patient-specific total knee replacement, *J Bone Joint Surg Br*, **94-B**(11), pp. 1457–1461.
- [2] Boonen, B., Schotanus, M. G. M., and Kort, N. P., 2012, Preliminary experience with the patient-specific templating total knee arthroplasty, *Acta Orthop*, **83**(4), pp. 387–393.
- [3] Conteduca, F., Iorio, R., Mazza, D., Caperna, L., Bolle, G., Argento, G., and Ferretti, A., 2012, Are MRI-based, patient matched cutting jigs as accurate as the tibial guides? *Int Orthop*, **36**(8), pp. 1589–1593.
- [4] Nunley, R. M., Ellison, B. S., Zhu, J., Ruh, E. L., Howell, S. M., and Barrack, R. L., 2012, Do patient-specific guides improve coronal alignment in total knee arthroplasty? *Clin Orthop Relat Res*, **470**(3), pp. 895–902.
- [5] Radermacher, K., Portheine, F., Anton, M., Zimolong, A., Kaspers, G., Rau, G., and Staudte, H. W., 1998, Computer assisted orthopaedic surgery with image based individual templates, *Clin Orthop Relat Res*, **354**, pp. 28–38.
- [6] Hafez, M. A., Chelule, K. L., Seedhom, B. B., and Sherman, K. P., 2007, Computer-Assisted Total Knee Arthroplasty Using Patient-Specific Templates: the Custom-made Cutting Guides, *Navigation and MIS in Orthopedic Surgery*, Springer, pp. 182–188.
- [7] Haselbacher, M., Sekyra, K., Mayr, E., Thaler, M., and Nogler, M., 2012, A new concept of a multiple-use screw-based shape-fitting plate in total knee arthroplasty, *J Bone Joint Surg Br*, **94-B**(SUPP XLIV), p. 65.
- [8] Asada, H. and By, A. B., 1985, Kinematic analysis of workpart fixturing for flexible assembly with automatically reconfigurable fixtures, *IEEE J Robot Autom*, **RA-1**(2), pp. 86–94.
- [9] Mattheijer, J., Herder, J. L., Tuijthof, G. J. M., Nelissen, R. G. H. H., Dankelman, J., and Valstar, E. R., 2013, Shaping Patient Specific Surgical Guides for Arthroplasty to Obtain High Docking Robustness, *J Mech Design*, **135**(7), p. 071001.
- [10] Brost, R. C. and Goldberg, K. Y., 1996, A complete algorithm for designing planar fixtures using modular components, *IEEE T Robot Autom*, **12**(1), pp. 31–46.
- [11] Chou, Y. C., Chandru, V., and Barash, M. M., 1989, A mathematical approach to automatic configuration of machining fixtures: analysis and synthesis, *J Eng Ind*, **111**(4), pp. 299–306.
- [12] Markenscoff, X., Ni, L., and Papadimitriou, C. H., 1990, The geometry of grasping, *Int J Robot Research*, **9**(1), pp. 61–74.
- [13] Bicchi, A., 1995, On the closure properties of robotic grasping, *Int J Robot Research*, **14**(4), pp. 319–334.
- [14] Trinkle, J. C., 1992, A quantitative test for form closure grasps, *Proceedings of the 1992 IEEE/RSJ International Conference on Intelligent Robots and Systems* (Vol. 3), pp. 1670–1677.

- [15] Dodou, D., Breedveld, P., and Wieringa, P. A., 2006, The role of geometry in the friction generated on the colonic surface by mucoadhesive films, *J Appl Phys*, **100**(1), p. 014904.
- [16] Bowden, F. P., Moore, A. J. W., and Tabor, D., 1943, The ploughing and adhesion of sliding metals, *J Appl Phys*, **14**(2), pp. 80–91.
- [17] Pottmann, H., Peternell, M., and Ravani, B., 1999, An introduction to line geometry with applications, *Comput Aided Des*, **31**(1), pp. 3–16.
- [18] Mason, M. T., 2001, *Mechanics of Robotic Manipulation*, The MIT Press.
- [19] Weinzierl, S., 2000, Introduction to monte carlo methods, arXiv:hep-ph/0006269.
- [20] Marsaglia, G., 1972, Choosing a point from the surface of a sphere, *Ann Math Stat*, **43**(2), pp. 645–646.
- [21] Fukuda, K., 2004, *Frequently asked questions in polyhedral computation*, Swiss Federal Institute of Technology, Lausanne and Zurich, Switzerland. Available at: <ftp://ftp.ifor.math.ethz.ch/pub/fukuda/reports/polyfaq040618.pdf>.
- [22] Dattorro, J., 2005, *Convex optimization & Euclidian distance geometry*, Meboo Publishing USA.
- [23] Fukuda, K., 1999, *cdd/cdd+ Reference Manual.*, Swiss Federal Institute of Technology, Lausanne and Zurich, Switzerland. Available at: <ftp://ftp.ifor.math.ethz.ch/pub/fukuda/cdd/cddman/cddman.html>.
- [24] Gómez, F., Ramaswami, S., and Toussaint, G., 1997, On removing non-degeneracy assumptions in computational geometry, *Algorithms and Complexity*, Springer, pp. 86–99.
- [25] Franc, V. and Hlavác, V., 2004, *Statistical pattern recognition toolbox for Matlab*, Center for Machine Perception, Czech Technical University, Prague, Czech Republic.
- [26] Baka, N., Kaptein, B. L., de Bruijne, M., van Walsum, T., Giphart, J. E., Niessen, W. J., and Lelieveldt, B. P. F., 2011, 2D–3D shape reconstruction of the distal femur from stereo X-ray imaging using statistical shape models, *Med Image Anal*, **15**(6), pp. 840–850.
- [27] Van den Broeck, J., Wirix-Speetjens, R., and Vander Sloten, J., 2015, Preoperative analysis of the stability of fit of a patient-specific surgical guide, *Comput Methods Biomech Biomed Engin*, **18**(1), pp. 38–47.
- [28] Lin, Q., Burdick, J. W., and Rimon, E., 2000, A stiffness-based quality measure for compliant grasps and fixtures, *IEEE T Robot Autom*, **16**(6), pp. 675–688.



CHAPTER 4

Docking Accuracy of Patient Specific Surgical Guides for Joint Replacement Surgery

Joost Mattheijer^{1,2}

Just L. Herder³

Dion C. Gijswijt⁴

Rob G.H.H. Nelissen¹

Jenny Dankelman²

Edward R. Valstar^{1,2,†}

¹Leiden University Medical Center, Dept. of Orthopaedics, Leiden, The Netherlands

²Delft University of Technology, Dept. of BioMechanical Eng., Delft, The Netherlands

³Delft Univ. of Tech., Dept. of Precision and Microsystems Eng., Delft, The Netherlands

⁴Delft University of Technology, Delft Inst. of Appl. Mathematics, Delft, The Netherlands

ABSTRACT

Patient specific surgical guides (PSSGs) are an aid to align implant components to bony and/or biomechanical landmarks during a surgical procedure. The PSSGs dock with matching geometrical features onto the joint surface. The accuracy of docking is influenced by geometrical deviations between the MRI/CT image used for planning and the actual bone morphology as encountered during surgery. Aim of this study is to introduce a new measure for the quantification of docking accuracy of PSSGs. Docking accuracy is measured by repeated simulated placements of the PSSG. Random bony deviations and a random application force of the surgeon are used as input for each simulation. The pose of the PSSG on the disturbed bone is found by an ICP algorithm modified for our application. In a numerical example with a distal femur, the docking accuracy measure is utilized to find optimal contact locations. The optimization also includes docking robustness to ensure that the surgeon is allowed to vary the application force considerably. The developed method can be used to develop a PSSG that can be docked stable and accurate onto the bone.

Keywords: Docking Accuracy, Docking Robustness, Surgical Guides, Joint Replacement, Workpiece Fixtures, Robotic Grasping.

1 INTRODUCTION

If a joint (e.g. hip, knee, etc.) is severely damaged by osteoarthritis, it can be replaced by a total joint replacement prosthesis. During the surgical replacement procedure – with limited surgical field exposure – part of the affected joint is removed by means of saw cuts and drill holes. The articular bony surfaces are shaped to match the artificial total joint components. To guide the saw cuts and drill holes in an accurate and time efficient manner, Patient Specific Surgical Guides (PSSGs) can be used [1, 2] (otherwise known as Patient Specific Instrumentation). The PSSGs are customized for each specific patient to accommodate for differences in bone morphology [3]. In the ideal situation, the dimensions of the PSSGs are determined for each specific patient and docking on the bone is possible in only one pose, enabling correct alignment of the saw and drilling guidance (Figure 1). The geometric fit of the PSSG combined with an applied force on the PSSG immobilizes the device, enabling the surgeon to use the guidance for accurate bone resections and an optimal implant alignment.

The geometric fit is determined pre-operative by the use of a virtual surface model of the bone, obtained either by Computed Tomography (CT) or Magnetic Resonance Imaging (MRI). Due to segmentation errors the virtual surface model does not represent exactly the actual bone surface as encountered during surgery. These geometric differences will be referred to as *unforeseen bony deviations*. Van den Broeck et al. [4] compared MRI and CT scans with optical scans in a study of human cadaveric knees. For the proximal tibia, they report an absolute error of 0.39 ± 0.37 mm when using MRI and 0.58 ± 0.26 mm when using CT. Rathnayaka et al. [5] report smaller errors for both MRI and CT in a study with cadaveric ovine femora. Although the magnitude of the unforeseen bony deviations is limited, it is uncertain what their effect is on the surgical guide's pose and thus alignment of the saw and drill guidance and subsequent bone cuts.

The accuracy of PSSG placement onto the bone, referred to as *docking accuracy*, is also an important issue in the related field of workpiece fixtures, where objects are fixated in a certain pose to facilitate machining [6-8]. Sakurai [9, 10] and later Xiong [11] employed a method based on screw theory to determine the final pose of workpieces for given errors at the contacts. The resulting final pose is defined by a differential rotation and translation. This method can also be used when there are more contact points than minimally required. Wang et al. [12, 13] implemented statistical methods to determine the docking accuracy.

There are substantial geometric differences when comparing workpiece fixtures with surgical guides and bone. For workpiece fixtures, the contact errors are only in the order of hundredths of millimeters, whereas for surgical guides, the unforeseen bony deviations

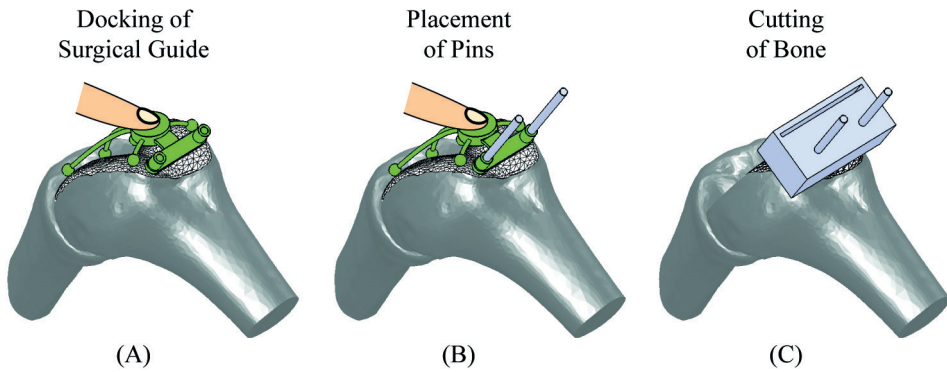


Figure 1. The usage of a surgical guide in knee replacement (adopted from [15]). (A) The guide is immobilized by a pushing force and a geometric fit with the bone surface. (B) The guidance for drilling is used to place pins. (C) A slotted saw block is slid over the pins, enabling a bone cut.

are in the order of tenths of millimeters. On top of that, arthritic deformed bone is characterized by a damaged and worn surface, much rougher than the machined workpieces. Finally, workpiece fixtures are usually designed for minimal contact, whereas PSSGs are primarily in need for robust contact during surgery [14, 15].

The methods of Sakurai, Xiong and Wang are first order methods (i.e. it is assumed that the workpiece can be approximated by an infinite plane at each contact point) and do not account for the curvature of contacting bodies. When these methods are used and the contacting bodies are in fact curved (i.e. anatomic geometries), larger contact errors will worsen the prediction of the final pose [16]. Second order methods enable finding the final pose more accurately, due to the better approximation of the curved surface of the contacting bodies [16-18]. However, first and second order methods are insufficient to find a good estimate when bony deviations occur and therefore numerical methods are proposed. To our best knowledge, there is no method known to determine the accuracy of docking a guide on rough surfaces.

The aim of this paper is to introduce a new measure to quantify docking accuracy of three-dimensional (3D) PSSGs. We modified an Iterative Closest Point algorithm (ICP) [19] by creating additional input, namely a set of bony deviations present underneath each contact. The docking accuracy is determined by repeated simulations of guide placement; a method known as Monte Carlo simulations. In every simulation, random bony deviations and a random application force of the surgeon are generated. The modified ICP algorithm is used to move the surgical guide to a final pose. For comparison the method described by Sakurai [9, 10] and Xiong [11] will be used.

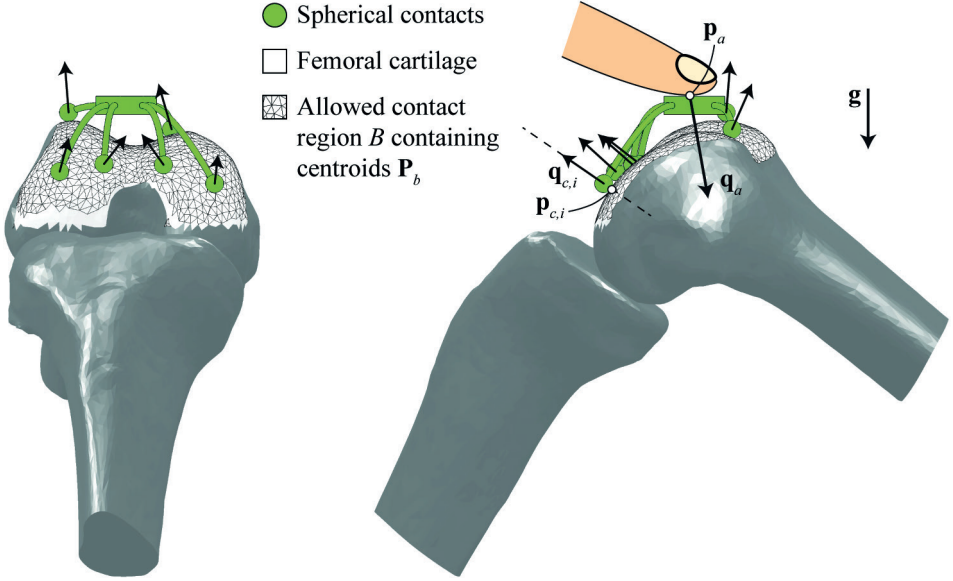


Figure 2. Forces acting on a surgical guide docked onto the femoral cartilage (adopted from [15]). The knee joint is typically directed upwards in joint replacement surgery (as shown here). The point of application \mathbf{p}_a and the line of action \mathbf{q}_a of the surgeon's pushing force are to a certain extent arbitrary. The reaction forces act along lines $\mathbf{q}_{c,i}$, directed normal to the bone. The variation allowed in \mathbf{q}_a depends on the contact point locations $\mathbf{p}_{c,i}$.

2 ROCKING OF SURGICAL GUIDES

A PSSG that is designed to fit on the distal end of the femur (i.e. for placement of the femoral knee component of a total knee prosthesis) will be used as example in this paper. The method created for the quantification of docking accuracy is, however, generic. The tibia and femur are shown in a typical orientation for knee surgery in Figure 2 and will remain as depicted. The method primarily concerns 3D PSSGs, though for visualization purposes a simplified two-dimensional (2D) example will be used.

A PSSG is prone to rocking when more than the minimum required number of contacts are present. This is illustrated in the 2D example of Figure 3. There is a bony deviation underneath contact two, leading to two possible final poses of the surgical guide (i.e. the poses of Figure 3A and D). The final poses of Figure 3B and C are fully determined by three contact points, though the fourth contact point violates a constraint, because it ends up underneath the bone surface. To the best of our knowledge, there is no method available in literature which can be used to quantify docking accuracy for an overdetermined pose.

The following assumptions are made: 1) We assume the bone and guide to be rigid, since PSSGs are generally constructed with relatively stiff materials, and subchondral bone

present in an osteoarthritic joint is hard. Although the cartilage is rather soft and will slightly affect the guide's pose, it will be neglected in this article (in general little or no cartilage is present in osteoarthritic joints), and 2) Friction between the bone and guide is neglected, thus only *fully determined* (final) poses of the PSSG are considered. In vivo surfaces are rather smooth due to slight natural lubrication of tissues.

Constraints used in our simulation are: 1) Region B is a restricted region for contact selection, wherein no contact set can be chosen which results in jamming of the PSSG (Figure 2). The angle between $-\mathbf{g}$ and the outward normal of all mesh triangles within region B is smaller than 75° . This angle is arbitrarily chosen below 90° (i.e. the maximum) to enhance ease of docking/undocking, and 2) To limit the number of possibilities for selection of a contact set to a finite number, contact within region B can only be selected from the triangles' centroids \mathbf{P}_b .

2.1 Final poses

The 2D example of Figure 3 shows what happens when there is an unforeseen deviation in the bony geometry (i.e. not visible at the planning CT / MRI). Three contact points are required for a *fully determined* pose (whereas 6 contact points are required for the 3D analogue) [6]. If the guide has more than minimal contact, there are several possibilities for a fully determined pose [14, 15]. The theoretical number of final poses with minimal contact with the bone can be calculated with the binomial coefficient [20]:

$$C(n, k) = \frac{n!}{k!(n-k)!} \quad (1)$$

This coefficient gives the number of combinations where k objects can be chosen from n objects. For the surgical guide, k is the number of contacts required for a fully determined pose and n the number of contacts the guide contains. For the example of Figure 3, the binomial coefficient equals $C(4, 3) = 4$, and hence, there are theoretically four final poses. However, constraints are violated for some of the final poses by the remaining contact (poses B and C), that is, due to the guide's translation and rotation the remaining contact ends up beneath the bone surface. Whether a final pose is feasible (i.e. does not violate any contact constraints) depends on the bony deviations. In this case, there is only a deviation under contact two, and thus, two of the four final poses are feasible (pose A and D).

The final poses of the 2D example of Figure 3 are derived using the linear method of Sakurai et al. [9]. In this method, it is assumed that the surgical guide has point contact with the bone and that contact occurs along infinite lines (or planes for the 3D analogue).

2.2 Force closure

The docking force is required for complete immobilization of the guide, a condition known as force closure [21]. Which of the final poses the guide ends up in depends on the line of action \mathbf{q}_a of the docking force. For example, the 2D surgical guide of Figure 3 ends up in pose A when force is applied along \mathbf{q}_a^A and in pose D when force is applied along \mathbf{q}_a^D (where the superscript indicates the corresponding pose in Figure 3). The line of action can vary to a certain extent when maintaining the surgical guide's final pose. The allowed variation is determined in the remainder of this section.

The line of action expressed in Plücker coordinates [22] is given by

$$\mathbf{q} = \begin{bmatrix} \mathbf{d} \\ \mathbf{m} \end{bmatrix} = \begin{bmatrix} \mathbf{d} \\ \mathbf{p} \times \mathbf{d} \end{bmatrix} \quad (2)$$

where \mathbf{d} is the line's direction vector and \mathbf{m} the moment vector relative to the origin. The moment \mathbf{m} can be found with the cross product $\mathbf{p} \times \mathbf{d}$, where \mathbf{p} is an arbitrary point on the line (e.g. the contact points $\mathbf{p}_{c,i}$ and application point \mathbf{p}_a in Figure 2). For 2D objects, like the example of Figure 3, we can find the moment with the 2D analog for the cross product $\det(\mathbf{p}, \mathbf{d})$ (which is then a single value m). A wrench \mathbf{w} can be used to define a force along \mathbf{q} [23].

$$\mathbf{w} = \lambda \mathbf{q} = \lambda \begin{bmatrix} \mathbf{d} \\ \mathbf{p} \times \mathbf{d} \end{bmatrix} = \begin{bmatrix} \mathbf{f} \\ \boldsymbol{\tau} \end{bmatrix} \quad (3)$$

where λ is the force magnitude. It should be noted that in general a wrench can be any combination of force \mathbf{f} and torque $\boldsymbol{\tau}$ components. In our case we only consider forces acting along a line, and hence, both the application wrench \mathbf{w}_a and the contact wrenches $\mathbf{w}_{c,i}$ are of the form of Eq. (3). Force closure is present if the summation of wrenches is zero.

$$\sum \lambda_{c,i} \mathbf{q}_{c,i} + \lambda_a \mathbf{q}_a = \mathbf{0}, \quad \forall \lambda \geq 0 \quad (4)$$

Force magnitudes λ are all nonnegative as every force on the guide is compressive. The limits of application line \mathbf{q}_a are found by rewriting Eq. (4).

$$\mathbf{q}_a \in K_a = \{ \mathbf{Q}_{nc} \boldsymbol{\lambda}_c \mid \boldsymbol{\lambda}_c \geq \mathbf{0} \} \quad (5)$$

where matrix \mathbf{Q}_{nc} contains the negated contact line vectors $-\mathbf{q}_{c,i}$ ordered in columns, and vector $\boldsymbol{\lambda}_c$ contains force magnitudes $\lambda_{c,i}$. Geometrically, K_a represents a polyhedral convex cone in wrench space [23]. For spatial objects K_a is six-dimensional whereas for planar objects K_a is three-dimensional. Eq. (5) generally states that the application line \mathbf{q}_a is

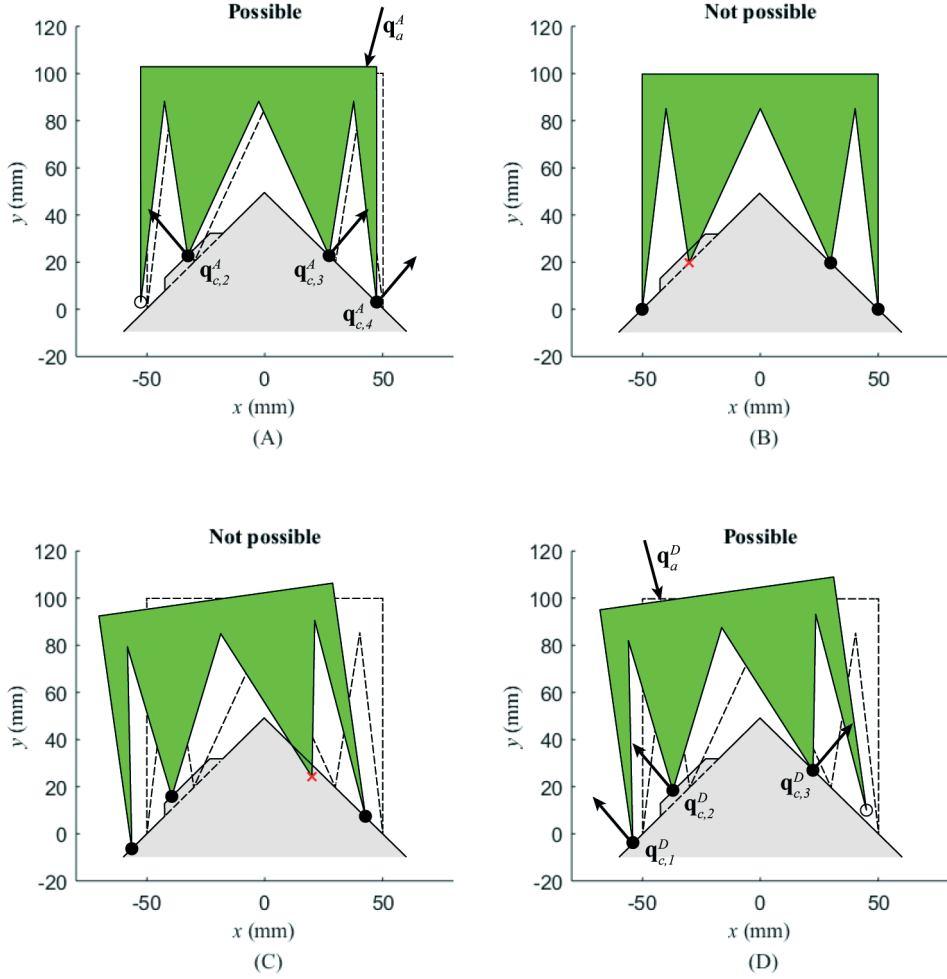


Figure 3. Rocking of a surgical guide on bone with unforeseen bony deviation. At contact two, there is an unforeseen bony deviation indicated by the offset line. The four subfigures show the surgical guide in four final poses, where the pose is fully determined by three contact points. In the final poses, the surgical guides are indicated by a continuous line. In the background of the subfigures, the planned pose is indicated by a dashed line. The contacts are indicated by their contact state with the bone: ● = in contact with the bone; ○ = above bone surface; x = underneath bone surface. Final poses *A* and *D* are feasible as the remaining contact ends up above the bone surface. In contrast, final poses *B* and *C* are not feasible as the remaining contact ends up underneath the bone surface. Application lines \mathbf{q}_a^A and \mathbf{q}_a^D are example lines of action that keep the surgical guide docked in the shown final pose. The direction of the normal forces is indicated by the contact lines $\mathbf{q}_{c,i}$.

allowed when it is contained within K_a . Note that the force magnitude λ_a is eliminated in Eq. (5) as it is only a scaling factor of \mathbf{q}_a , that is, λ_a has no effect on containment within K_a .

The two feasible final poses of the 2D example (Figure 3A and D) have different subsets of contact points contacting the bone, and consequently, there are different limits for \mathbf{q}_a for

the final poses. Figure 4 shows these limits by line spaces L_a^A and L_a^D , representing all application lines allowed, and thus, contained within convex cones K_a^A and K_a^D . The representation of the line spaces in Figure 4 is created by only considering lines with unit direction, in which case the coordinates of \mathbf{q}_a lie on a cylinder with a radius of one. The surface of the cylinder is unrolled – like the label of a tin can – to form the shown representation. Thus, line spaces L_a^A and L_a^D are the unrolled cylinder intersections of convex cones K_a^A and K_a^D . The boundary of the line spaces is curved because of the intersection between the convex cones and cylinder. The direction of \mathbf{q}_a is indicated by an angle instead of x - and y -components. This angle will be referred to as the application angle θ_a and is zero in the negative y -direction (i.e. the downward direction in Figure 3).

For force closure, the coordinates of the application line \mathbf{q}_a must be contained within either L_a^A or L_a^D . Two example application lines \mathbf{q}_a^A and \mathbf{q}_a^D are shown in Figure 3 and 4 wherefore force closure is obtained. In general, when the surgeon docks the guide onto the bone, the application line \mathbf{q}_a of the docking force is random to a certain extent (i.e. the surgeon makes small iterations with the PSSG to find a stable pose). Hence, the chance that the guide ends up in a certain final pose is depending on the corresponding line space size. For our 2D guide, line spaces L_a^A or L_a^D are roughly the same size. When a guide contains more contact points or contacts at other places (e.g. closer together), smaller line spaces may result. The smaller these line spaces are the less likely it is that the guide will end up in the corresponding final pose.

3 MODIFIED ITERATIVE CLOSEST POINT ALGORITHM

The bony deviations force the surgical guide and its contact points to a final pose. The ICP algorithm is used to find this final pose by rotating and translating the surgical guide iteratively. To find the final pose, an extra input of bony deviations is created in the modified ICP algorithm. In the algorithm, for simplicity, the bony deviations are not added to the bone, but to the surgical guide. This is done by virtual adding (or subtracting) a layer to (or from) the spherical contact points (Figure 5B). These thickened or thinned contact points will be referred to as *bony deviation spheres*. In the final pose, the surgical guide is oriented such that the bony deviation spheres make contact with the undisturbed bone (Figure 5C). The final pose is not influenced by shifting the bony deviations from the bone to the surgical guide (Figure 5C).

In a normal ICP algorithm, every point in the first set is matched to the nearest point in the second set. The distance between these matched points is subsequently minimized in the iterative process of the algorithm (for details see [19]). In our modified ICP algorithm, a match is made between the closest points on the undisturbed bone $\mathbf{p}_{b,i}$ and bony deviation spheres $\mathbf{p}_{d,i}$ (Figure 5B). The closest points on the undisturbed bone $\mathbf{p}_{b,i}$ are the

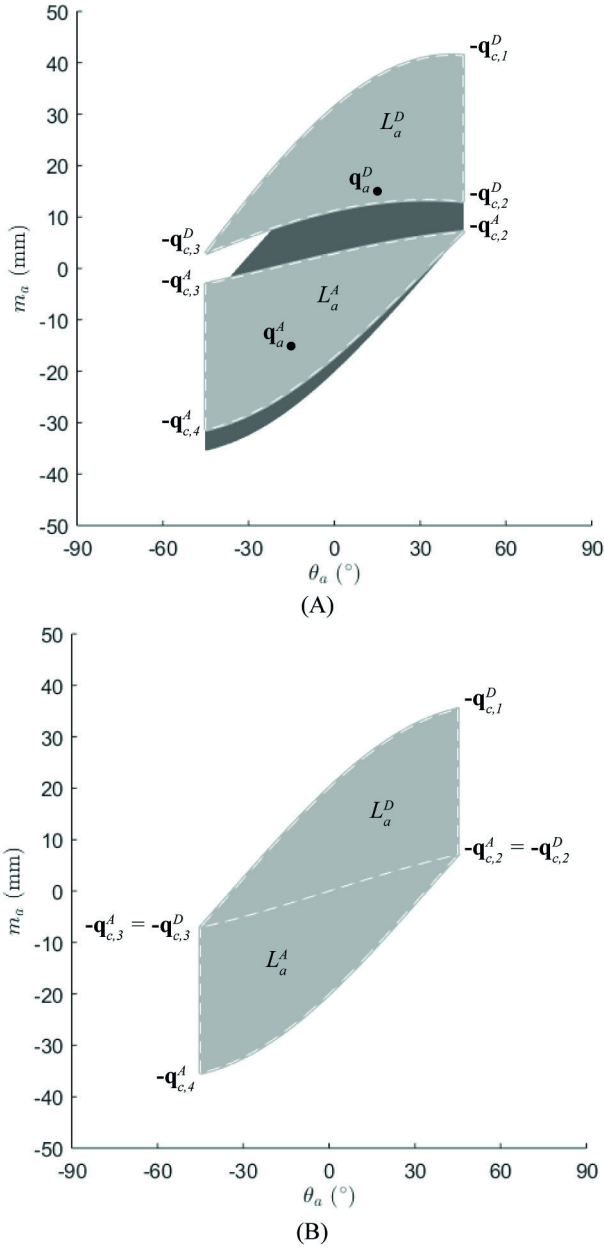


Figure 4. (A) Line spaces L_a^A and L_a^D indicating the limits of the line of action \mathbf{q}_a applied on the surgical guide of Figure 3. The superscript in the lines of action and line spaces indicate the corresponding final pose in Figure 3. The two line spaces L_a^A and L_a^D are respectively spanned by the contact lines $\mathbf{q}_{c,i}^A$ and $\mathbf{q}_{c,i}^D$. Two example application lines \mathbf{q}_a^A and \mathbf{q}_a^D are shown, which are also shown in Figure 3. These application lines \mathbf{q}_a^A and \mathbf{q}_a^D can vary within the limits of their own line space. (B) Line spaces L_a^A and L_a^D when the unforeseen bony deviation depicted in Figure 3 is infinitesimally small. The line spaces merge and completely cover the line space of the planned pose L_a (indicated dark gray in top figure and located behind L_a^A and L_a^D).

closest points from each contact center $\mathbf{p}_{c0,i}$, which can be determined with a signed distance algorithm [24]. Note that this point can be anywhere on the triangular mesh and not necessarily on a triangle's corner point. The closest points on the bony deviation spheres $\mathbf{p}_{d,i}$ lie on the lines between $\mathbf{p}_{c0,i}$ and $\mathbf{p}_{b,i}$, and are calculated as follows.

$$\mathbf{p}_{d,i} = \mathbf{p}_{c0,i} - (r_{c,i} + e_{d,i}) \mathbf{n}_{b,i}, \quad (6)$$

where

$$\mathbf{n}_{b,i} = \frac{1}{s_i} (\mathbf{p}_{c0,i} - \mathbf{p}_{b,i}). \quad (7)$$

Here, $r_{c,i}$ is the radius of the contact sphere, $e_{d,i}$ is the size of the bony deviation, $\mathbf{n}_{b,i}$ is the outward normal of the bone at $\mathbf{p}_{b,i}$, and s_i the signed distance between $\mathbf{p}_{c0,i}$ and the bone. Note that when a bony deviation sphere penetrates the bone, $\mathbf{p}_{d,i}$ is actually the furthest penetrating point. The outward normals $\mathbf{n}_{b,i}$ are also used as plane normals in the point-to-plane minimization process of ICP. When the ICP algorithm is finished, the surgical guide is in the final pose and the matched points of the bony deviation spheres $\mathbf{p}_{d,i}$ and bone $\mathbf{p}_{b,i}$ intersect.

4 DOCKING ACCURACY USING MONTE CARLO SIMULATIONS

A rotational docking accuracy measure A_θ and translational docking accuracy measure A_v are created to determine prior to the actual placement (i.e. before surgery), how accurate the surgical guide can be docked onto the bone. The docking accuracy will be derived by a Monte Carlo simulation, wherein the docking is repeatedly simulated for different bony deviations \mathbf{e}_b and a different application line \mathbf{q}_a . In every repetition of the Monte Carlo simulation, a new set of random bony deviations \mathbf{e}_b and a new random application line \mathbf{q}_a is created. The random bony deviations \mathbf{e}_b are scalar signed distances drawn from a normal distribution. The application line \mathbf{q}_a is randomized with random direction \mathbf{d}_a and random moment \mathbf{m}_a (according to the methods described in [15]). The final pose is subsequently determined as follows:

- 1) The random application line \mathbf{q}_a is checked for containment within the wrench cone K_a of the planned pose. In the planned pose, every contact makes contact with the undisturbed bone.
- 2) If $\mathbf{q}_a \in K_a$, a minimal subcone K_a^i is searched wherein \mathbf{q}_a is contained. This minimal subcone K_a^i corresponds to a minimal contact set (i.e. six contacts).

- 3) The modified ICP algorithm is used to find the final pose where the bony deviation spheres – of the minimal contact set – are in contact with the undisturbed bone (as depicted in Figure 5). The output of the algorithm is a translation vector \mathbf{t} and a rotation vector $\mathbf{\theta}$ (i.e. axis-angle representation [23]).
- 4) The found final pose is checked for violation of any contact constraints, that is, the bony deviation spheres of the remaining contacts are checked for penetration with the undisturbed bone.
- 5) When penetration occurs, the final pose is not feasible. Steps 2-4 are repeated until a feasible final pose is found.

The process above is repeated until n application lines have resulted in n feasible final poses. The more final poses, the better the Monte Carlo simulation will estimate docking accuracy. The simulation results in a distribution of n feasible final poses.

Measures A_θ and A_v are created in a similar way, so for brevity, we will only explain the rotational docking accuracy A_θ . The magnitudes of all the rotation vectors $\mathbf{\theta}$ form a half distribution, because all values are positive. The dispersion D_θ of this half distribution is determined by taking the eightieth percentile of the observed rotation vectors $\mathbf{\theta}$. This is a similar measure for dispersion as the more familiar inter-decile range, which is used to quantify the dispersion of distributions that are *not* half. The rotational docking accuracy A_θ is then defined as the inverse of dispersion D_θ , that is $A_\theta = D_\theta^{-1}$.

The standard error in A_θ and D_θ are determined by bootstrapping methods [25]. Hereto, the rotation vector magnitudes are resampled, in order to recalculate A_θ and D_θ . Recalculation is done a number of times (we will use one thousand repetitions), and subsequently, the standard error is defined as the standard deviation of all resulting A_θ 's or D_θ 's.

5 DIMENSIONAL OPTIMIZATION

The rotational docking accuracy measure A_θ is now used in an example, where we optimize the contact set \mathbf{P}_c^* of a PSSG. The guide is planned to dock onto the distal femur shown in Figure 2. This bone model is a mean statistical shape adopted from [26]. Alongside A_θ , the contact efficiency measure η_c from [15] is used to ensure that the surgical guide can be docked in a stable manner (we refer to [15] for details on how this measure is calculated).

The number of contacts is set to twelve as this has shown to lead to relatively high contact efficiency η_c [15]. The rotational docking accuracy A_θ and contact efficiency η_c are

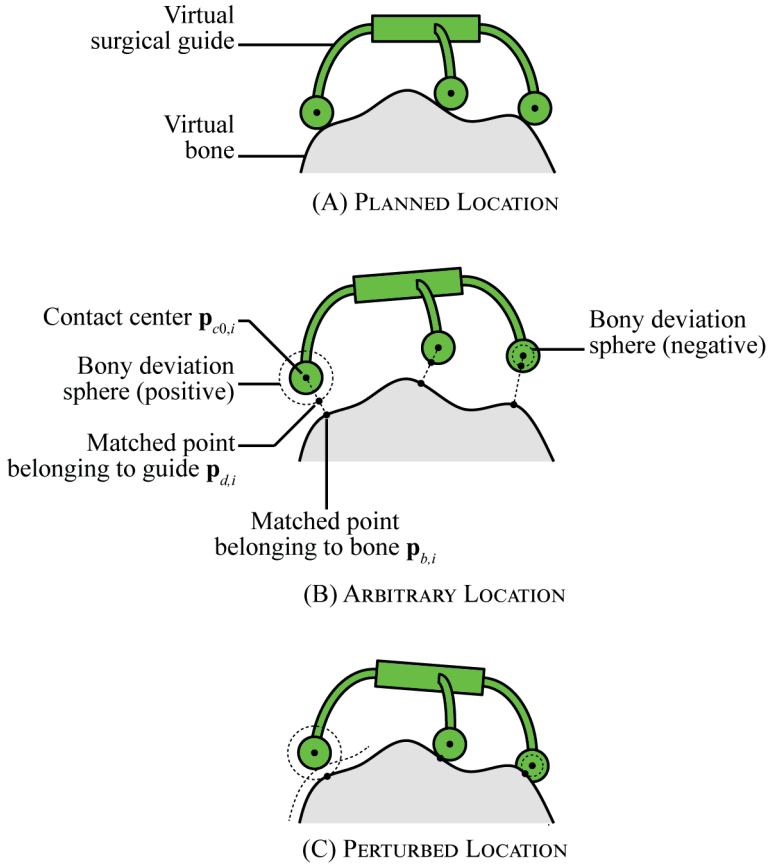


Figure 5. Point matching for the modified ICP algorithm. (A) The surgical guide is posed as planned. (B) The surgical guide is in an intermediate pose at an iteration of the ICP algorithm. A point match is made between points belonging to the bone and points belonging to the guide. The matched points belonging to the bone $\mathbf{p}_{b,i}$ are the closest points to contact centers $\mathbf{p}_{c0,i}$. The bone offset spheres are an offset from the contacts with an offset value equal to the bony deviation. The matched points belonging to the guide $\mathbf{p}_{d,i}$ are the intersection between the bony deviation spheres and the lines between $\mathbf{p}_{c0,i}$ and $\mathbf{p}_{b,i}$. (C) The surgical guide is in the final pose, which is the result of the minimization with the ICP algorithm. The matched points belonging to the bone and guide intersect with each other.

combined to find a surgical guide that can be stably docked, and at the same time, has low sensitivity to unforeseen bony deviations. The following multi-objective optimization is created to realize this:

$$\max f(\mathbf{P}_c) \text{ subject to } \mathbf{P}_c \in \mathbf{P}'_c \quad (8)$$

$$f(\mathbf{P}_c) = w_1 A_\theta(\mathbf{P}_c) + w_2 \eta_c(\mathbf{P}_c) \quad (9)$$

The weight factors w_1 and w_2 are included to scale the two objectives. Weight factor w_2 is set to one, such that $w_2 \cdot f_2$ equals one when the contact efficiency is one (i.e. maximal). Weight factor w_1 is set to $\pi/18$, such that $w_1 \cdot f_1$ is one when dispersion D_θ is $\pi/18$ radians (i.e. ten degrees). The diameter of the contacts is set to 5 mm. The standard deviation (SD) of the bony deviations is set to 0.5 mm, which is in the same order as reported by van den Broeck et al. [4]. The number of random application lines is set to 100.000 for calculation of η_c and to 300 for calculation of A_θ . We use far less application lines for A_θ as the calculation of A_θ is very time consuming (about 15 min for one contact set). The relative error of the Monte Carlo integration in the calculation of η_c is about 0.02 [15, 27]. The standard error in the calculation of D_θ is about 0.007 radians (i.e about 0.4°) [25].

Altering the locations of contact with the bone can be expected to result in local minima of the combined objective function f . Hence, it would be ideal to calculate f for all contact sets with twelve contacts (i.e. brute-force search). However, this would be too time expensive for our application. Instead, contacts in \mathbf{P}_c are optimized one at the time as follows. An initial contact set \mathbf{P}_c is selected randomly from the basis contact set \mathbf{P}_c [14, 15]. The basis contact set \mathbf{P}_c excludes the centroids from \mathbf{P}_b that do not contribute to the robustness. An advantage of this is that every subset of \mathbf{P}_c only contains contacts that contribute the robustness as well. Subsequently, in every iteration the location of one contact is optimized (also selected from \mathbf{P}_c). Hereto, first η_c is determined for all possible locations of the individual contact.

The three locations for the individual contact that result in the largest η_c are further investigated by calculating the combined objective function f . The combined objective function f is also calculated for the initial location of the contact. The contact is set to the location that results in the largest of the four values f . The remaining contacts are optimized in the same fashion until the complete contact set \mathbf{P}_c is optimized. This contact set \mathbf{P}_c is then selected as the initial set in a subsequent optimization cycle. The optimization is performed for three cycles, enabling us to examine whether the method converges.

5.1 Results

The optimization results for a surgical guide with twelve contact points are shown in Figure 6. Instead of the rotational docking accuracy, the rotational dispersion is shown, quantified in degrees. The final poses in the derivation of rotational dispersion are found by our modified ICP algorithm (Sec. 3-4). For comparison, also the *linear rotational dispersion* is included. The method to derive the linear rotational dispersion is as described in Sec. 4, with the difference that step 2-5 are interchanged with the linear method described by Sakurai [9, 10] and Xiong [11].

The dispersion D_θ decreases in the first iterations and then fluctuates around five degrees. The contact efficiency η_c increases over the iterations to a value of about 0.6. This is a bit less than the 0.75 found by Mattheijer et al. [15], though it should be noted that they only optimized for robustness. The objective is optimal at the twenty-fifth iteration ($f^* = 2.979$). The rotational dispersion is 4.2 ± 0.3 degrees and the contact efficiency is 0.62 ± 0.02 . For this iteration, the linear rotational dispersion is with 3.8 ± 0.2 degrees quite close to the ICP rotational dispersion, but is far off for other iterations. Figure 7 shows dispersions derived for the same guides as Figure 6, though the standard deviation of bony deviations is now set to one hundredth of the original value (i.e. 0.005 mm instead of 0.5 mm). The result is that the dispersion values of the ICP method and the linear method are much closer to each other; the error bars of the two methods are nearly identical (Figure 7).

6 DISCUSSION

This article presents new measures for rotational and translational docking accuracy of surgical guides. The measures can be used to optimize contact geometry dimensions such that accurate placement of surgical guide (PSSG) onto the bone is facilitated. Besides accuracy, it is beneficial to have a surgical guide that is robust, i.e. large variation is allowed in the line of action of the applied force. Docking accuracy and docking robustness are combined to obtain a surgical guide that can be docked accurate and stable onto the bone.

Surgical guides generally contain more contact points than minimally required, in order to obtain a robust fit [14, 15]. Our method to derive docking accuracy is suitable for more than the minimally required number of contact points. Since there are generally multiple final poses possible giving a geometric fit, the final pose the surgical guide ends up depends on the applied docking force. In our method, the final pose can be found for known bony deviations and known docking force.

The modified ICP algorithm used finds the final pose iteratively. In each iteration, a signed distance function determines the distance of the contact points to the bony geometry [24]. In our method, an exact final pose is found due to the implementation of the signed distance function. In the first and second order methods found in literature [9, 17, 18], the final pose is approximated. The inclusion of the signed distance function also enabled us to use spherical contacts instead of point contacts.

What we generally observe when the linear method is used is that the bony deviations *tessellate* the wrench space (Figure 4). When the bony deviations underneath the contacts decrease to infinitesimal small bony deviations, the contact lines will approach the contact

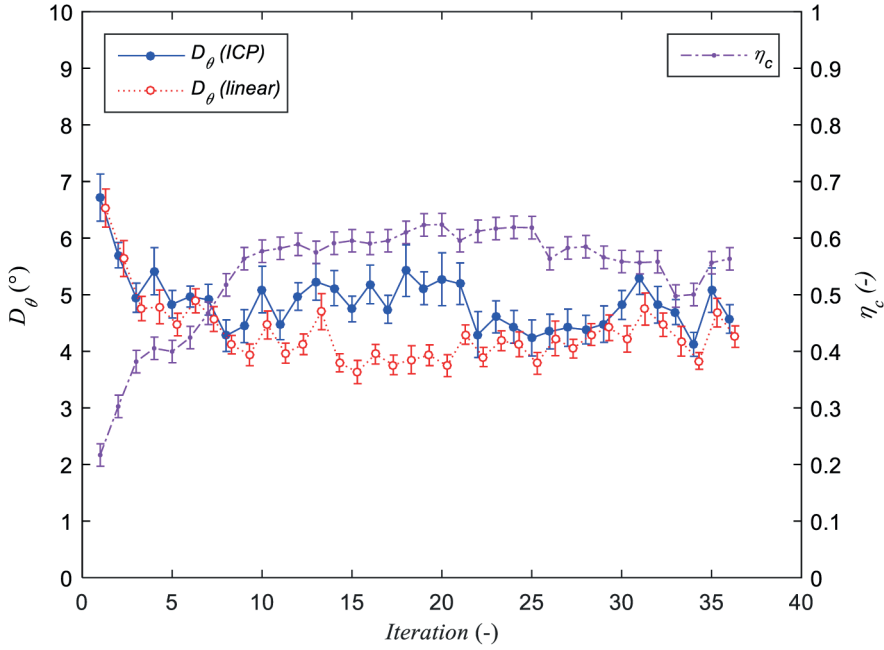


Figure 6. Optimization results for a surgical guide with twelve contacts. The bony deviations are set to a SD of 0.5 millimeter. The dispersion D_θ calculated with ICP is indicated by the filled dots and continuous line. The dispersion D_θ calculated with the linear method is indicated by the open dots and dotted line. The contact efficiency η_c is indicated by the points and the dash-dotted line.

lines corresponding to the planned pose. Consequently, the separate line spaces in Figure 4A will merge into one larger line space (figure 4B) identical to the line space of the planned pose L_a (indicated dark gray in Figure 4A and located behind the line spaces L_a^A and L_a^D).

The tessellation of wrench space by known bony deviations can be explained as follows. The possible final poses can be determined by a linear program [[9], page 75], [11]. By duality of this linear program, it can be shown that polyhedral cone K_a of the wrench space can be decomposed into simplicial cones, i.e. cones for which the corresponding matrix \mathbf{Q}_{nc} is nonsingular. Thus, for the 2D example of Figure 3 \mathbf{Q}_{nc}^A and \mathbf{Q}_{nc}^D are nonsingular. The simplicial cones are a tessellation of K_a . The tessellation phenomenon is known as the basis decomposition theorem and was first described by Walkup and Wets [[28], page 471]. We refer the reader to Loera et al. [[29], page 13] for more details on the theorem. The consequence of the wrench space tessellation by known bony deviations is twofold: (1) a known application line will always lead to one final pose; (2) the limits for the application line are only slightly affected by the bony deviations. The line spaces joined

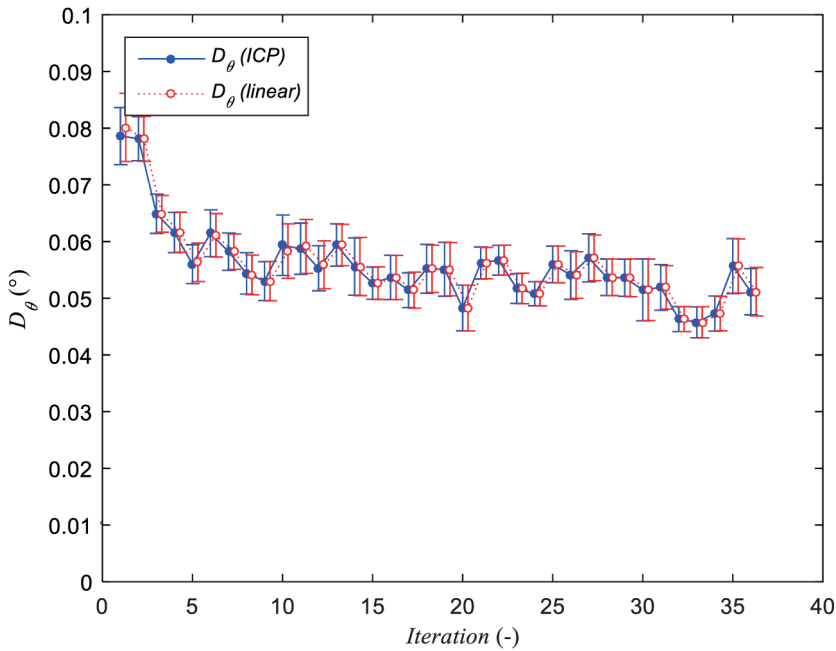


Figure 7. Dispersion results when the bony deviations are changed to a SD of 0.005 mm. The dispersion D_{θ} calculated with ICP is indicated by the filled dots and continuous line. The dispersion D_{θ} calculated with the linear method is indicated by the open dots and dotted line.

together remains roughly the same in shape and size as the line space of the planned pose.

Despite the accurately found final poses, the modified ICP algorithm is rather slow. When using the modified ICP algorithm, the calculation of docking accuracy takes about fifteen minutes. In comparison, when using the linear method of Sakurai, the calculation takes less than a minute. Future research needs to be carried out, to compare how methods for finding the final pose of a guide on a morphological complex anatomic structure with soft and hard surfaces, work in practice. We suggest that the algorithms are used on data of many different patients, including patients with very rough arthritic bone surfaces.

7 CONCLUSION

Docking accuracy measures are created for the preoperative optimization of the geometric fit between surgical guides and an opposing joint surface. Surgical guide placement is simulated repeatedly for evaluation of docking accuracy, using random bony deviations and a random application force of the surgeon. Only one final pose of the surgical guide is possible for a known application force. The final poses on the possibly

rough arthritic bone are found precisely using a modified ICP algorithm. The measures can be used for surgical guides having more than the minimum required number of contact points. In an optimization of a surgical guide containing twelve contacts, docking accuracy is combined with docking robustness to find a surgical guide that docks both accurately and stably. For future research we suggest assessing the docking accuracy measure in practice on a large patient group including severe arthritic bone.

8 ACKNOWLEDGMENTS

Competing interest: None declared.

Funding: This work is supported by the Dutch Technology Foundation STW, which is part of the Netherlands Organization for Scientific Research (NWO), and which is partly funded by the Ministry of Economic Affairs [Grant number NIG 10812].

Ethical approval: Not required.

9 REFERENCES

- [1] Krishnan, S. P., Dawood, A., Richards, R., Henckel, J., and Hart, A. J., 2012, A review of rapid prototyped surgical guides for patient-specific total knee replacement, *J Bone Joint Surg Br*, **94-B**(11), pp. 1457–1461.
- [2] Nunley, R. M., Ellison, B. S., Zhu, J., Ruh, E. L., Howell, S. M., and Barrack, R. L., 2012, Do patient-specific guides improve coronal alignment in total knee arthroplasty? *Clin Orthop Relat Res*, **470**(3), pp. 895–902.
- [3] Mahfouz, M., Abdel Fatah, E., Bowers, L., and Scuderi, G., 2012, Three-dimensional Morphology of the Knee Reveals Ethnic Differences, *Clin Orthop Relat Res*, **470**, pp. 172–185.
- [4] Van den Broeck, J., Vereecke, E., Wirix-Speetjens, R., and Vander Sloten, J., 2014, Segmentation accuracy of long bones, *Med Eng Phys*, **36**(7), pp. 949–953.
- [5] Rathnayaka, K., Momot, K. I., Noser, H., Volp, A., Schuetz, M. A., Sahama, T., and Schmutz, B., 2012, Quantification of the accuracy of MRI generated 3D models of long bones compared to CT generated 3D models, *Med Eng Phys*, **34**(3), pp. 357–363.
- [6] Asada, H. and By, A. B., 1985, Kinematic analysis of workpart fixturing for flexible assembly with automatically reconfigurable fixtures, *IEEE J Robot Autom*, **RA-1**(2), pp. 86–94.
- [7] Brost, R. C. and Goldberg, K. Y., 1996, A complete algorithm for designing planar fixtures using modular components, *IEEE T Robot Autom*, **12**(1), pp. 31–46.

- [8] Chou, Y. C., Chandru, V., and Barash, M. M., 1989, A mathematical approach to automatic configuration of machining fixtures: analysis and synthesis, *J Eng Ind*, **111**(4), pp. 299–306.
- [9] Sakurai, H., 1990, Automatic setup planning and fixture design for machining, Ph.D. thesis, Massachusetts Institute of Technology.
- [10] Sakurai, H., 1992, Automatic setup planning and fixture design for machining, *J Manuf Syst*, **11**(1), pp. 30–37.
- [11] Xiong, Y. and Xiong, X., 2007, Algebraic structure and geometric interpretation of rigid complex fixture systems, *IEEE T Autom Sci Eng*, **4**(2), pp. 252–264.
- [12] Wang, M. Y., 2000, An optimum design for 3-D fixture synthesis in a point set domain, *IEEE T Robot Autom*, **16**(6), pp. 839–846.
- [13] Wang, M. Y., 2002, Characterizations of localization accuracy of fixtures, *IEEE T Robot Autom*, **18**(6), pp. 976–981.
- [14] Mattheijer, J., Herder, J. L., Tuijthof, G. J. M., Nelissen, R. G. H. H., Dankelman, J., and Valstar, E. R., 2013, Shaping Patient Specific Surgical Guides for Arthroplasty to Obtain High Docking Robustness, *J Mech Design*, **135**(7), p. 071001.
- [15] Mattheijer, J., Herder, J. L., Tuijthof, G. J. M., and Valstar, E. R., 2015, Docking Robustness of Patient Specific Surgical Guides for Joint Replacement Surgery, *J Mech Design*, **137**(6), p. 062301.
- [16] Carlson, J. S., 2001, Quadratic sensitivity analysis of fixtures and locating schemes for rigid parts, *J Manuf Sci Eng*, **123**(3), pp. 462–472.
- [17] Wang, M. Y., Liu, T., and Pelinescu, D. M., 2003, Fixture kinematic analysis based on the full contact model of rigid bodies, *J Manuf Sci Eng*, **125**(2), pp. 316–324.
- [18] Luo, C., Zhu, L., and Ding, H., 2013, A unified distance function framework for workpiece fixturing modeling and analysis, *IEEE T Autom Sci Eng*, **10**(4), pp. 1166–1172.
- [19] Low, K.-L., 2004, Linear least-squares optimization for point-to-plane ICP surface registration, Tech. rep., Chapel Hill, University of North Carolina.
- [20] Brualdi, R. A., 2009, *Introductory combinatorics*, 5th ed., Pearson Education, Inc.
- [21] Lakshminarayana, K., 1978, Mechanics of form closure, ASME Paper, **78-DET-32**.
- [22] Pottmann, H., Peternell, M., and Ravani, B., 1999, An introduction to line geometry with applications, *Comput Aided Des*, **31**(1), pp. 3–16.
- [23] Mason, M. T., 2001, *Mechanics of Robotic Manipulation*, The MIT Press.
- [24] Baerentzen, J. A. and Aanaes, H., 2005, Signed distance computation using the angle weighted pseudonormal, *IEEE Trans Vis Comput Graphics*, **11**(3), pp. 243–253.
- [25] Efron, B. and Tibshirani, R. J., 1994, *An introduction to the bootstrap*, Chapman and Hall, Inc.

- [26] Baka, N., Kaptein, B. L., de Bruijne, M., van Walsum, T., Giphart, J. E., Niessen, W. J., and Lelieveldt, B. P. F., 2011, 2D–3D shape reconstruction of the distal femur from stereo X-ray imaging using statistical shape models, *Med Image Anal*, **15**(6), pp. 840–850.
- [27] Weinzierl, S., 2000, Introduction to monte carlo methods, arXiv:hep-ph/0006269.
- [28] Walkup, D. and Wets, R., 1969, Lifting projections of convex polyhedra, *Pac J Math*, **28**(2), pp. 465–475.
- [29] De Loera, J. A., Rambau, J., and Santos, F., 2010, *Triangulations: Structures for Algorithms and Applications*, 1st ed., Springer Publishing Company, Inc.



CHAPTER 5

A Novel Intraoperatively Adjustable Patient Specific Surgical Guide for Knee Replacement Surgery

Joost Mattheijer^{1,2}

Tim O. Herrebrugh²

Rob G.H.H. Nelissen¹

Jenny Dankelman²

Edward R. Valstar^{1,2,†}

¹Leiden University Medical Center, Dept. of Orthopaedics, Leiden, The Netherlands

²Delft University of Technology, Dept. of BioMechanical Eng., Delft, The Netherlands

ABSTRACT

During knee replacement surgery, positioning the femoral component is a complex task. Aim of this study is to develop and evaluate a novel patient specific surgical guide, that allows optimizing femoral component positioning.

A surgical guide is designed containing spring plungers, which can be configured to have a geometric fit with bone. The spring plungers contain a mechanism to visualize bone contact. Surgeons can use the visual feedback to remove spring plungers disturbing the fit. We assessed the surgical guide with non-experts ($n = 14$) and experts ($n = 2$). They were asked to place the guide on a plastic bone model. Either none or one spring plunger was set with additional disturbance. The users were asked to detect disturbance, and if present, remove it and reposition the guide.

Non-experts and experts correctly removed *any* spring plunger in 69% and 81% of cases, respectively, and precisely the *disturbing* spring plunger in 27% and 69% of cases. When disturbance was initially absent, non-experts recognized this in 62% and experts in 92% of cases. Disturbances present in the *final position* caused, for non-experts, significant increase in translational error ($p = 0.03$) and rotational error ($p = 0.02$). For experts, this caused no significant increase in translational error ($p = 0.13$), whereas rotational error was significantly larger ($p = 0.04$).

In conclusion, although the surgical guide supported experts in recognizing disturbance, non-experts were mostly unable to recognize this. Hence, when the surgical guide is developed further for clinical practice, extensive training is recommended.

Keywords: Patient Specific, Surgical Guides, Joint Replacement, Adjustable, Configurable.

1 INTRODUCTION

Failure of knee prostheses (i.e. end-point revision surgery) is associated with malalignment of prosthetic components [1]. In the Netherlands, 27.1% of major knee revision surgeries are related to malalignment of the prosthesis [2]. Positioning of the femoral component in knee replacement surgery is a complex task, because anatomical reference points (e.g. the hip center) are difficult to assess. This study focuses on a modality to optimize positioning of the femoral component.

Prior to placement of the femoral component, the distal femur is shaped to match the inner surface of the prosthetic component. To align the different bony cutting planes of the femur for accommodating a correct position of the implant, cutting blocks with saw slots are attached to the bone. Alignment of the cutting blocks is determined using anatomical references. When placing the cutting blocks, surgeons have to accommodate for differences in bone anatomy [3, 4]. With conventional instrumentation (CI), both the determination of mechanical axis and epicondylar axis show large inter-surgeon variability [5, 6]. Intramedullary rods are often used with CI for referencing the shaft of long bones like the femur. The right point for entering the intramedullary cavity can vary between patients depending on for example varus or valgus deformities [3]. To overcome the alignment difficulties and variabilities, alternative referencing tools were developed.

Computer navigation (CN) is such an alternative [7], using markers attached to instruments and bone. CN shows contradictory results with respect to accuracy of component position compared to CI [8-10], probably because of the high variability of intraoperative determined landmarks, which are used as input to CN systems. Another alternative is the use of patient specific surgical guides (PSSGs; otherwise known as Patient Specific Instrumentation), which are based on preoperative 3D images of the patient, and can be tailor made to fit the patient's anatomy. PSSGs were introduced to have the advantages of a computer aided planning, without the disadvantage of intraoperative registration. However, results in obtaining the planned alignment are mixed. Compared to CI, PSSGs are reported either to improve alignment [11-15], get similar results [16-22] or worsen alignment [23].

State of the art PSSGs are disposable products made of one piece and therefore cannot be adjusted intraoperatively to correct alignment [24]. The disposable surgical guides are generally 3D printed by an external company. Average lead times for production are around 20 to 30 days [25], during which the remnants of cartilage or subchondral bone may have changed. Intraoperatively, surgeons often alter from the preoperative surgical plan due to unforeseen circumstances like imbalance of the knee, the thickness of bone cuts and sizing/positioning of components [21].

Attempts have been made to develop configurable and reusable PSSGs that allow for adjustments during surgery. Haselbacher [26] proposed a PSSG wherewith a geometric fit can be created by setting the depth of threaded pins relative to a base plate. The base plate of the PSSG contains threaded holes ordered in a rectangular grid giving the surgeon many options for configuration. Kroes [27] developed a grid-based guide in which the pins are clamped all at once by creating a shear action between sandwiched plates.

Positioning of current disposable and configurable PSSGs is based on the fit of the device with the opposing bone surface. The surgeon judges the placement by the stability of the guide-bone interface. Inaccuracies in the preoperative 3D image and changes to the cartilage or subchondral bone, can make it difficult to judge the stability of positioning. Some companies offer rods which can be connected to the PSSG to check alignment with for example the hip center. Nevertheless, to our best knowledge, there is no direct method or mechanism to double check the positioning between bone and guide.

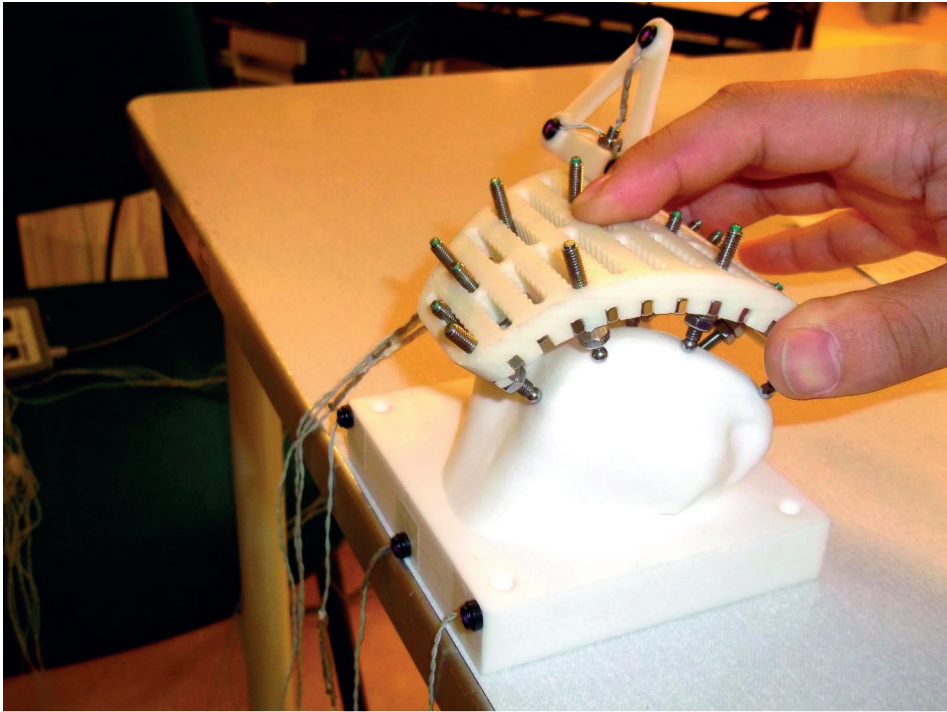
The aim of this article is to develop and evaluate an intraoperatively adjustable PSSG which can be set according to a predetermined fit and also contains a mechanism to visualize contact with the bone. The surgeon can use this visual feedback to check if the PSSG is correctly positioned, and if applicable, remove contacts that obstruct correct positioning.

2 METHODS

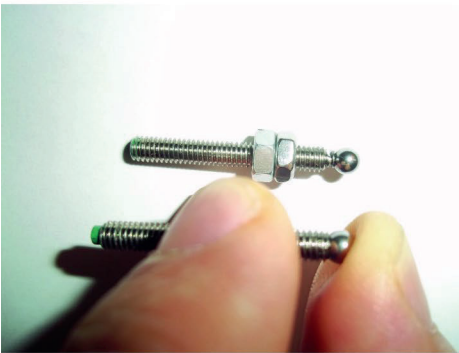
2.1 Intraoperatively adjustable PSSG

The intraoperatively adjustable guide consists of a base that allows spring plungers to be set to a certain depth (Figure 1). Contact of the spring plunger's spherical tip is indicated by a green protruding pin end (Figure 1B), which is rigidly connected to the spherical contact. Hence, there is a one-to-one relation between the tip's depression and the pin end's protrusion. A light spring prevents the green pin end from protruding due to gravity or movement. When the guide is configured and placed onto the bone (Figure 1A), the green pin ends protrude only from the spring plungers that contact the bone.

The depth of the spring plungers is set by adjusting the position of a nut on the threaded spring plunger. A second nut is used to interlock the first nut. The spring plungers are inserted from the inside of the guide's base and connect with a magnetic layer (Figure 1C). The magnetic connection allows for quick removal of the contact points. The spring plungers are placed in a grid consisting of rows with overlapping holes allowing for planning contact on key support points like the cartilage edge. The overlapping holes have the advantage that contact with the bone can be set for a wide variety of knees without using an overcomplicated mechanism. The shape and design of the guide's base



(A)



(B)



(C)

Figure 1. The design of our intraoperatively adjustable PSSG. (B) The spring plunger includes a protruding pin end to show that spherical contact makes contact. (C) The spring plungers are inserted into the desired holes in the guide's base. (A) The position of the PSSG is tracked during placement with an optical tracking system.

determine where contact points can be placed. The lateral contour of the base follows the lateral curved contour of the femur (Figure 1).

Figure 2 shows the typical usage of the configurable guide. First, the alignment of the prosthetic components is virtually planned on a computer. The guide is subsequently configured to the calculated settings. The depth of the spring plungers is set, and the

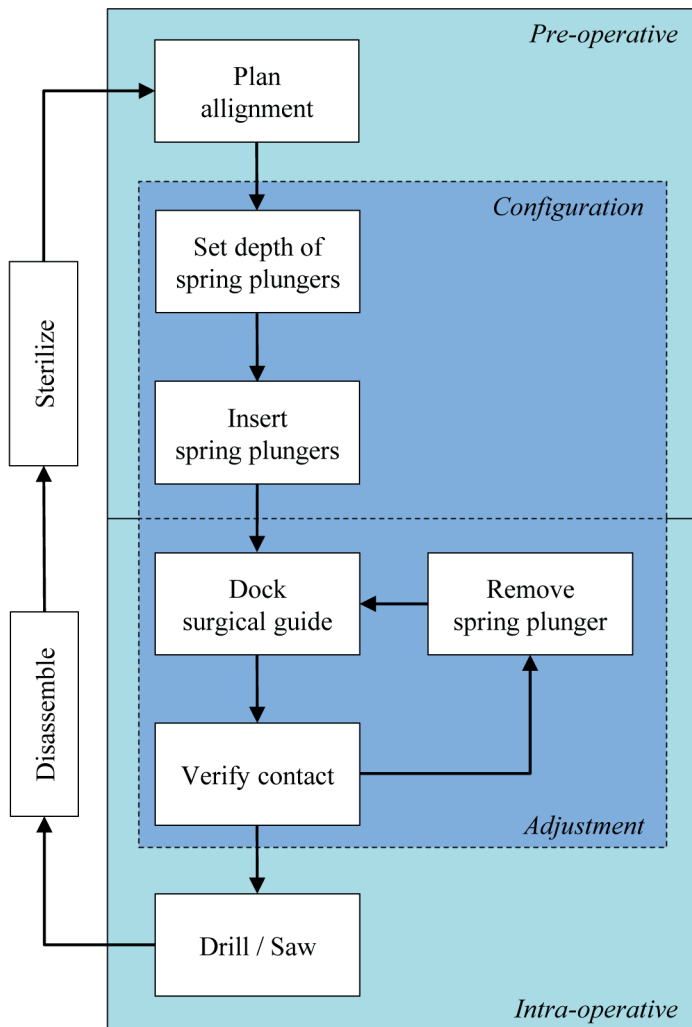


Figure 2. Usage of the intraoperatively adjustable PSSG. Preoperatively, the alignment is planned and the surgical guide is configured. Intraoperatively, the surgical guide is docked and spring plungers that disturb the fit can be removed. After surgery, the surgical guide can be disassembled and sterilized for reuse.

spring plungers are inserted in the right holes. The guide is docked onto the bone and contact of the spring plungers is verified. The spring plungers are configured such that the green pin ends fully protrude when the surgical guide is in the planned position and all spring plungers are fully compressed. When only a few green pin ends protrude or do not protrude fully, the surgeon can remove the spring plungers that prevent a good fit. This can be repeated until a good fit is found.

2.2 Experimental setup

The surgical guide prototype is tested on a 3D printed distal femur, which is manufactured by selective laser sintering (SLS) using nylon (PA2200) (Figure 1A). This bone model is the mean shape derived from a statistical shape model from Baka et al. [28]. The Optotrak Certus system is used to track the motion of the surgical guide relative to the bone. A triangular marker tree is attached to the guide and markers are placed on the bone.

A contact set is derived by optimizing for docking robustness by the method of Mattheijer et al. [29]. The optimal contact set allows the surgeon to vary the location and direction of the docking force to a great extent. Before the experiments, the *planned position* was determined performing five placements of the PSSG without any disturbances (TH). The center of mass of the PSSG's curved base is considered as its origin.

The spring plunger locations for the found contact set are indicated in Figure 3 and the depths of the spring plungers are listed in Table 1. Because the printed model of the guide's base deviates from the digital model and is slightly flexible, the depth settings were altered manually in such a way that all green pin ends protrude when the correct alignment is reached. Two spring plungers jammed because the bone was locally too steep relative to the axis of the spring plungers, therefore these were moved to a neighboring grid location. One spring plunger was moved from J01 to H01 and another from L02 to J02. Spring plungers 1 to 4 were omitted from the disturbance selection, because they showed too much play and were fixed on the guide with an additional nut.

Two sets of spring plungers are available, one set with settings exactly as described in Table 1 and another set is with disturbances introduced. The disturbing spring plungers have a depth setting which is one millimeter deeper than the settings from Table 1. The guide is fitted with the first set by default. The presence of a bump on the bone model (i.e. an osteophyte or bone defect) can be mimicked by exchanging one of the spring plungers from the default configuration with a corresponding one from the second set.

2.3 User tasks

The users performed the following tasks:

- 1A) Place the PSSG on the printed model and recognize if the fit was undisturbed or disturbed.
- 1B) If the position was felt to be disturbed, the user was allowed to remove one spring plunger to improve the fit. The user was allowed to reconsider and remove another spring plunger, although only one could be left out for the final

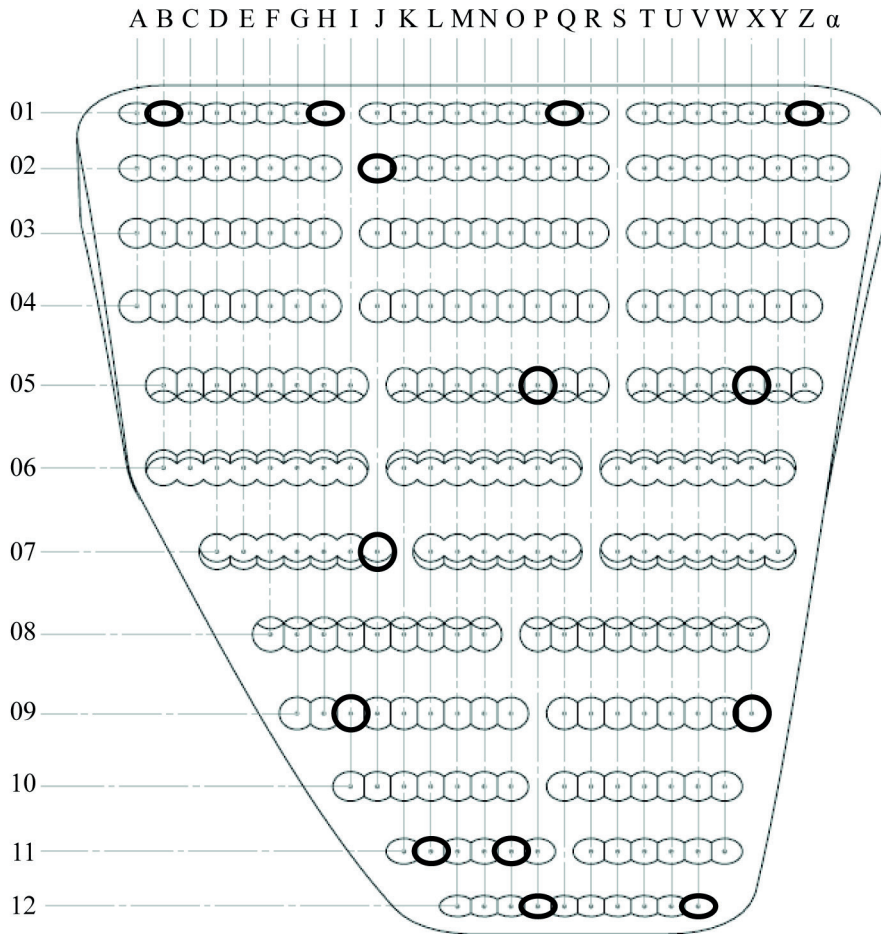


Figure 3. The selected locations for the spring plungers in the guide's base.

placement. The map depicted in Figure 3 was available to the user to help relocating removed spring plungers.

- 2) When the fit was considered optimal, the PSSG was kept in place and the final position was recorded for two seconds by the optical tracking system.

2.4 User groups

The experiments were performed by *non-experts* and *experts*. The non-expert group included fourteen users with no previous experience and were a staff member or student from the orthopedic department of the Leiden University Medical Center. The *expert group* included the two designers of the PSSG (JM and TH) with a lot of previous experience with the PSSG.

Table 1. The location and depth setting for the spring plungers of the PSSG.

Spring plunger	Location ^a	Depth ^b (mm)
1	B01	15.5
2	H01	14.6
3	Q01	18.0
4	Z01	11.7
5	J02	18.0
6	P05	18.3
7	X05	13.0
8	J07	11.3
9	I09	11.6
10	X09	11.3
11	L11	13.0
12	O11	17.2
13	P12	18.6
14	V12	14.1

a. The locations of the spring plungers are depicted in Figure 3.

b. The depth setting is measured from the top face of the top nut to the bottom of the spherical contact.

The *non-experts* were subjected to six PSSG configurations, three with and three without a disturbance. The first configuration for non-experts was without disturbance and enabled the user to feel the geometric fit. The remaining five configurations were randomly ordered. If a disturbance was present, the disturbing spring plunger was randomly selected. The first configuration with and without disturbance enabled initial experience for the non-experts and these results were not included in the data analysis.

The configurations in the *expert group* were randomly ordered. To have equal size groups, the experts performed placements until the number of placements with and without a disturbance equals the number of the non-expert group. Placements performed because either the with or without group did not reach this number yet were omitted from the analysis.

2.5 Data analysis

To determine how well the users performed Task 1A and 1B, the right and wrong decisions of users were compared using contingency tables. The following null hypothesis and alternative hypothesis were defined:

H_0 : the PSSG has an undisturbed fit

H_A : the PSSG has a disturbed fit

The removal of the disturbing spring plunger is a categorical task (with the spring plunger numbers as categories). We reduced this to a binary task by only considering if the right spring plunger was selected. The significance of recognizing disturbed fits was tested with the Pearson's chi-squared test and the effect size was determined with the phi coefficient.

The *final positions* of the PSSG were compared to the *planned position*. The *final positions* were divided into two groups: (1) a disturbing spring plunger was still present in the final position; (2) either no disturbing spring plunger was present or the user had removed the disturbing spring plunger. The translational error, defined as the absolute translation of the PSSG's origin, and the rotational error, defined as the absolute rotation determined from an axis-angle representation were analyzed with box plots. The difference in translational and rotational error was tested with one-tailed Mann-Whitney U test. The effect size was analyzed with the probability of superiority [30], i.e. the probability that the positional error of a random sample of one group is larger than a random sample of the other group.

3 RESULTS

The total number of placements for *non-experts* and *experts* were both 52 (i.e. for both groups 26 with and 26 without a disturbance). The results of one non-expert were omitted as this user relocated one of the spring plungers to a different location in the grid. Hence, the configuration of the guide did not comply with the experiment anymore.

Table 2 shows the contingency table for non-experts. The lack of disturbance was correctly predicted in 16 out of 26 cases (i.e. specificity is 62%) and the presence in 18 out of 26 cases (i.e. sensitivity is 69%). The correct prediction of presence of a disturbance is statistically significant ($\chi^2 = 4.952, p = 0.025$). The phi coefficient shows a moderate relationship [31] between prediction and reality ($\phi = 0.309, p = 0.05$). The non-experts had trouble finding the disturbing spring plunger. When a disturbance was present, the disturbing spring plunger was removed only in 7 out of the 26 cases (i.e. 27%).

Table 3 shows the contingency table for experts. The lack of a disturbance was correctly identified in 24 out of 26 cases (i.e. specificity is 92%) and the presence of disturbance in 21 out of 26 cases (i.e. sensitivity is 81%). Like for the non-experts, correct prediction is statistically significant ($\chi^2 = 28.144, p < 0.001$). There is a strong relationship [31] between prediction and reality for the experts ($\phi = 0.736, p < 0.001$). The experts performed better than the non-experts in finding a disturbance. The expert users removed the disturbing spring plunger from the PSSG in 18 out of 26 cases (i.e. 69%).

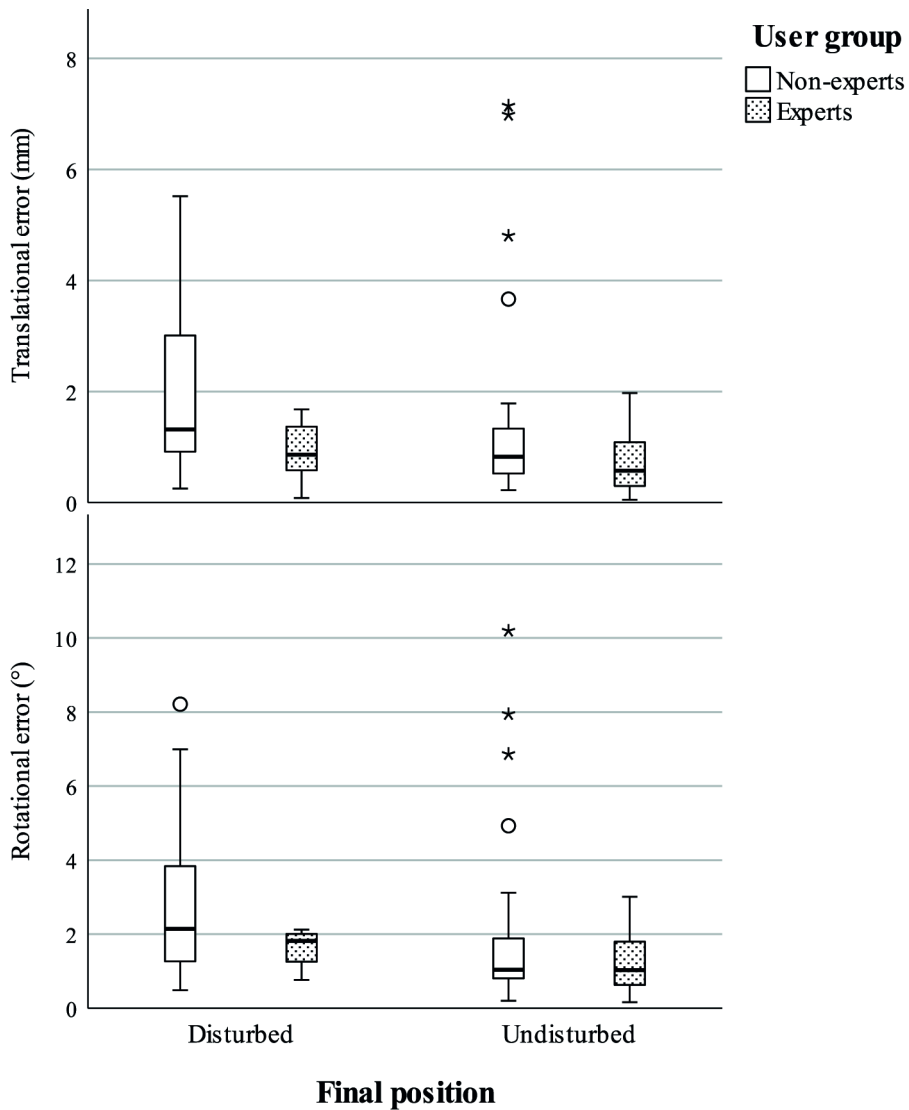


Figure 4. The translational error (Top) and the rotational error (Bottom) due to disturbance presence in the *final position*. Undisturbed final positions correspond to the cases underlined in Table 2 and 3.

Figure 4 shows the error in the final position of the PSSG for both non-experts and experts. The undisturbed final positions correspond to the underlined cases in Table 2 and 3. The range in translational and rotational error is larger for the non-experts. The maximum translational error is 7.2 mm for the non-experts and 2.0 mm for the experts. The maximum rotational error is 10.2 degrees for the non-experts and 3.0 degrees for the experts.

Table 2. Decisions of the *non-expert users* to accept either H_0 or H_A .

			Reality	
			H_A is True	H_0 is True
Decision	Accept H_A	Count	18(11/ <u>7</u> ^a)	<u>10</u> ^b
		% within Reality	69%	38%
	Accept H_0	Count	8	<u>16</u> ^b
		% within Reality	31%	62%

Underlined numbers indicate undisturbed final positions, where:

a. the disturbing spring plunger was removed;

b. there was no disturbance present in the initial configuration.

The box plots show that the median is larger when a disturbance is present. The largest difference in median values is seen for the rotational error of non-experts; with plunger disturbance, the median equals 2.1 degrees, and without plunger disturbance, the median equals 1.0 degrees. For the non-experts, a significantly larger translational error ($U = 213$, $p = 0.03$, $\hat{p}_{a>b} = 0.66$) and rotational error ($U = 203$, $p = 0.02$, $\hat{p}_{a>b} = 0.68$) are found. For the experts, the translational error is not significantly larger ($U = 131$, $p = 0.13$, $\hat{p}_{a>b} = 0.63$), but the rotational error is ($U = 107$, $p = 0.04$, $\hat{p}_{a>b} = 0.70$). The probability of superiorities $\hat{p}_{a>b}$ are all above 0.50, showing that a larger positional error is more likely when a disturbance is present.

4 DISCUSSION

The novel PSSG presented in this article can be configured to have a geometric fit with the opposing bone and can be adjusted in case unforeseen bony deviations occur. The PSSG supported expert users in most cases to recognize which spring plunger disturbed the fit with the bone, whereas the inexperienced users were in the majority of cases unable to recognize the disturbing plunger.

Compared to guides with a flat base (like the guides of Haselbacher [26] and Kroes [27]), the curved base has several advantages. The guide can be docked more stably when the surgeons docking force is closer to the bone [32, 29] and the guide is more stable due to a lower center of gravity. Furthermore, it is an advantage that the spring plungers can have a shorter length because of the shorter distance to the bone. From a lateral point of view, the holes for the locating pins are radially patterned. Consequently, they are directed relatively normal to the bone. The main advantage of this is that when the spring plungers contact the bone, they are less likely to get jammed. On top of the close proximity of the guide's base, the relatively normal direction makes that the spring plungers' length can be even shorter. Moreover, the radial pattern creates a denser grid of possible contact points

Table 3. Decisions of the *expert users* to accept either H_0 or H_A .

			Reality	
			H_A is True	H_0 is True
Decision	Accept H_A	Count	21(3/ <u>18</u> ^a)	<u>2</u> ^b
		% within Reality	81%	8%
	Accept H_0	Count	5	<u>24</u> ^b
		% within Reality	19%	92%

Underlined numbers indicate undisturbed final positions, where:

a. the disturbing spring plunger was removed;

b. there was no disturbance present in the initial configuration.

on the bone. Hence, there are more options to select a suitable contact set. These advantages make the PSSG more compact and easier to handle.

The aim of removing the disturbing spring plunger from the PSSG is to obtain more accurate placement. When a disturbance was not present in the final position, many placements of the non-experts stayed within 2 mm and 3 degrees error. When a disturbance was still present for the experts (i.e. only eight positions), the range in positional errors was strikingly smaller. For both non-experts and experts, the medians of the positional errors were greater when a disturbance was still present. Correspondingly, the probability of superiority showed that positional errors are likely to be greater when a disturbance was still present. From this we can conclude that it is beneficial for the alignment to have disturbances removed.

We observed that many users had trouble interpreting the green pin ends to test positioning. In multiple instances users tested the effect of many different plunger removals and eventually settled with one where they were not completely satisfied with. We also noticed that one of the non-expert users persevered in finding the disturbance by taking a lot of time (we did not set a time limit), which ultimately resulted in finding the correct disturbance. Expert users were far better than non-experts in both finding the disturbance and positioning the guide, even with a disturbance present in the final position. This stresses the importance of training when a new device is used. When the disturbance was removed, both the non-expert and expert users could position the PSSG accurately in many cases. We conclude that the contact detection mechanism requires training, and even then, does not always result in correct removal. Nevertheless, even without correct removal, the green pin ends allow trained users to find an accurate position.

The PSSG itself had some limitations. Since, the bone was too steep for some spring plungers, we had to move them to prevent jamming. Moreover, the guide was not perfectly rigid and therefore some spring plungers had to be fixed to prevent play inside

the guide's base. The play of other spring plungers was considerably less, though compromised the guide's fit somewhat. We also benefitted from the imperfect fit, because the experiment was now more focused on the effectiveness of contact detection.

Our study had some other limitations. As these were the first experiments with our novel PSSG, we performed the experiments on a 3D printed plastic bone model. The cartilage layer covering real bone is quite soft, and consequently, disturbances might be less prominent as the PSSG can adapt. In our experiment, we wanted to test the user's ability to remove one disturbance first. Having more disturbances present would be interesting to investigate. Furthermore, we only tested the positioning of the PSSG in our study; thereby disregarding the saw cuts. Future research should include the making of the saw cuts as an additional step which also might affect the positional error of implant components.

In conclusion, our study showed that a contact detection and disturbance removal mechanism improves PSSG alignment. The better the alignment of the PSSG onto the bone, the better the alignment of implant components. The contact detection and removal mechanism did not prove to be simple though. However, training could help to place the guide faster and more accurate. Next step is to integrate our designed PSSG in a more realistic setting, to test whether it enables surgeons to improve alignment during surgery and to get more certainty in correctness of placement.

5 ACKNOWLEDGMENTS

This research is supported by the Dutch Technology Foundation AES, which is part of the Netherlands Organisation for Scientific Research (NWO), and which is partly funded by the Ministry of Economic Affairs (Project No. NIG 10812).

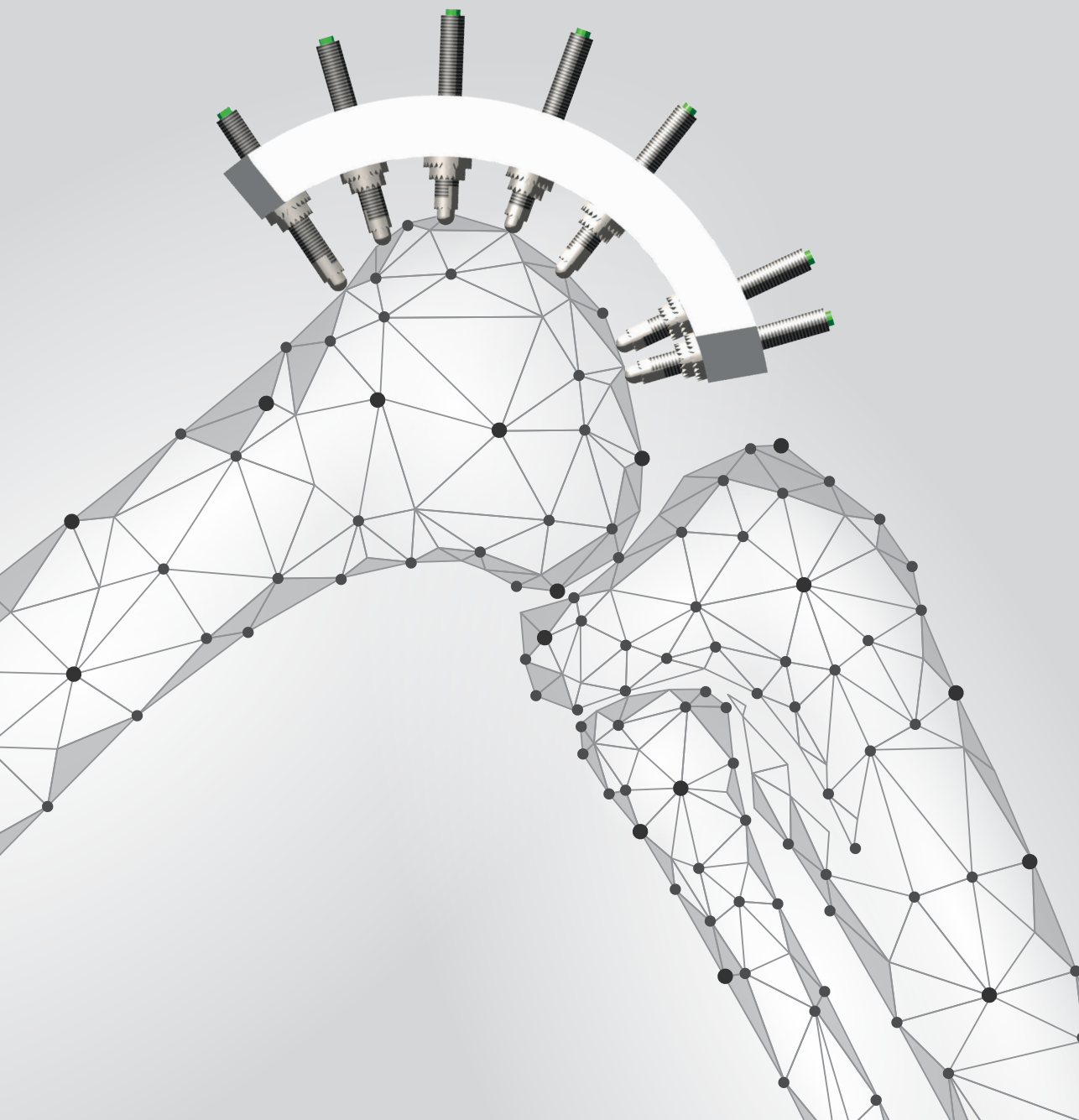
REFERENCES

- [1] Ritter, M. A., Faris, P. M., Keating, E. M., and Meding, J. B., 1994, Postoperative Alignment of Total Knee Replacement Its Effect on Survival. *Clin Orthop Relat Res*, **299**, pp. 153–156.
- [2] Reus, A., Spekenbrink-Spooren, A., van Steenbergen, L. N., Denissen, G. A. W., Rijnsburger, E., and van der Togt, C. R., 2018, Online LROI annual report 2018, Tech. rep., Dutch Arthroplasty Register (LROI), 's-Hertogenbosch, The Netherlands.
- [3] Laskin, R. S., 2003, Instrumentation pitfalls: you just can't go on autopilot! *J Arthroplasty*, **18**(3), pp. 18–22.

- [4] Mahfouz, M., Abdel Fatah, E., Bowers, L., and Scuderi, G., 2012, Three-dimensional Morphology of the Knee Reveals Ethnic Differences, *Clin Orthop Relat Res*, **470**, pp. 172–185.
- [5] van der Linden-van, H. M. J., Bos, J., Van der Heide, H. J. L., Nelissen, R. G. H. H., et al., 2011, A computed tomography based study on rotational alignment accuracy of the femoral component in total knee arthroplasty using computer-assisted orthopaedic surgery, *Int Orthop*, **35**(6), pp. 845–850.
- [6] van der Linden-van der Zwaag, H. M. J., Valstar, E. R., van der Molen, A. J., and Nelissen, R. G. H. H., 2008, Transepicondylar axis accuracy in computer assisted knee surgery: a comparison of the CT-based measured axis versus the CAS-determined axis, *Comput Aided Surg*, **13**(4), pp. 200–206.
- [7] van der Linden-van der Zwaag, H. M. J., Wolterbeek, R., and Nelissen, R. G. H. H., 2008, Computer assisted orthopedic surgery; its influence on prosthesis size in total knee replacement, *Knee*, **15**(4), pp. 281–285.
- [8] Cheng, T., Zhao, S., Peng, X., and Zhang, X., 2012, Does computer-assisted surgery improve postoperative leg alignment and implant positioning following total knee arthroplasty? A meta-analysis of randomized controlled trials? *Knee Surg Sports Traumatol Arthrosc*, **20**(7), pp. 1307–1322.
- [9] Hetaimish, B. M., Khan, M. M., Simunovic, N., Al-Harbi, H. H., Bhandari, M., and Zalzal, P. K., 2012, Meta-analysis of navigation vs conventional total knee arthroplasty, *J Arthroplasty*, **27**(6), pp. 1177–1182.
- [10] van Strien, T., Kaptein, B., van Erkel, A., Valstar, E., Nelissen, R., et al., 2009, Computer assisted versus conventional cemented total knee prostheses alignment accuracy and micromotion of the tibial component, *Int Orthop*, **33**(5), p. 1255.
- [11] Anderl, W., Pauzenberger, L., Kölblinger, R., Kiesselbach, G., Brandl, G., Laky, B., Kriegleder, B., Heuberger, P., and Schwameis, E., 2016, Patient-specific instrumentation improved mechanical alignment, while early clinical outcome was comparable to conventional instrumentation in TKA, *Knee Surg Sports Traumatol Arthrosc*, **24**(1), pp. 102–111.
- [12] Chan, W. C.-W., Pinder, E., and Loeffler, M., 2016, Patient-specific instrumentation versus conventional instrumentation in total knee arthroplasty, *J Orthop Surg (Hong Kong)*, **24**(2), pp. 175–178.
- [13] Heyse, T. J. and Tibesku, C. O., 2014, Improved femoral component rotation in TKA using patient-specific instrumentation, *Knee*, **21**(1), pp. 268–271.
- [14] Mannan, A. and Smith, T. O., 2016, Favourable rotational alignment outcomes in PSI knee arthroplasty: a level 1 systematic review and meta-analysis, *Knee*, **23**(2), pp. 186–190.
- [15] Vide, J., Freitas, T. P., Ramos, A., Cruz, H., and Sousa, J. P., 2017, Patient-specific instrumentation in total knee arthroplasty: simpler, faster and more accurate than

- standard instrumentation—a randomized controlled trial, *Knee Surg Sports Traumatol Arthrosc*, **25**(8), pp. 2616–2621.
- [16] Boonen, B., Schotanus, M. G. M., Kerens, B., van der Weegen, W., Hoekstra, H. J., and Kort, N. P., 2016, No difference in clinical outcome between patient-matched positioning guides and conventional instrumented total knee arthroplasty two years post-operatively, *J Bone Joint Surg Br*, **98**(7), pp. 939–944.
- [17] Cavaignac, E., Pailhé, R., Laumond, G., Murgier, J., Reina, N., Laffosse, J. M., Bérard, E., and Chiron, P., 2015, Evaluation of the accuracy of patient-specific cutting blocks for total knee arthroplasty: a meta-analysis, *Int Orthop*, **39**(8), pp. 1541–1552.
- [18] Fu, H., Wang, J., Zhou, S., Cheng, T., Zhang, W., Wang, Q., and Zhang, X., 2015, No difference in mechanical alignment and femoral component placement between patient-specific instrumentation and conventional instrumentation in TKA, *Knee Surg Sports Traumatol Arthrosc*, **23**(11), pp. 3288–3295.
- [19] Huijbregts, H. J. T. A. M., Khan, R. J. K., Sorensen, E., Fick, D. P., and Haebich, S., 2016, Patient-specific instrumentation does not improve radiographic alignment or clinical outcomes after total knee arthroplasty: A meta-analysis, *Acta Orthop*, **87**(4), pp. 386–394.
- [20] Mannan, A., Smith, T. O., Sagar, C., London, N. J., and Molitor, P. J. A., 2015, No demonstrable benefit for coronal alignment outcomes in PSI knee arthroplasty: a systematic review and meta-analysis, *Orthop Traumatol Surg Res*, **101**(4), pp. 461–468.
- [21] Sassoon, A., Nam, D., Nunley, R., and Barrack, R., 2015, Systematic review of patient-specific instrumentation in total knee arthroplasty: new but not improved, *Clin Orthop Relat Res*, **473**(1), pp. 151–158.
- [22] Yan, C. H., Chiu, K. Y., Ng, F. Y., Chan, P. K., and Fang, C. X., 2015, Comparison between patient-specific instruments and conventional instruments and computer navigation in total knee arthroplasty: a randomized controlled trial, *Knee Surg Sports Traumatol Arthrosc*, **23**(12), pp. 3637–3645.
- [23] Chen, J. Y., Yeo, S. J., Yew, A. K. S., Tay, D. K. J., Chia, S.-L., Lo, N. N., and Chin, P. L., 2014, The radiological outcomes of patient-specific instrumentation versus conventional total knee arthroplasty, *Knee Surg Sports Traumatol Arthrosc*, **22**(3), pp. 630–635.
- [24] Stronach, B. M., Pelt, C. E., Erickson, J., and Peters, C. L., 2013, Patient-specific total knee arthroplasty required frequent surgeon-directed changes, *Clin Orthop Relat Res*, **471**, pp. 169–174.
- [25] Thienpont, E., Bellemans, J., Delport, H., Van Overschelde, P., Stuyts, B., Brabants, K., and Victor, J., 2013, Patient-specific instruments: industry's innovation with a surgeon's interest, *Knee Surg Sports Traumatol Arthrosc*, **21**(10), pp. 2227–2233.

- [26] Haselbacher, M., Sekyra, K., Mayr, E., Thaler, M., and Nogler, M., 2012, A new concept of a multiple-use screw-based shape-fitting plate in total knee arthroplasty, *J Bone Joint Surg Br*, **94-B**(SUPP XLIV), p. 65.
- [27] Kroes, T., Valstar, E., and Eisemann, E., 2015, Numerical optimization of alignment reproducibility for customizable surgical guides, *Int J Comput Assist Radiol Surg*, **10**(10), pp. 1567–1578.
- [28] Baka, N., Kaptein, B. L., de Bruijne, M., van Walsum, T., Giphart, J. E., Niessen, W. J., and Lelieveldt, B. P. F., 2011, 2D–3D shape reconstruction of the distal femur from stereo X-ray imaging using statistical shape models, *Med Image Anal*, **15**(6), pp. 840–850.
- [29] Mattheijer, J., Herder, J. L., Tuijthof, G. J. M., and Valstar, E. R., 2015, Docking Robustness of Patient Specific Surgical Guides for Joint Replacement Surgery, *J Mech Design*, **137**(6), p. 062301.
- [30] Grissom, R. J. and Kim, J. J., 2012, *Effect sizes for research: Univariate and multivariate applications*, 2nd ed., Routledge/Taylor & Francis Group, New York, NY, USA.
- [31] Rea, L. M. and Parker, R. A., 2014, *Designing and conducting survey research: A comprehensive guide*, 4th ed., John Wiley & Sons, San Francisco, CA, USA.
- [32] Mattheijer, J., Herder, J. L., Tuijthof, G. J. M., Nelissen, R. G. H. H., Dankelman, J., and Valstar, E. R., 2013, Shaping Patient Specific Surgical Guides for Arthroplasty to Obtain High Docking Robustness, *J Mech Design*, **135**(7), p. 071001.



CHAPTER 6

General Discussion and Conclusion

1 GENERAL DISCUSSION

Our goal was to develop preoperative planning tools for joint replacement surgery which can be used to find optimal settings for Patient Specific Surgical Guides (PSSGs). The PSSGs are set according to a pre-operative plan and are used intra-operatively for accurate placement of the joint replacement prosthesis. Accurate positioning is aimed to improve patient outcome and reduce the need for revision surgery.

1.1 Docking robustness in theory and practice

In our work, docking robustness measures were created for both two-dimensional (Chapter 2) and three-dimensional surgical guides (Chapter 3). These measures can be used to find optimal settings for a surgical guide with reference to the joint surface of a specific patient. Optimized settings ensure that the surgical guide can be most stably docked. Experimental validation of two-dimensional PSSGs showed that the stability of the surgical guide can be reliably predicted using our methods (Chapter 2). Optimization of contact locations with a three-dimensional distal femur (Chapter 3) showed that 12 contact points already result in a relatively stable position (with 0.74 contact efficiency out of a maximum 1.00). Minimal contact however – i.e. using 6 contact points - showed to be relatively unstable (with 0.18 contact efficiency out of a maximum 1.00). Hence, a tradeoff exists between the complexity of the device and its stability on the joint surface.

Docking robustness has also been investigated by few other researchers. Van den Broeck et al. [1] adopted measures for workpiece fixturing and robotic grasping (introduced by Lin et al. [2]) and performed an assessment on 3D printed PSSGs. The experiments show that guide designs with a better score resulted in better stability. Müller et al. [3] introduced a method for robotically testing PSSGs for acetabulum replacement. The PSSG was placed on a printed acetabulum model where after force and torques were robotically applied in a planned sequence. The PSSG could subsequently be evaluated using visualization maps for reaction forces and displacements. The visualization maps show what variation is allowed in the surgeon's docking force, and hence, are an indicator for docking robustness.

The measures of Van den Broeck et al. [1] are comparable to our 2D and 3D docking robustness measures. However, contact that does not allow greater variation in the surgeon's applied force, unnecessarily affects the stability measures of van den Broeck. In contrast to our measures, where contact which does not affect the surgeon's applied force is considered redundant. Broeck et al. also indicate that from the mathematical model it is expected that forces or torques are identical when inverting direction, whereas the experiments showed an asymmetric response. The robotic testing method of Müller et al. could prove to be a valuable tool for physically evaluating the stability measures. Hereto,

the measures would first need to be tested for suitability in experiments on plastic bones models before validation is performed on cadaveric bones. The visualization maps of Muller et al. could also be appropriate for planning software to depict the quality of PSSGs. Translational displacement errors would be a welcome addition to the visualization maps of Müller et al. for fully assessing positional accuracy.

1.2 Docking accuracy in theory and practice

In our work, a docking accuracy measure was created to evaluate the influence of geometrical deviations between the CT/MRI image and the bone as observed in surgery (Chapter 4). This measure can be used in combination with docking robustness to find optimal contact locations for both accurate and stable positioning on the joint surface. The method is virtually tested on a three-dimensional bone model of the distal femur. Accuracy can be evaluated with both a linear and non-linear method, where the linear method deviates more from the non-linear method for increasing bone deviations. The methods remain to be validated in practice.

Kroes et al. [4]. introduced a computer-assisted method for selecting and optimizing PSSG contact points. The docking of the surgical guide is virtually simulated to find positional errors between the docked position and the planned position. Every PSSG instance is virtually docked multiple times using slightly different approach paths. User-selected and computer-optimized contact sets were compared in a physical experiment. Computer-optimized contact sets resulted in a better reproducibility of the planned position. Müller et al. [3] assessed accuracy of PSSG docking onto the acetabulum in their method where forces and torques were robotically applied. Visualization maps show the forces and torques applied and the resulting tilt error relative to the acetabulum. The method to find docking accuracy is different for our measure and the measure of Kroes et al. We search for fully determined positions (i.e. positions with six contact points), where Kroes et al. use virtual physics to simulate the docking. Our method further considers possible anatomic deviations between the CT/MRI image and the bone as observed during surgery. It would be interesting to see the effect of these bony deviations in physical simulation as performed by Kroes et al. This physical simulation can hence be compared with our computational method and cadaveric experiments. The virtual bone in the physical simulation should ideally show realistic geometrical deviations between CT/MRI image and the actual bone at the time of surgery. The docking accuracy methods can be validated in computational time and accuracy compared to reality. Validation can be performed by visualization maps as presented by Müller et al. [3].

1.3 Configurable and non-configurable PSSGs

Our configurable PSSG contains a novel mechanism for detecting contact with an opposing joint surface (Chapter 5). The contact mechanism visualizes which contacts are in contact with the bone by protruding green pin ends. The PSSG can be positioned using a geometric fit and can be adjusted by removing one of the contacts when overall contact appears to be suboptimal. The surgical guide was tested in a physical experiment where a disturbance between PSSG and bone was intentionally present. Users with no previous experience with the PSSG were mostly not able to recognize disturbance. User with experience were able to recognize disturbance and often removed the contact that allowed disturbance. Extensive training is therefore considered necessary for using this device or a future counterpart. Improvement in usability of the device is considered appropriate as correct pin removal is not a straightforward process.

Haselbacher [5] et al. were the first to propose a configurable surgical guide. Their device consists of a rectangular base plate with a rectangular grid of holes and threaded pins which can be set to match the joint surface. Kroes et al. developed a similar device where the base plate consists of three sandwiched plates, whereof shear action onto the middle plate clamps all pins at once [6]. Both surgical guides were intended to be used for the replacement of the joint surface of the distal femur.

In contrast to the devices of Haselbacher et al. [5] and Kroes et al. [4], our device was designed with a curved base, thereby created the following advantages. The surgeon's docking force is closer to the bone, and hence, the docking is more robust [6, 7]. The lower center of gravity of the device additionally enhances the stability of docking. Due to the short distance between the curved base and the bone, the contact pins can have short length making the device more compact. In practice however, docking of our configurable PSSG onto a three-dimensional femur model did not result in a greatly stable position. Reasons for the relatively unstable position may be one of the following. Contact of the surgical guide is selected within a grid, and hence, possible features of the bone which can be used to obtain a stable fit might not even be selectable (e.g. the cartilage rim or bony deformations). The tested bone model had a smooth joint surface. The natural shape of the femur is such that movement - especially about its hinge-like axis - is promoted. Bone with severe arthritis may have more pronounced features enabling a more stable fit. Though the device is presumably lighter than the PSSG of Haselbacher and Kroes, weight is still rather high. The lighter the device is the more the surgeon would be able to feel the interaction with the joint surface.

Non-configurable PSSGs were also developed in recent years. Zimmer introduced PSSGs for glenoid replacement surgery [8-10]. The surgical guide contains drill guidance for the creation of a central hole in the glenoid. Throckmorton et al. [9] compared the PSSG to

conventional TKA on arthritic cadaveric knees with five surgeons of varying experience level. The positioning with PSSGs was significantly more accurate for both version and inclination. Lau et al. [10] obtain greater variance in alignment than previous studies and conclude that larger studies are required. Wright medical introduced another PSSG for glenoid replacement surgery [11]. Software is included with the PSSG system which enables the surgeon to plan prosthesis placement and PSSG positioning in advance. The surgeon picks contact points on the anterior and posterior glenoid rim for support of the PSSG. The plan is sent to Wright medical for 3D printing the PSSGs. Berhouet et al. [11] evaluated PSSG placement in a prospective study with 10 patients undergoing TSA. Four contact pillars are used for the PSSGs in this study. The resulting rotation of the glenoid component varied considerably from its planning. In order to improve rotational alignment more contact pillars are suggested by Berhouet et al.

The PSSG of Zimmer is designed to be seated on the anterior rim of the glenoid. This could however be insufficient for creating a well-defined position. In contrast, the PSSG of Wright medical also allows support on the posterior rim of the glenoid. Wright Medical however allows users to select where contact is made. Kroes et al. showed that a computer-selected contact set was better than a user-selected contact set for docking accuracy. Hence, measures for docking robustness and docking accuracy could show be valuable in finding an optimal fit and can therefore be a valuable addition to the pre-operative planning software of these devices.

1.4 Future perspective

The configurable guides designed by Haselbacher, Kroes and us all have a grid mechanism for contact. Disadvantage of such design is that contact can only be selected within a finite set of points. Important locations for contact like the cartilage rim or severe deformities due to arthritis might not even be selectable. PSSGs fabricated by 3D printed can be designed for full surface contact or contact at specific areas. Configurable PSSGs can possibly be developed for contact with crucial locations, though this would require possibilities for fine adjustments. Due to the complexity of such device, usability for the surgeon may decrease. Dedicated tooling could possibly be developed for configuring the device in the operating room. However, the configurable PSSG itself would remain complex, and possibly heavy and clumsy due to its configurability. Hence, 3D printing may be a more viable solution for creating a usable and compact device that allows contact in crucial locations.

Our configurable PSSG design (Chapter 5) provides the surgeon with the usual tactile feedback and additionally gives visual feedback for correct positioning. For future devices it is advisable to make the additional user feedback easier to understand. A method to accomplish this is by bundling contact information into one signal. Micro contact switches

can for instance be used as inserts in contact pillars of 3D printed PSSGs (Figure 1A). A microprocessor can combine the contact information into one audible signal (e.g. a beep tone) or one visual signal (e.g. LEDs). Interval between beeps or multiple LEDs can distinguish for degree of contact (i.e. sub-minimal contact, minimal contact and over-determined contact). During surgery, one or two contact pillars may be removed from the PSSG for increased alignment. As alternative for the micro contact switches, four-bar mechanisms may be used for every contact, transferring contact information to the microprocessor by actuation (Figure 1B). This would enable simple assembly of a dedicated microprocessor and a complex 3D printed PSSG. The surgeon or scrub nurse could perform the assembly in the operating room.

The docking robustness and docking accuracy measures can further be used in developing PSSGs. One could for example investigate whether there are more generic regions on the joint surface which promote reliable docking. If so, PSSGs can be designed to have a generic shape, with the possibility to have only slight adjustments for every individual patient. Another topic of research could be the association between docking accuracy and docking robustness. This could result in design parameters for a PSSG that can be docked stable and is not susceptible for errors in the virtual image (i.e. the CT/MRI image). Research can also be performed in simplifying the required virtual image procedure. A device could for example be developed which only needs partial information of the joint surface (e.g. only certain slices or specific regions) and is yet able to be positioned accurate and stable. This would enable using lower resolution images and thereby decreasing cost and lead time.

2 GENERAL CONCLUSION

This PhD thesis gives developers insight in how PSSGs – as a generic concept with patient specific adjustments – can be dimensioned for both robust and accurate docking. PSSG requirements can be set such that contact is selected in crucial locations at the joint surface. Thus, the possibility is created that other areas, not enhancing the geometric fit, can be discarded for image processing and 3D printing of the guide. The PSSG designed for this thesis has an additional visual feedback, allowing surgeons to double-check the position intraoperatively. Future research could focus on simplifying the device design while remaining accuracy; increasing device usability; simplifying the virtual image procedure; and identifying the relation between docking accuracy and docking robustness. When optimizing intraoperative implant positioning using preoperative information as input, it remains a challenge not to distract the surgeon from the patient's operating field and aim of surgery as such. In the end the PSSG is a mean to reach the goal: optimal implant placement. The latter is predictive for a long-lasting good functioning implant in the patient.

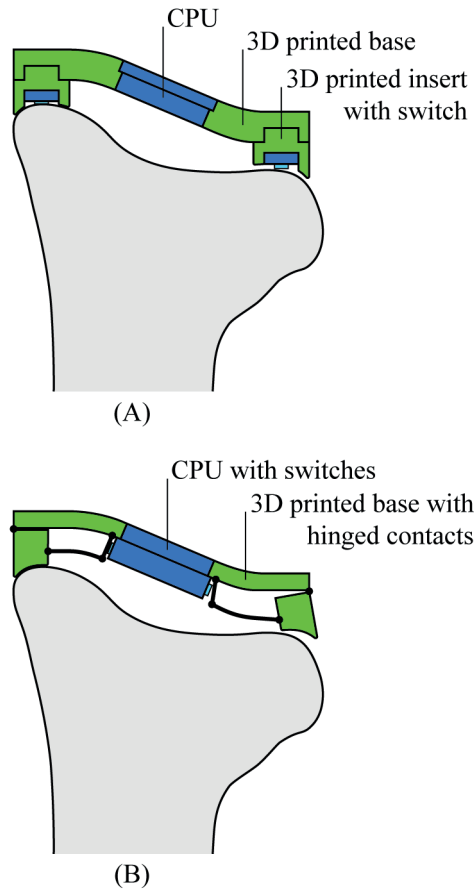


Figure 1. Envisioned future printed PSSGs with contact feedback. (A) PSSG comprising a printed base, printed inserts with contact switches and a CPU. (B) PSSG comprising a printed base with hinged contacts and a CPU with contact switches.

REFERENCES

- [1] Van den Broeck, J., Wirix-Speetjens, R., and Vander Sloten, J., 2015, Preoperative analysis of the stability of fit of a patient-specific surgical guide, *Comput Methods Biomech Biomed Engin*, **18**(1), pp. 38–47.
- [2] Lin, Q., Burdick, J. W., and Rimon, E., 2000, A stiffness-based quality measure for compliant grasps and fixtures, *IEEE T Robot Autom*, **16**(6), pp. 675–688.
- [3] Müller, S., Rawohl, M., Kahrs, L. A., and Ortmaier, T., 2018, Robot based evaluation of the quality of form closure of patient specific instruments, *SMIT2018-IBEC2018 Joint Conference*.

- [4] Kroes, T., Valstar, E., and Eisemann, E., 2015, Numerical optimization of alignment reproducibility for customizable surgical guides, *Int J Comput Assist Radiol Surg*, **10**(10), pp. 1567–1578.
- [5] Haselbacher, M., Sekyra, K., Mayr, E., Thaler, M., and Nogler, M., 2012, A new concept of a multiple-use screw-based shape-fitting plate in total knee arthroplasty, *J Bone Joint Surg Br*, **94-B**(SUPP XLIV), p. 65.
- [6] Mattheijer, J., Herder, J. L., Tuijthof, G. J. M., Nelissen, R. G. H. H., Dankelman, J., and Valstar, E. R., 2013, Shaping Patient Specific Surgical Guides for Arthroplasty to Obtain High Docking Robustness, *J Mech Design*, **135**(7), p. 071001.
- [7] Mattheijer, J., Herder, J. L., Tuijthof, G. J. M., and Valstar, E. R., 2015, Docking Robustness of Patient Specific Surgical Guides for Joint Replacement Surgery, *J Mech Design*, **137**(6), p. 062301.
- [8] Pietrzak, W. S., 2014, Shoulder alignment obtained with the Signature glenoid guide system: a cadaver study. Biomet Orthopedics Inc., Warsaw, IN, USA.
- [9] Throckmorton, T. W., Gulotta, L. V., Bonnarens, F. O., Wright, S. A., Hartzell, J. L., Rozzi, W. B., Hurst, J. M., Frostick, S. P., and Sperling, J. W., 2015, Patient-specific targeting guides compared with traditional instrumentation for glenoid component placement in shoulder arthroplasty: a multi-surgeon study in 70 arthritic cadaver specimens, *J Shoulder Elbow Surg*, **24**(6), pp. 965–971.
- [10] Lau, S. C. and Keith, P. P. A., 2018, Patient-specific instrumentation for total shoulder arthroplasty: not as accurate as it would seem, *J Shoulder Elbow Surg*, **27**(1), pp. 90–95.
- [11] Berhouet, J., Rol, M., Spiry, C., Slimane, M., Chevalier, C., and Favard, L., 2018, Shoulder patient-specific guide: First experience in 10 patients indicates room for improvement, *Orthop Traumatol Surg Res*, **104**(1), pp. 45–51.

DANKWOORD

Daar is dan het moment, mijn thesis is afgerond en ik mag de betrokken mensen bedanken voor hun steun en bijdrage. Het is een uitdagend en uiterst interessant project geweest met raakvlakken in vele vakgebieden, als orthopedie, engineering, visualisatie en wiskunde. Dankzij de inhoudelijke maar ook morele steun kan ik dit traject met voldoening afronden.

Allereerst wil ik Edward[†] bedanken voor zijn enthousiaste en toegewijde steun bij mijn onderzoek. Als promotor heb jij 'guidance' gegeven in projectafbakening, het koppelen aan de juiste mensen en het schrijven van artikelen. Tot mijn spijt kun je niet meer bij de verdediging van mijn promotie zijn. Ik weet dat je hier met verve aan had deelgenomen.

Jenny en Rob, jullie zijn vanaf het eerste uur betrokken in dit onderzoekstraject. Ik ben bijzonder dankbaar voor de trouwe begeleiding. Door het gehele project hebben jullie mij onvoorwaardelijke steun geboden. Jenny, bedankt voor jouw kritische maar tegelijk ook pragmatische blik op het onderzoek. Rob, mijn dank voor jouw inspiratieve inzicht en ideeën voor gewrichtsvervangende instrumentarium. In het speciaal wil ik mijn dank naar jullie uiten voor de geboden hulp in de eindfase. Dankzij jullie toewijding heb ik de laatste stappen kunnen zetten in de afronding van mijn thesis.

Mijn oprechte dank voor de Stichting Technische Wetenschappen en de leden van de gebruikerscommissie. De financiering heeft het project mogelijk gemaakt en de bijdrage van commissieleden in tussentijdse sessies is behulpzaam geweest om de haalbaarheid tegen het licht te houden. Enrike, Jochem en andere collega's hebben mij in en buiten deze sessies veel inzicht gegeven in instrumentarium en de complexiteit van conventionele chirurgie. Mijn dank voor het mogen bijwonen van operaties en de waardevolle discussies over instrumenten.

Vele anderen hebben mij geholpen in het onderzoek. Ten eerste, Just, wie een belangrijke bijdrage heeft geleverd. Met jou heb ik altijd uiterst interessante discussies gehad over robuustheid en nauwkeurigheid van geometrische fits. Jij hebt me de goede weg gewezen. Mijn speciale dank voor jouw inzicht en kritisch inhoudelijke blik op het schrijven van de artikelen. In de beginfase is Edward samen met Gabriëlle begonnen met begeleiding bij mijn onderzoek. Ik wil jou Gabriëlle bedanken voor de structurering van niet alleen de eerste artikelen maar ook het onderzoek als geheel.

In dit multidisciplinair onderzoek ben ik met vele mensen uit andere vakgebieden in aanraking gekomen. In de eerste plaats Thomas, met wie ik in dit project samenwerkte waarbij hij de visualisatie voor zijn rekening nam. Thomas, ik heb met plezier met jou aan dit onderzoek gewerkt. Dank voor de vele koffiepauzes waarin we konden sparren over

projectuitdagingen en instrumentideeën. Ook wil ik Thomas zijn begeleiders Charl en Elmar bedanken voor de vele interessante discussies en projectafstemming. Bart wil ik graag bedanken met het helpen inzicht te verkrijgen in computer algoritmes en het meedenken aan instrumentideeën. Voor lastige wiskundige vraagstukken ben ik in contact gekomen met Johannes en Dion. Ik wil jullie bedanken voor de geboden hulp bij deze belangrijke onderdelen van het onderzoek. Ook wil ik Hein en Tim bedanken voor de ontwikkeling van instrumentprototypes en de daarbij horende experimenten in hun masterfase.

Tijdens mijn promotie heb ik in Delft en Leiden gewerkt om zowel van het technische als het klinische aspect kennis op te doen. Hierdoor heb ik veel promovendi en andere collega's leren kennen. Emiel bedankt voor jouw hulp met de laatste loodjes van mijn eerste artikel. Francois, met veel plezier heb ik met jou intense squashpartijen gespeeld. Buurvrouwen Claire, Claudia, en ook de vele andere collega's in Leiden, bedankt voor alle gezelligheid. Alex en collega's van instrumentele zaken wil ik graag bedanken voor zijn hulp met het vervaardigen van prototypes. In Delft heb ik een plezierige tijd gehad met de vele collega technici. Met Gert en Steven heb ik aan vergelijkbare projecten gewerkt waardoor we ook van elkaar konden leren. Ik wil jullie en alle andere collega's uit Delft bedanken voor de mooie tijd.

Vrienden en familie wil ik graag bedanken voor alle morele steun. Myron en Boudewijn bedankt voor de vele leuke reizen en alle gezellige avonden in Rotterdam en Utrecht. Ik ben vereerd dat jullie mijn paranimfen zijn. Nick en Joost bedankt voor de mooie vakanties en poolavonden. Paulien en Sjoerd, we gaan snel weer eens bowlen. Alle teamgenoten en vrienden van de volleybalvereniging bedankt voor de sportieve en gezellige tijd. Reinier, Matthijs, Johan, Richard en Wilco bedankt voor de leuke studietijd en ik kijk uit naar ons volgende jaarlijks etentje.

Mijn ouders Erik en Catrien, broer Jaap en zus Marloes hebben mij altijd met een luisterend oor bijgestaan. Zonder jullie steun had ik hier nu niet gestaan. Ik wil jullie van harte bedanken voor alle motiverende woorden en afleiding.

CURRICULUM VITAE

Joost Mattheijer was born on 4 April 1981 in Alkmaar, The Netherlands. In 1998 he started his technical education with a bachelor's in mechanical engineering at the Amsterdam University of Applied Sciences. After his graduation in 2002 he worked at KH Engineering, an engineering office, on varying projects among which the development of testing facilities for the European Space Agency. In 2004 he continued his education by enrolling for a master's in biomedical engineering at the Delft University of Technology. Obtaining a general interest in medical devices he proceeded his master in 2009 by assisting Prof. dr. ir. Paul Breedveld with the further development of his graduation project – a colonoscope propulsion device – and a steerable forceps for eye surgery. Prof. dr. ir. Edward Valstar[†] invited him in 2010 to join a PhD research project on intraoperative guidance instrumentation for arthroplasty. After his main research he started a job in 2015 at Oftavinci Research, an ophthalmic company where he developed surgical instruments for treatment of vitreoretinal diseases. While working there he continued finalizing his PhD research, whereof you read here the result in the form of this dissertation.

LIST OF PUBLICATIONS

Scientific articles

Mattheijer, J., Herder, J. L., Tuijthof, G. J. M., Nelissen, R. G. H. H., Dankelman, J., and Valstar, E. R., 2013, Shaping Patient Specific Surgical Guides for Arthroplasty to Obtain High Docking Robustness, *J Mech Design*, 135(7), p. 071001.

Mattheijer, J., Herder, J. L., Tuijthof, G. J. M., and Valstar, E. R., 2015, Docking Robustness of Patient Specific Surgical Guides for Joint Replacement Surgery, *J Mech Design*, 137(6), p. 062301.

Mattheijer, J., Herder, J. L., Gijswijt, D.C., Nelissen, R. G. H. H., Dankelman, J., and Valstar, E. R., 2019, Docking Accuracy of Patient Specific Surgical Guides for Joint Replacement Surgery, submitted.

Mattheijer, J., Herrebrugh, T.O., Nelissen, R. G. H. H., Dankelman, J., and Valstar, E. R., 2019, A Novel Intraoperatively Adjustable Patient Specific Surgical Guide for Knee Replacement Surgery, submitted.

Presentations and abstracts

Mattheijer, J., Herder, J. L., Tuijthof, G. J. M., Nelissen, R. G. H. H., and Valstar, E. R., Robust Docking of Surgical Guides, Oral presentation at the 24th conference of the Society for Medical Innovation and Technology, September 20-22, 2012, Barcelona, Spain.

Mattheijer, J., Herder, J. L., Tuijthof, G. J. M., Nelissen, R. G. H. H., Dankelman, J., and Valstar, E. R., Shaping Patient Specific Templates for Arthroplasty to Obtain High Docking Robustness, Poster presentation at the 20th annual meeting of the European Orthopaedic Research Society, September 26-28, 2012, Amsterdam, The Netherlands.

Mattheijer, J., Herder, J. L., Tuijthof, G. J. M., Nelissen, R. G. H. H., Dankelman, J., and Valstar, E. R., Shaping Patient Specific Templates for Arthroplasty to Obtain High Docking Robustness, Oral presentation at the 4th Dutch Conference on Bio-Medical Engineering, January 24-25, 2013, Egmond aan Zee, The Netherlands.

